AD NUMBER

AD913898

NEW LIMITATION CHANGE

TO

Approved for public release, distribution unlimited

FROM

Distribution authorized to U.S. Gov't. agencies only; Test and Evaluation; JUL 1973. Other requests shall be referred to US Air Force Avionics Laboratory, Attn: AAA, Wright-Patterson AFB, OH 46433.

AUTHORITY

AFAL ltr, 7 May 1979

AFAL-TR-73-170

TITAN VEHICLE ELECTROSTATIC ENVIRONMENT

J. E. NANEVICZ   G. R. HILBERS

Stanford Research Institute
Menlo Park, California

D D C

OCT 17 1973

C

TITAN VEHICLE ELECTROSTATIC ENVIRONMENT

J. E. NANEVICZ   G. R. HILBERS

Stanford Research Institute
Menlo Park, California

27 OCT 1973

Copy No. 39

FOREWORD

This report was prepared by Stanford Research Institute, Menlo Park, California, on Air Force Contract F33615-70-C-1406, Project No 6091. The program was administered by the Air Force Avionics Laboratory, Air Force Systems Command, Systems Avionics Division, Wright-Patterson AFB, Ohio. The Air Force project engineers directing the technical aspects of the study were Claude Austin and Capt D F Wilkerson of the Avionics Synthesis and Analysis Branch, AFAL/AAA.

This work began in February 1970 and concluded in December 1972. The research was conducted by the Electromagnetic Sciences Laboratory of the Electronics and Radio Sciences Division of Stanford Research Institute. The principal investigator, Dr J E Nanevicz, was responsible for research activity under Stanford Research Institute Project 8428.

The authors submitted this report 5 March 1973.

This Technical Report has been reviewed and is approved.

COZIER S KLINE, Colonel, USAF
Chief, System Avionics Division
AF Avionics Laboratory

ii

ABSTRACT

Ground and flight instrumentation was developed and employed for
the study of vehicle electrification during the launch of two Titan IIIC
rockets. The flight instrumentation operated and gathered data from
ignition to payload orbit injection at 19,400 nmi. The first launch
occurred under clear-weather conditions and provided data on rocket-
motor electrification at liftoff and in the ionosphere. On the second
launch, clouds existed in the launch area so that this flight provided
data on vehicle electrification during flight through precipitation.

The results of the experiment indicate that rockets become electrified
by the action of the engines at liftoff, and that precipitation-particle
impact also produces electrification. Streamer discharges were measured
resulting from precipitation-static electrification of a dielectric
surface on the front of the rocket. Results from the atmospheric portion
of the flight indicate that the electrostatic behavior of a large
rocket is similar to that of a jet aircraft.

In the flight through the ionosphere, it was found that operation
of the main engines and altitude-control rockets produced readily detected
signals in the electrostatic sensors. This indicated that rocket-exhaust
constituents were being returned to the vicinity of the vehicle.

Data from the ground instrumentation indicate that the electro-
static fields in the vicinity of the pad at launch are dominated by
charges on the clouds generated by the launch.

Instrumentation and the results of the tests are discussed in con-
siderable detail. Where appropriate, results are compared to theoretical
analyses or to earlier measurements on aircraft and rockets.

CONTENTS

ILLUSTRATIONS

TABLES

ACKNOWLEDGMENTS

I INTRODUCTION

Rockets and space vehicles can acquire electrical charge of various amounts from such processes as triboelectric charging from particulate matter; plasma processes in the ionosphere, radiation belts, and solar wind; photoelectric charging from high-energy radiation; and engine charging from various processes occurring in the combustion chambers of rocket engines. Of these charging processes, triboelectric charging and engine charging were known to be capable of producing detrimental vehicle potentials that lead to sparks, corona, and streamers.[1-7*]

On the Titan IIIC vehicle, anomalous Missile Guidance Computer (MGC) responses have been observed during the flights of Vehicles C-10 and C-14. The anomalous responses occurred at 84 kft for the C-10 and at 58 kft for the C-14 flight. Ground tests of the MGC indicate that similar responses can be produced by sparks to the computer case or by electrical discharges near the computer system. In addition, the Titan IIIC payload fairing is coated with an ablating material on which charge may accumulate, and the fairing was not positively bonded to the missile frame. Thus, it was strongly suspected that the anomalies observed on Vehicles C-10 and C-14 were of electrostatic origin.

The objectives of this program were to study the vehicle electrification mechanisms and charging-current magnitudes on the Titan IIIC rocket vehicle in an effort to better understand the processes by which electromagnetic impulses capable of affecting system operation might be generated. The objectives were achieved by developing and calibrating special flight-test instrumentation and installing and operating it on

---

*References are listed at the end of the report.

two Titan IIIC rockets during scheduled firings. The instrumentation was designed to measure vehicle potential, charging current arriving on a metal frontal surface, streamers generated on a small dielectric frontal surface, and ion current flow and electric field in the vehicle's plasma environment.[8]

Actual installation of the instrumentation on the Titan IIIC test vehicle was accomplished at the Eastern Test Range by the Martin-Marietta Corporation on a separate contract.

During the Titan III instrument development and fabrication period, Apollo 12 was struck by lightning during launch. As a result, SRI scientists participated in two series of ground experiments (one on Apollo 13 and the second on Apollo 14) to investigate the electrical characteristics of the Apollo rocket and its plume.[9] These Apollo experiments were conducted with no electrostatic instrumentation on the rocket, while the Titan IIIC experiments were to be conducted with no ground-based electrostatic instrumentation. It was observed that both programs would be considerably strengthened at relatively little expense if provisions were made to include ground-based measurements on the Titan program. In addition, since the Saturn booster is liquid-fueled, and the first stage of the Titan booster is solid-fueled, the acquisition of relatable data from both vehicles affords an opportunity to compare the characteristics of solid- and liquid-fueled motors. Accordingly, a set of ground-based field meters was fabricated and emplaced around the Titan IIIC launch complex for each launch.

In this report, data measured for flights C-20 and C-21 of the Titan III vehicle are presented. The data include ground-based measurements as well as flight-test data measured during light-off, below the ionosphere, and in the ionosphere. Ground-based measurements from the Apollo 13 and 14 flights are also included for comparison. Many details of the experiment are given in Appendices A through D.

2

Following the two Titan IIIC flights, a set of similar electrostatic-study instrumentation was fabricated by SRI and installed on a satellite to be launched into synchronous orbit. A brief description of this instrumentation system is given in Appendix E of this report.

II DESCRIPTION OF INSTRUMENTATION

A. Flight Instruments

The instrumentation system was developed[8] to measure the following parameters during the flight of the test vehicle:

(1) Instantaneous vehicle potential

(2) Charging rate

(3) Impinging-particle count

(4) Streamer discharge PRF

(5) Streamer discharge current

(6) Ambient electron density.

An electric-field-meter system is used to measure vehicle potential. The field strength measured at a point on the surface of the vehicle by the field meter is directly proportional to the vehicle potential ($V \approx -10\ E$ for the vehicle configuration at launch in free space); thus a measure of the field strength is tantamount to a measure of vehicle potential. The vehicle can be charged by frictional electrification caused by rocket-engine operation.

A charging patch located on the nose of the rocket is used to measure the charging produced by impinging dust or precipitation particles only.[10] The charging-rate patch consists of an electrically isolated conductor on the outside of the vehicle, subject to the impingement of dust or precipitation. The electronic circuitry associated with this patch is designed to measure the current flowing to the patch and to count the number of particles impinging.

In an effort to further study the breakdown process occurring on a rocket vehicle, provisions were made to count the streamer pulses generated

5

by charging of a small, insulating region on the vehicle nose. The electronic circuitry used for the streamer studies includes provisions for measuring the streamer current and for counting the number of streamers generated.

The Langmuir probes for studies during orbit injection are similar to those designed and fabricated by SRI for use by AFCRL in their Trailblazer experiments.[11] The probe consists of an isolated conductor biased negatively with respect to the skin so that it collects saturation ion current. The magnitude of the current is related to the electron density in the immediate vicinity of the probe.[12] Although a fixed-bias ion probe does not permit the determination of electron temperature, its simplicity and compatibility with the rest of the instrumentation dictated its choice.

One of the overriding constraints on the program was that the electrostatic-study instrumentation be carried on a "piggy-back" basis. It could not interfere in any way with either the mechanical or electrical functioning of either the rocket or the payload. This meant that the sensors had to be designed in such a way that there was no question of their mechanical integrity, and that their installation did not compromise the integrity of the vehicle and payload system. These constraints limited the sensor designs that could be considered. For example, it was not possible to consider sensors mounted on booms or struts protruding from the mold lines of the rocket since such a design would require extensive analysis and testing to verify its mechanical integrity in the Titan IIIC launch environment.

1. Field Meter

The field meter developed for this program is of the rotating-vane design. The detector head is mounted in a hole in the skin in such a manner that the meter vanes are exposed to the exterior of the vehicle as shown in Figure 1. Movement of the grounded rotor shown in the figure
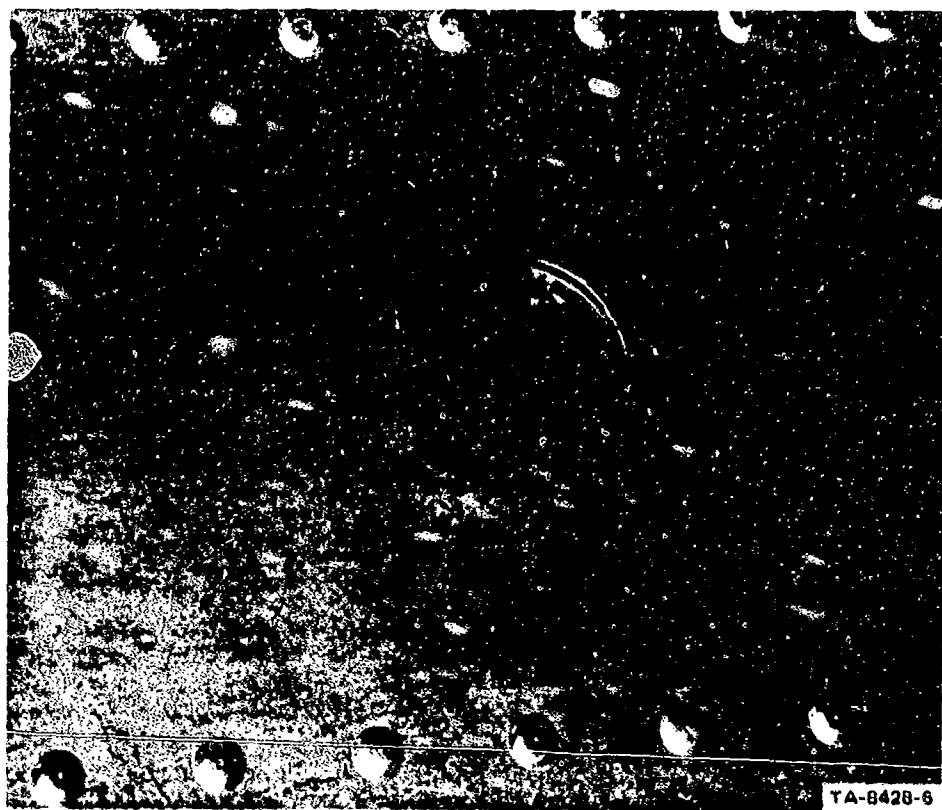
TA-8428-6

FIGURE 1   FIELD-METER INSTALLATION ON TITAN III ROCKET

causes the stator to be alternately exposed to and shielded from the
exterior environment.   In this way an alternating signal is generated
in the stator as the rotor chops the ambient electric field at the skin
or as it chops a convection current to the skin.   These two signals are
in phase quadrature,[8] and for low-altitude airborne measurements, only
the "in-phase" signal generated by chopping the true electric field is
measured.   Although the "quadrature" response of the field meter to
convection currents is not a very useful physical parameter, it does
provide a basis for evaluating the behavior of the field meter in the
ionosphere.   In the present field-meter system, therefore, both the
"in-phase" and "quadrature" components of the stator signal are detected.

7

To ensure its proper operation, the field meter must not be located near plastic surfaces, which may accumulate charge and distort the electric field at the meter location. In determining a location for the field-meter sensor, the transtage[13] (Stage III) of the vehicle was attractive because this section remains intact and operational until payload orbital injection seven hours after launch. This part of the fairing is covered with a 5-mil-thick layer of special, thermal-control silicone paint of sufficient electrical quality to maintain an electric charge on its surface for extended periods of time. This problem was overcome by installing a 21-by-30-inch sheet of Alzak (an electropolished, anodized soft aluminum) on the skin of the vehicle surrounding the field meter. This material has optical characteristics that make it suitable for use as a thermal-control material on the surface of the Titan IIIC, and laboratory tests demonstrated that it retains a sufficiently small charge on its surface to permit it to be used around the field meter.

2. Charging Rate and Particle Counter

The charging rate and particle count are determined with one sensor and appropriate signal processing. The particle counting is done by processing pulses produced by individual particle charge deposited on the sensor plate, and the charging rate is obtained from the average current flowing to the plate as a result of these charge deposits. Using data from aircraft flight tests for particle density and charge per particle, the maximum charging rate and counting rate at Mach 1 should be of the order of one milliampere per square meter and 10^7 particles per second per square meter. A patch area of the order of 100 cm^2 could thus collect a maximum current of 10 µA and intercept particles at a maximum rate of 10^5 particles per second. Since these maximum rates occur infrequently even on aircraft, the sensing system was designed with a dynamic range such that the lower, more frequently encountered

8

rates can be measured. The patch area of 100 cm^2 thus provides adequate current sensitivity and particle discrimination, and with such an area the capacitance of the patch is sufficiently low that reasonable particle pulse amplitudes are produced.

A photograph of the particle sensor used on the Titan IIIC is shown in Figure 2. The entire assembly is made of 0.090-inch-thick stainless-steel pieces cemented to a fiberglass substrate. The particle electrode is simply the 3-by-30-cm rectangle of stainless steel shown in the lower part of the photograph. For best particle-pulse definition, the sensor should be a conducting strip with its longest axis oriented at right angles to the flight path. With this arrangement, particles remain close to the skin as they cross the sensor electrode and gap, and generate short, high-amplitude pulses. Ideally, the dimensions of the particle-counting probe along the direction of flight should be smaller, and the probe should be located away from the body of the vehicle--for example, on a boom extending out from the body. Such an idealized design was not possible within the constraints of the present program. Accordingly, the design of Figure 2 represents the nearest practical approach to the idealized design.

The instrumentation for studying frontal charging is shown in block form in Figure 3. Particles impinging on the sensor induce current pulses, the ac components of which are fed through the coupling capacitor, C, to the input of the pulse amplifier located immediately behind the sensor. The input resistor, R, is chosen to that RC_s (where C_s is the stray capacitance to ground of the input circuit) is small compared to the time between successive pulses. The pulses out of the amplifier are fed to an absolute-value amplifier. The unipolar pulses from the output are used to trigger a pair of one-shot multivibrators. The output from each multivibrator is integrated and used to drive a
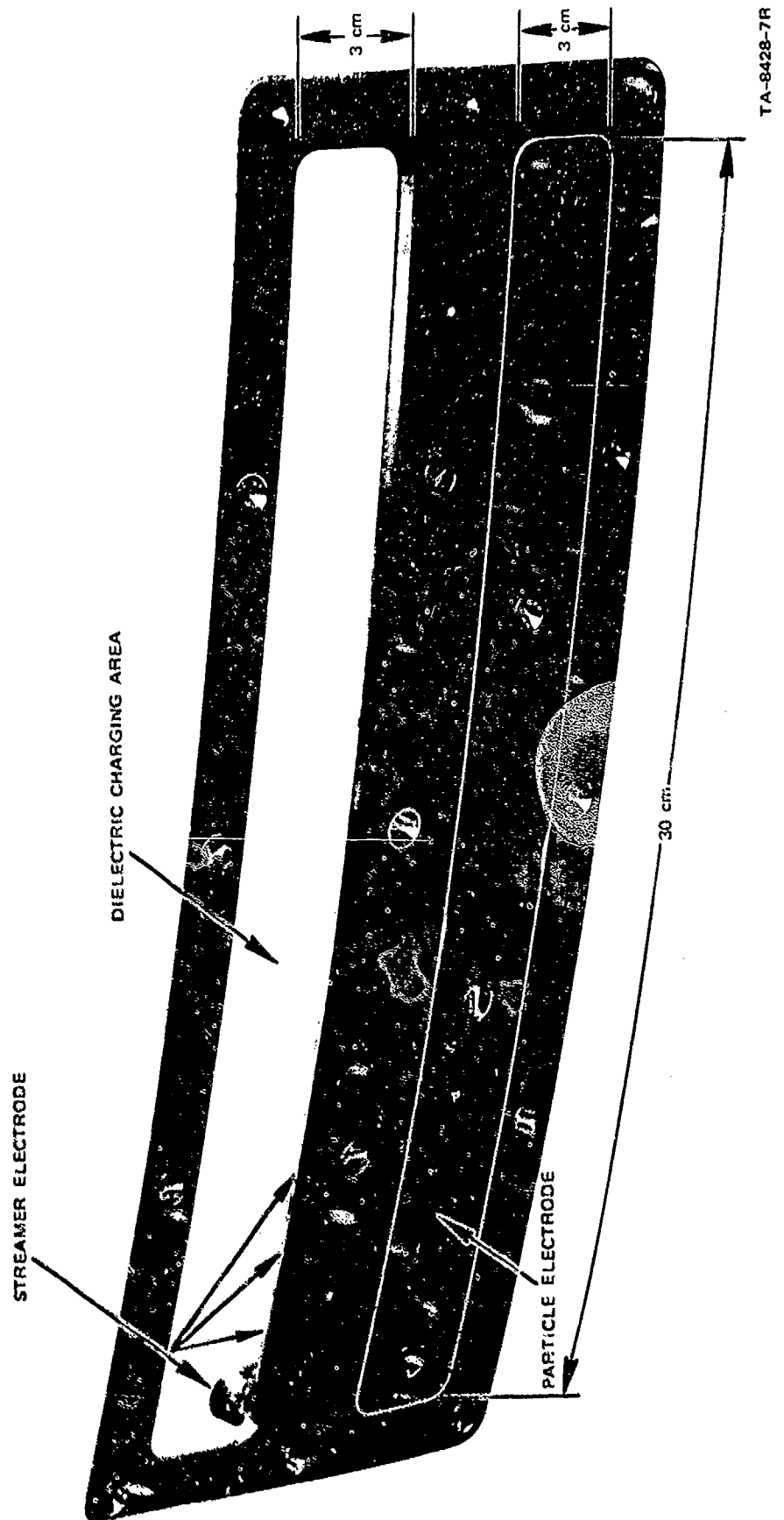
FIGURE 2   PARTICLE/STREAMER SENSOR

STREAMER ELECTRODE

DIELECTRIC CHARGING AREA

PARTICLE ELECTRODE

3 cm

3 cm

30 cm

TA-8428-7R

10
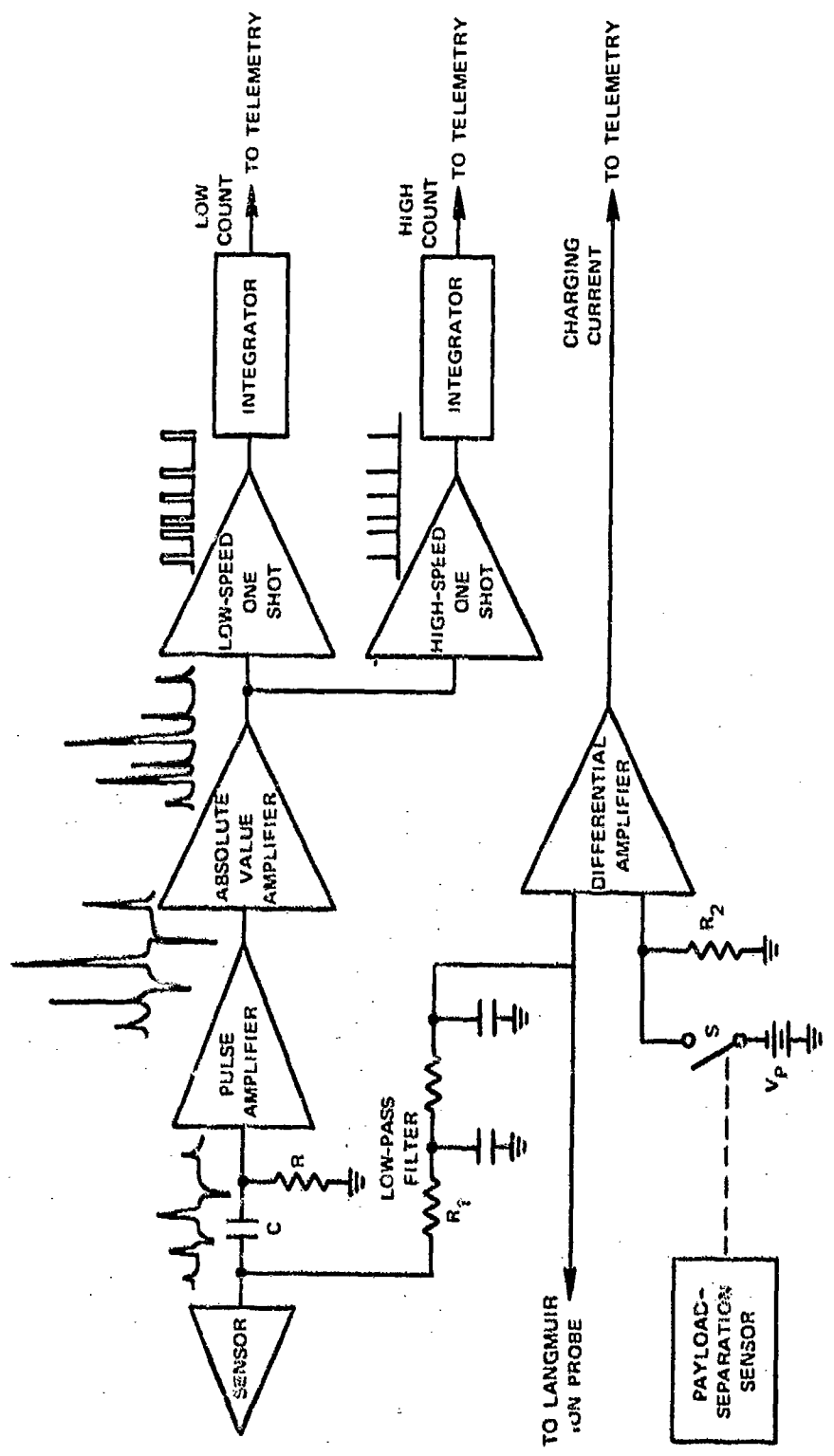
FIGURE 3   BLOCK DIAGRAM OF CHARGING-RATE AND PARTICLE-COUNT SYSTEM

TA-8428-4

11

channel of the telemetry system. Since all of the output pulses produced by a particular multivibrator are of identical shape, the output from the integrator is linearly proportional to the PRF of the pulses at the input. Thus the output is linearly proportional to the particle impingment rate. Wider dynamic range for the system is achieved by setting the multivibrator constants such that the top multivibrator produces wider pulses than the lower one. Thus, for a given pulse rate, the top multivibrator produces a higher dc output from its integrator than the lower multivibrator.

The dc component of the current deposited on the probe flows to ground through the low-pass RC filter, the input resistance of the differential amplifier, and R_2. The voltage developed by this current flowing through the differential-amplifier input is amplified and used to drive a telemetry channel. The value of the low-pass-filter input resistor R_1 is chosen to be high with respect to R. Also, R_1 is located physically close to the probe so that the charging-current circuitry is effectively decoupled from the particle-counting circuitry. Switch S is open the entire time that frontal-charging measurements are being made, so that the power supply V_p is not connected to the differential amplifier during this time. (Actually, the switch is open as long as the payload fairing is on the vehicle.) The purpose of the power supply, the switch, and the ion-probe lead is to permit the particle-current circuitry to be used as a Langmuir ion probe in the ionosphere. It was largely this ability to use the same dc-current-measuring circuitry both for low-altitude frontal-charging studies and for ionospheric-electron-density measurement that dictated the choice of the fixed negatively biased Langmuir ion probe for electron-density determination.

3. Streamer Counter and Dielectric Charging

The streamer patch is designed to provide a direct measure of frontal-dielectric-surface charging and streamer-discharge occurrence. The streamer pulse rate and the streamer current to an isolated dielectric patch were measured using signal-processing electronics similar to that used with the particle-charging system discussed in the previous section.

Since the charge transferred in a streamer discharge is at least an order of magnitude greater than that transferred in an individual particle impact, it is possible to discriminate between streamers and particles striking the patch. Furthermore, the intercept area for particles was made small by using only a fine conducting border about a dielectric surface as the streamer collector. A streamer patch about the same size as the charging-rate patch thus has about the same average charging current, while the streamer pulse count will be about one-tenth the count of the particle patch.

The form of the sensor evolved for streamer studies is shown in the upper part of the photograph of Figure 2. A region of dielectric 3 by 30 cm is exposed to impinging particles. The streamer electrode is a 0.005-inch-thick strip of stainless steel insulated from the rest of the structure and protruding 0.005 inch onto the dielectric from the lower edge of the rim around the dielectric region. Charge deposited on the dielectric surface is relieved by streamers to the streamer electrode or to the surrounding metal structure. These streamer discharges generate pulses in the streamer-sensor electrode. The dc current flowing to the streamer electrode is very nearly equal to one-half the charging current arriving on the isolated dielectric region (the other half of the current flows to the grounded surrounding structure).

The electronic system used for the streamer studies is of the same form as that indicated in Figure 3. Since streamer pulses are much

13

more energetic than the pulses generated by individual precipitation or dust particles, the gain of the pulse amplifier in the system is reduced. The dc-current-measuring system is identical to that used in the particle-charging studies, since the charging areas are very nearly the same in the two cases, and the currents should be the same. The design of the system is such that the streamer-current electronics are used to measure current from a second Langmuir ion probe in the ionosphere.

4. Summary of Characteristics and Sensitivities

The characteristics and sensitivities of the various components of the Titan IIIC instrumentation system are shown in Table 1. It is

Table 1

SUMMARY OF TITAN IIIC INSTRUMENTATION CHARACTERISTICS AND SENSITIVITIES

Sensor	Parameters Measured	Nominal Range
Field meter	Electric field (high gain)	± 10 kV/m
	Electric field (low gain)	± 300 kV/m
	Convection current (high gain)	± 0.1 mA/m^2
	Convection current (low gain)	± 3 mA/m^2
Particle Counter	Particle impacts (low count)	0 to 1,000 pps
	Particle impacts (high count)	0 to 20,000 pps
Streamer Counter	Streamer pulses (low count)	0 to 500 pps
	Streamer pulses (high count)	0 to 10,000 pps
Particle-current sensor	Current (high gain)	± 0.1 μA
	Current (low gain)	± 3 μA
Ion Probe No. 2	Current (high gain)	0 to 0.1 μA
	Current (low gain)	0 to 3 μA
Streamer-current sensor	Current (high gain)	± 0.1 μA
	Current (low gain)	± 3 μA
Ion Probe No. 1	Current (high gain)	0 to 0.1 μA
	Current (low gain)	0 to 3 μA

evident that dymanic range was achieved by employing two linear data-output channels (differing in sensitivity by up to 30 dB) for each parameter measured. The sensitivity limits for each measurement were established using best estimates for expected values of the measured parameter. Details of these considerations are presented in Ref. 8.

5. Installation of Test Vehicle

The general form of the Titan IIIC test vehicle and the physical placement of the electrostatic-study instrumentation on it are shown in Figure 4. All of the electronics and sensors are located either in the transtage or the payload fairing. Both of these structures stay with the vehicle throughout the early staging. The payload fairing is jettisoned 280 seconds into the flight at an altitude of 400,000 feet. The transtage remains intact and operating until the time of payload orbit injection.

A more detailed illustration of the instrument locations is given in Figure 5. The particle/streamer sensor is installed on the outside surface of a door in the nose of the payload fairing. (The preamplifier associated with this sensor is located immediately behind the sensor on the inside of the door.) This location was chosen because it places the surface of the sensor at roughly 45° to the axis of the rocket. This location is away from the stagnation region at the nose, but still not so far back on the rocket that the sensor is shielded from the particles. A location on the vehicle at 90° from the target direction was chosen to minimize changes in particle impingement resulting from changing airflow patterns about the probe during vehicle maneuvering. The in-flight maneuvering of the Titan IIIC is such that the pitch of the rocket (in the plane of the target direction) is non-zero, and changes from time to time during the flight. No deliberate changes are made, however, in the yaw direction, and the yaw angle is maintained near zero

15

PARTICLE/STREAMER
SENSOR ON OUTSIDE

PAYLOAD FAIRING
PREAMPLIFIER ON
INSIDE

PAYLOAD
FAIRING

LANGMUIR PROBE AND
FIELD-METER SENSORS
ON OUTSIDE

ELECTRONICS PACKAGE
ON INSIDE

TRAN-
STAGE

SKIRT

SECOND
STAGE

BOOSTER
STAGE

FIRST
STAGE

BOOSTER
STAGE
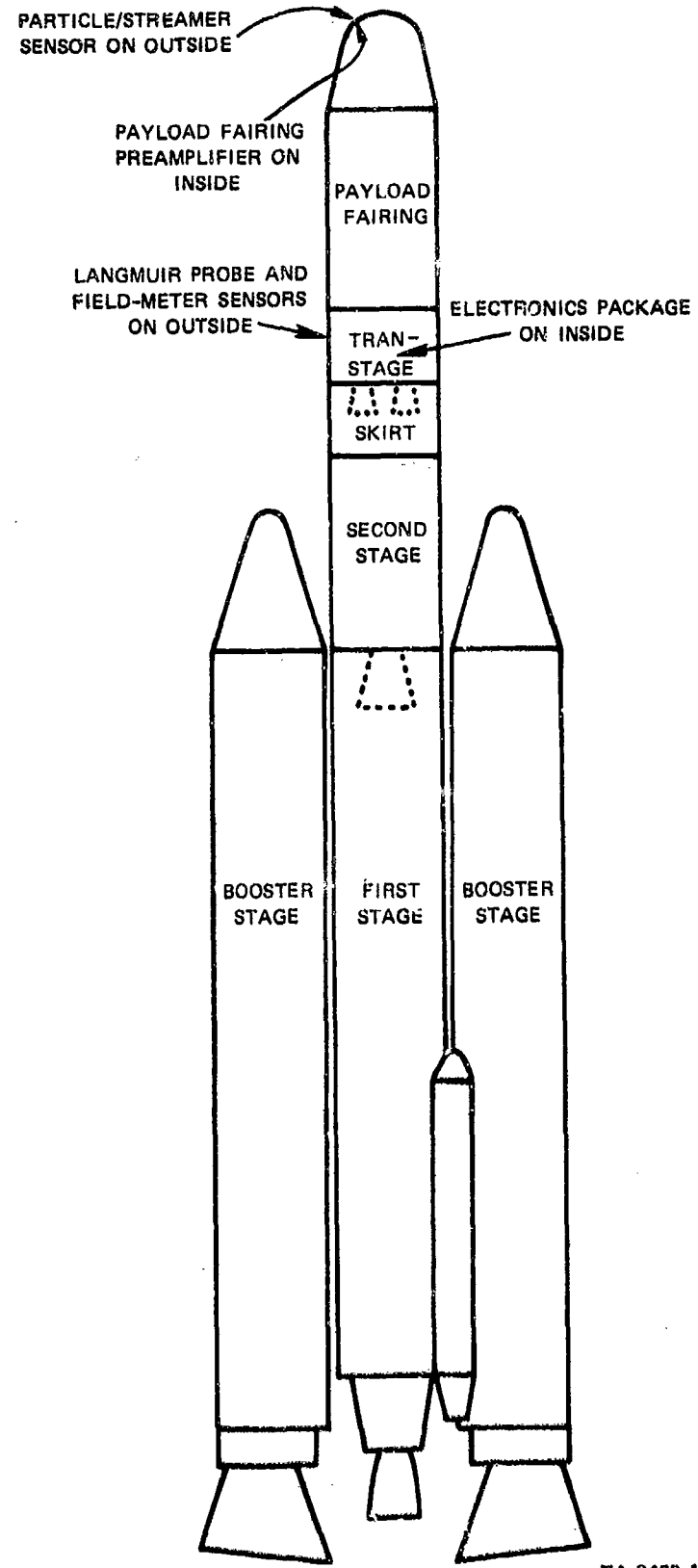
TA-8428-10

FIGURE 4   SKETCH OF TITAN IIIC TEST VEHICLE
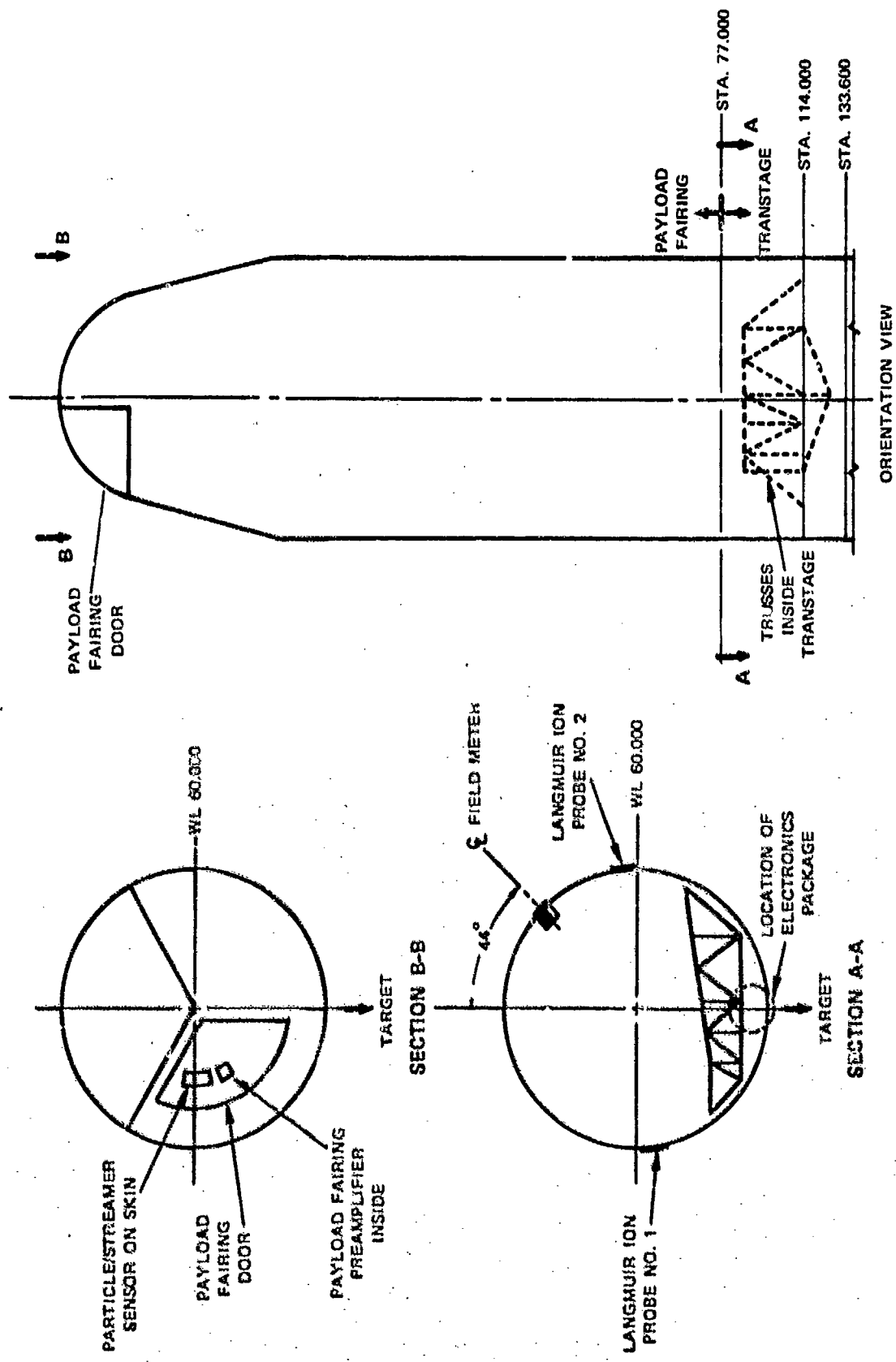
FIGURE 5 LOCATION OF INSTRUMENTATION AND SENSORS ON TITAN IIIC TEST VEHICLE

TA-8428-11

17

throughout the flight. Thus the airflow patterns about the sensor should be constant during flight.

To avoid particle impingement, the field-meter sensor was located on the side of the rocket away from the target direction. Since the vehicle operates in a pitched-up attitude during much of the launch trajectory, the back side of the vehicle is shielded from particles.

B. Ground Instruments

1. Titan

As was indicated earlier, the purpose of the Titan ground experiments was to generate data to supplement those from the flight vehicle, and to provide a common set of measurements to unify the Apollo and Titan electrostatic experiments. As is indicated in Ref. 9, the Apollo experiments were designed to use launch perturbations in the ground-electrostatic-field structure to infer as much as possible about the electrical appearance of the launch vehicle (e.g., whether the vehicle is highly charged, and whether the conducting portion of the plume is thousands of feet long). The SRI Apollo instrumentation consisted largely of field motors arrayed on the ground around the launch pad and on the launch tower. A similar ground installation was used for the Titan launches.

A drawing of the launch pad showing the five ground field-meter locations is given in Figure 6. Field motors were installed at the following stations:

- Track by tower (A), 320 ft from pad
- Guard gate (B), 610 ft from pad
- Outside fence (C), 1090 ft from pad
- Flame trench (D), 430 ft from pad
- Umbilical tower (E), 170 ft above pad
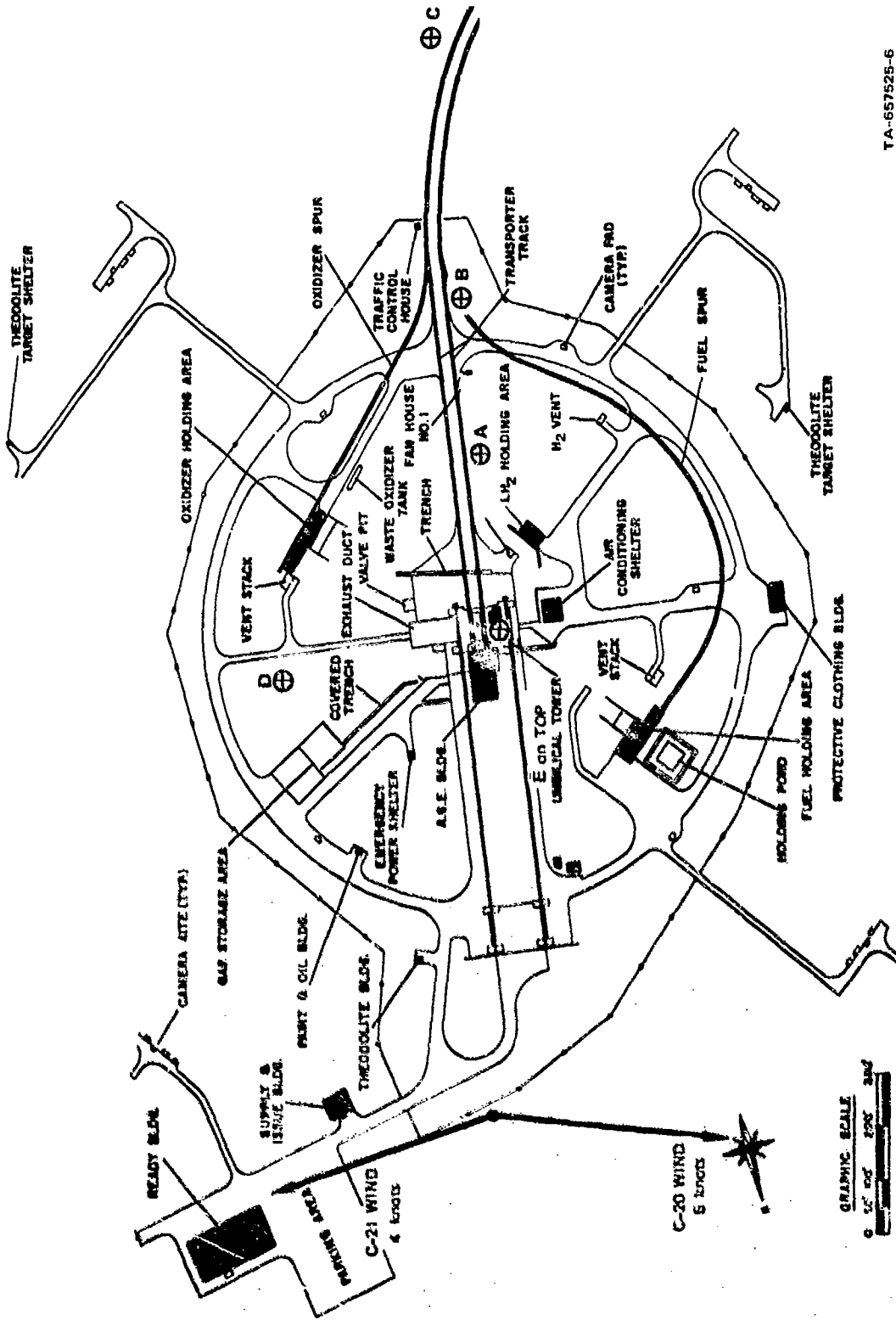
FIGURE 6   GROUND FIELD-METER INSTALLATION ON TITAN III FIRING

TA-657525-6

19

During the early part of a Titan launch, the exhaust is directed east-ward via the single exhaust duct extending east of the pad as shown in Figure 6. To minimize coupling to the exhaust products (which generally are charged), a set of field meters A, B, and C was set out in a line to the south of the pad at right angles to the exhaust duct. Field meter D was positioned slightly north of the exhaust-duct axis to couple strongly to the exhaust products. Field-meter E was located on the top of the 170-ft umbilical tower to couple strongly to the rocket as it moves by the tower, in an effort to measure the potential of the vehicle as it moves by.

A photograph of a typical ground field-meter installation is shown in Figure 7. All the electronics and the strip-chart recorder were housed in a plywood box that protected the system from the weather and provided a convenient base for sandbagging to protect the instrumen-tation from the launch blast. The field-meter detector head is positioned upside down $13\frac{1}{4}$ inches above ground and a few feet toward the pad from the instrumentation box. (Inverted-field-meter operation avoids problems with the motor bearing and insulator design when the sensor must be operated in the rain.) Electrostatic cage calibrations provided the true ambient electrostatic field from the field that was read at the detector face.

A photograph of the field-meter installation on top of the umbilical tower is shown in Figure 8. The field-meter detector head is positioned upside down 20 inches above the top of the tower. The field meter installed on the umbilical tower is one of the heavy-duty units developed for the Titan III onboard field measurements, and was qualified to a 160-dB acoustic environment, and to a 1360-g peak shock.[8] Electrostatic cage calibrations indicate that the ambient electrostatic field at the field-meter location on top of the tower is 27% of the field reading at the meter face. Also, the ambient field that would exist at ground level

FIGURE 7   TYPICAL TITAN III GROUND FIELD-METER INSTALLATION

STRUCTURE
OVER PAYLOAD —
MOVED AWAY
FOR LAUNCH

FIELD-
METER
HEAD

EDGE OF
ROOF

FIELD-METER
ELECTRONICS

ROOF OF
LAUNCH
TOWER

SANDBAGS
OVER SIGNAL
AND POWER
CABLES

TA 857525-3
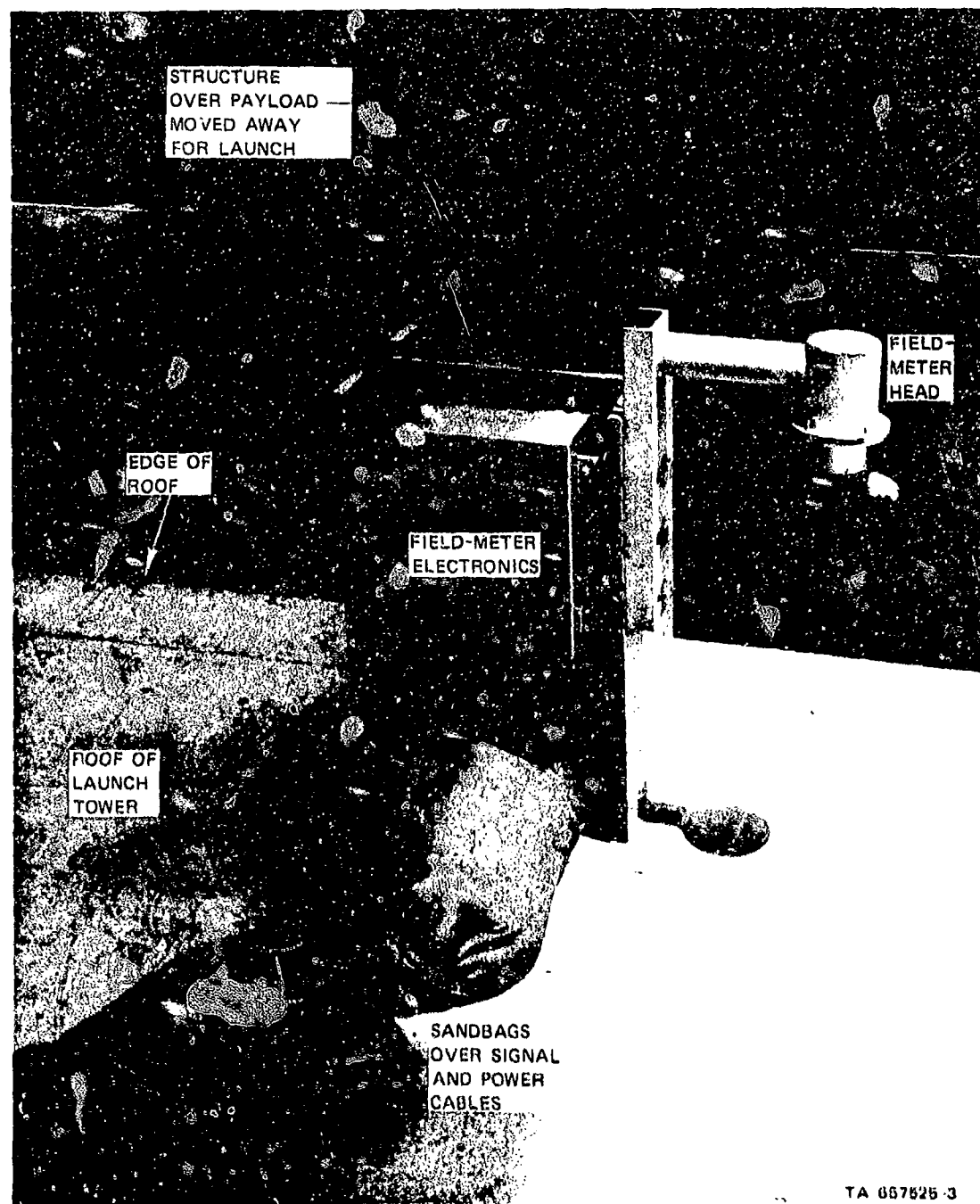
FIGURE 8   FIELD-METER INSTALLATION ON TITAN III UMBILICAL TOWER

is 12% of the ambient field at the top of the tower at the field-meter location. Thus, to obtain true tower-top fields, field-meter-E readings must be multiplied by 0.27 while, to obtain the true ambient earth's field, field-meter-E readings must be multiplied by $0.12 \times 0.27 = 0.032$.

2. Apollo Launch Instrumentation

The SRI field-meter layout used during the Apollo 14 launch[9] is shown in Figure 9. Field meters for the Apollo 14 launch, and also for the Apollo 13 launch, were installed at the following locations:

- Crawlerway, 5740 ft from pad
  (slightly north along crawlerway road for Apollo 13)

- Slidewire, 2780 ft from pad

- Parking lot, 2500 ft from pad (only Apollo 13)

- Camera pad 5, 1310 ft from pad

- Camera pad 4, 1300 ft from pad

- Umbilical tower--LUT, 340 ft above pad (only Apollo 14).

During Apollo launches the exhaust is channeled into two flame trenches: one extending north of the pad and the other south of the pad as shown in Figure 9.

The main Apollo array of three field meters, at camera-pad 5, crawlerway, and slidewire sites, is located along a line roughly at right angles to the flame trenches and is analogous to the main Titan array of three field meters south of the Titan launch pad. Apollo field-meter sites at camera-pad 4 and the parking-lot (Apollo 14 only) are comparable to the Titan flame-trench site in that they all couple tightly to the flame trenches. It should be noted that Apollo sites are located further away from the pad than the Titan sites. A field-meter installation was also placed 340 ft up the 380-ft launch umbilical tower (LUT) for the Apollo 14 launch to couple strongly to the Saturn as it was passing the tower.

23
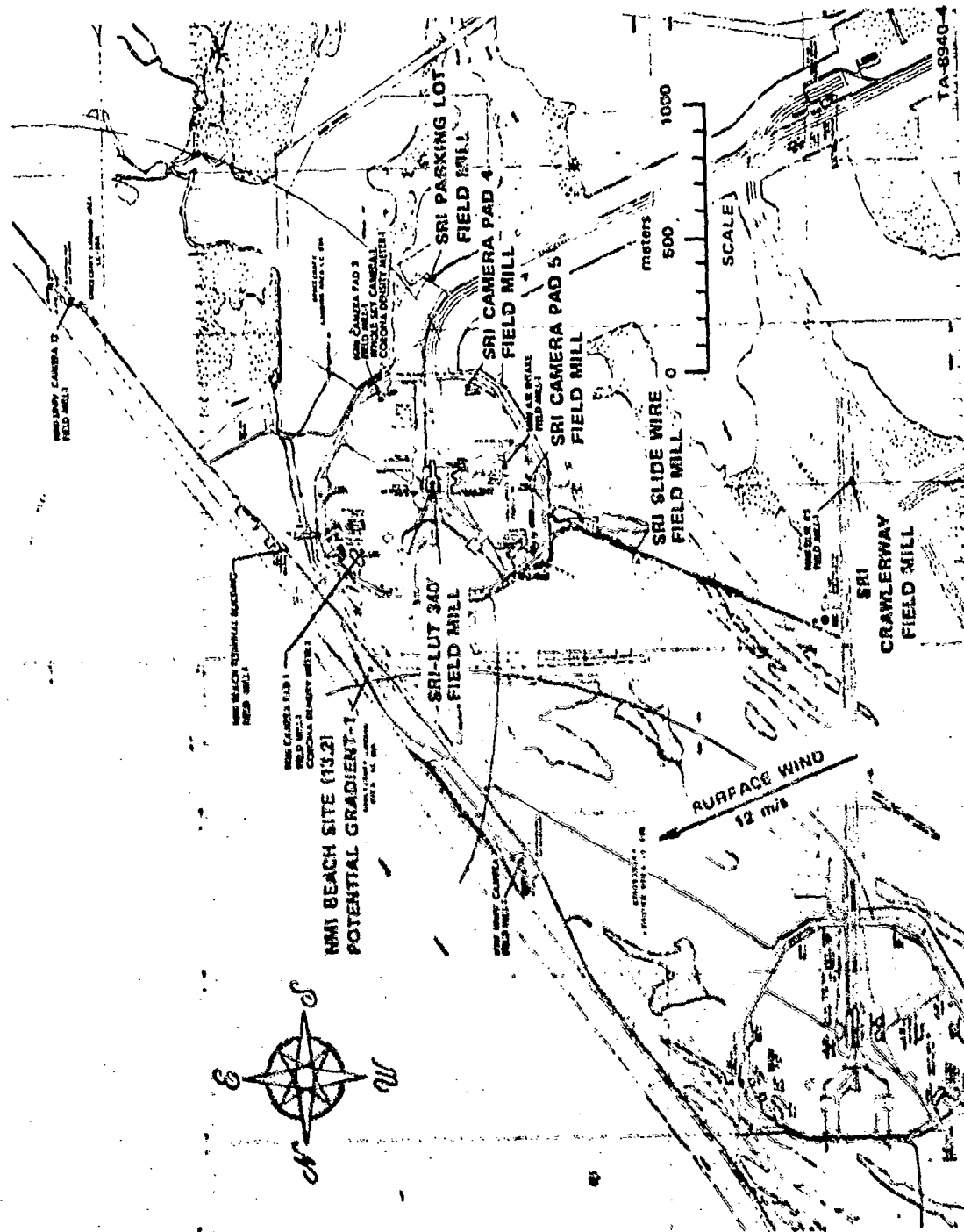
FIGURE 8   INSTRUMENTATION FOR APOLLO 14 LAUNCH

24

III DESCRIPTION OF FLIGHT

A. Titan IIIC-20

The Titan IIIC-20 flight was conducted in early Spring of 1971.
Time of SRM ignition was 0743:01.24 GMT.

A general Titan III mission is described as follows:[14] The vehicle
is launched at the Air Force Eastern Test Range (AFETR) on a 93° flight
azimuth. The transtage and payload are injected into an orbit of 80 × 95
nmi at the completion of the Stage II burn. The transtage engines are
then ignited and a transfer maneuver is performed at the first equatorial
crossing (over the Atlantic). This transfer maneuver produces an orbit
with an apogee of 19,323 nmi. When the apogee is reached, the transtage
engines are ignited for the second time and a plane change/circularization
maneuver is performed. This maneuver produces a synchronous orbit (19,323
nmi) in the equatorial plane. Shortly after the second shutdown of the
transtage engines, the vehicle is reoriented to the payload-separation
attitude. Following payload separation the Attitude Control System (ACS)
and main engines of the transtage are disabled, and the Titan III por-
tion of the mission is completed. Thermal maneuvers are performed while
the rocket is in the transfer orbit orientation. This orientation re-
sults in the transtage roll axis being aligned within 20° of the launch-
site inertial vertical with the outer gimbal equal to ± 160°. This
roll-axis attitude is held constant while a back-and-forth roll
maneuver of ± 112° amplitude is maintained. At each extreme there is
a dwell time of 276 ±5s. The roll rate used is 1.0 + 0.1, -0°/s.
Launch time is chosen such that the insolation vector is within a 60°
half-angle cone measured forward and aft from a plane normal to the
transtage roll axis. During the transfer period, these thermal-orientation

maneuvers are interrupted three times to allow the attitude control system to orient the vehicle to an attitude that permits the ground station to receive telemetry data from the vehicle.

A clear stable atmosphere and no cloud formations existed in the AFETR area at the time of the Titan IIIC-20 launch.

All test instruments worked on the ground and in flight to synchronous orbit. Interesting electric-field data were recorded on the ground prior to launch and up to 1 or 2 minutes after launch (corresponding to vehicle altitudes of 36 to 135 kft). Flight-test data were obtained during the following six telemetry windows:

	Approximate Altitude
Boost phase	40 to 400,000 ft
First transtage burn	80 to 150 nmi
Coast phase	310 to 430 nmi
	1350 to 1450 nmi
	1830 nmi
Second transtage burn and payload ejection	19,300 nmi

A post-flight reconstruction of the C-20 trajectory was made available by Martin Marietta Corp. covering all powered phases of flight. ACS activity was identified on the reconstruction for all telemetry windows. Sun orientation relative to vehicle roll axis and roll plane was also available for vehicle flight events during ionosphere flight.

B.   Titan IIIC-21

The Titan IIIC-21 flight was conducted in Fall 1971. Time of SRM ignition was 0309:05.44 GMT.

26

The general mission of the C-21 flight is similar to that described for the C-20 vehicle except that a double payload was released at 19,400 nmi during sequential times.

Flight-test data were obtained in the following seven telemetry windows:

	Approximate Altitude
Boost phase	20 to 500,000 ft
Park orbit	80 nmi
First transtage burn	100 to 200 nmi
Transfer orbit	4,200 nmi
	14,200 nmi
	18,600 nmi
Second transtage burn and satellite ejections	19,400 nmi

Data concerning powered flight trajectory, ACS activity, and flight-event sun orientation were made available for the C-21 flight by Martin Marietta Corp. ACS jet pressure data were also provided for correlation with electrical measurements.

IV LIFT-OFF PHASE

A. Airborne Data

1. Titan IIIC-20

Onboard instrument data for the first minute after launch are shown in Figure 10. In general, particle and streamer sensor activity was very minimal. This is to be expected in view of the clear weather conditions at the time of launch. In fact, the only indications from these two sensors in this flight regime consist of a few particle counts (25 to 50 pps measured starting at roughly 20 kft altitude). There was no accompanying indication of particle or streamer current and no change in vehicle potential indicating charge accumulation on the rocket. It is not clear, therefore, what interpretation should be placed on the burst of particle-counter activity.

The field-meter record at the time of launch is far more interesting. In view of the existing stable and clear meteorological conditions at launch, rocket charging is evidently caused by processes in the ionized rocket exhaust. It is seen that the C-20 vehicle begins charging negatively about 2 s after SRM ignition. (See Appendix A for polarity convention adopted in this report.) The rocket potential remains at approximately -20 kV until about 7 s after liftoff (at 0743:09.5), when the rocket altitude is 650 ft. The subsequent abrupt increase in negative potential can be interpreted to indicate that the highly conductive portion of the rocket exhaust breaks contact with the ground at 650 ft. This behavior is consistent with the Apollo work of Uman;[15] he has indicated that the visible rocket plume (length approximately 625 ft at ground level) is a uniformly good conductor, but that the

29
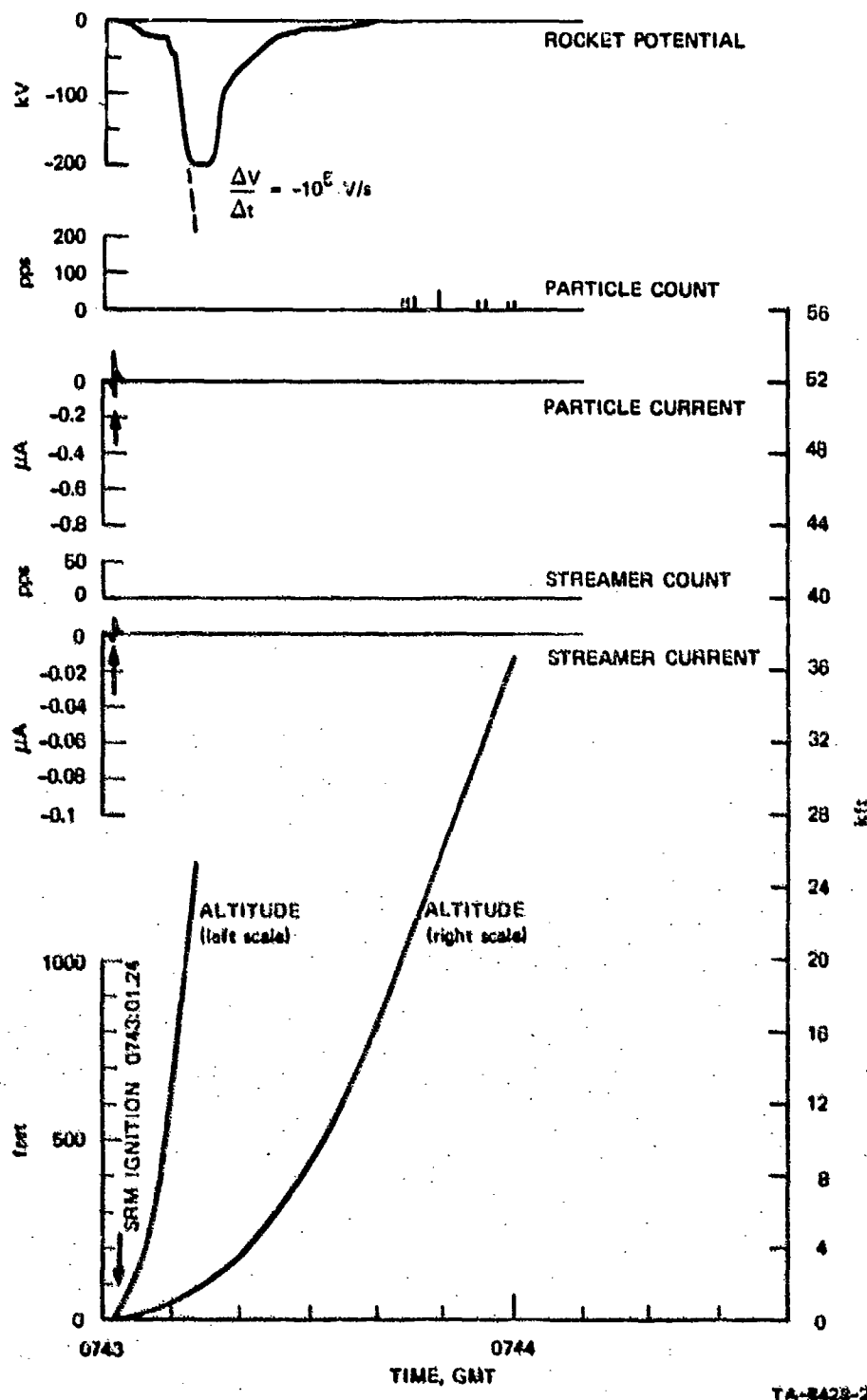
FIGURE 10   LAUNCH DATA FROM TITAN IIIC-20

conductivity drops quite rapidly with further increasing distance along the exhaust trail.

Launch movies indicate that when the rocket reached an altitude of about 600 ft, the exhaust clouds in the vicinity of the pad changed from a grayish, white appearance to a reddish, orange appearance. The portion of the rocket plume impinging on the pad also exhibited this change at about 1000 ft rocket altitude. This visible change in exhaust characteristics apparently indicates a cooler exhaust and a concomitant reduction in plume conductivity.

The C-20 vehicle reaches 200 kV negative potential about 12 s after SRM ignition at an altitude of 1.4 kft. The potential is held nearly constant at 200 kV for nearly 5 s. (Limiting probably occurs as the result of corona discharges from vehicle extremities.) Altogether, the rocket potential remains above 50 kV between 800 and 4000 ft (9 to 20 s after ignition). At these altitudes the vehicle, as viewed by camera, is trailed by an exhaust plume removed from local exhaust clouds generated in the launch area. The vehicle returns to approximately zero potential 34 s after launch at an altitude of 12 kft. At this altitude the rocket plume is not visible in the launch movies. This behavior agrees with aircraft experience where engine-charging current monotonically decreases as the aircraft climbs.

We may now use the rate of change of rocket potential to estimate rocket-engine charging current. From Figure 10 we observe that, during the period of rapid potential increase, $\Delta V / \Delta t = -10^5$ V/s. From measurements made on a scale model of the Titan IIIC vehicle, the self-capacitance C of the vehicle is 1000 pF. The charging current i_{ch} is given by

$$
\begin{aligned}
i_{ch} &= C \, \Delta V / \Delta t \\
&= -10^{-9} \times 10^5 \\
&= -100 \quad ,
\end{aligned}
\tag{1}
$$

31

Both the polarity and magnitude of the charging current are in good
agreement with engine charging current observed on large American jet
aircraft.[16] These currents were in the range 100 to 200 μA for "dry"
takeoffs (with the aircraft charging negatively), and increased by a
factor of 3 to 5 during water injection. In a series of tests on 17
small solid-fueled motors, Boeing measured charging currents in connection
with its minuteman program.[17] The motors were in the 200-to-500-lb
thrust range. The charging currents varied from less than 0.1 μA for the
200-lb-thrust-motors, to slightly over 2 μA for the 500-lb-thrust-motors.
The motors apparently charged to a negative polarity. Although it is
not clear how one should scale data from a 200-to-500-lb rocket, to
apply a Titan IIIC with a thrust of 1.2×10^{6} lb at least the polarities
are in agreement, and the small rocket-motor c   nt is substantially
smaller.

If we assume that the rocket-motor charging processes remained
unchanged from liftoff to 650 ft altitude, we can estimate the plume
resistance R_p required to restrict the vehicle potential to 20 kV during
this time. Employing Ohm's law

$$R_p = \frac{V}{I}$$

where V = Vehicle potential

I = Charging current

and substituting numerical values, we obtain

$$R_p = \frac{2 \times 10^{4}}{100 \times 10^{-6}}$$

$$= 200 \ \text{MΩ} \ .$$

2.   Titan IIIC-21

Data generated by onboard instruments during the first minute
after C-21 launch are shown in Figure 11. This record obviously shows

32
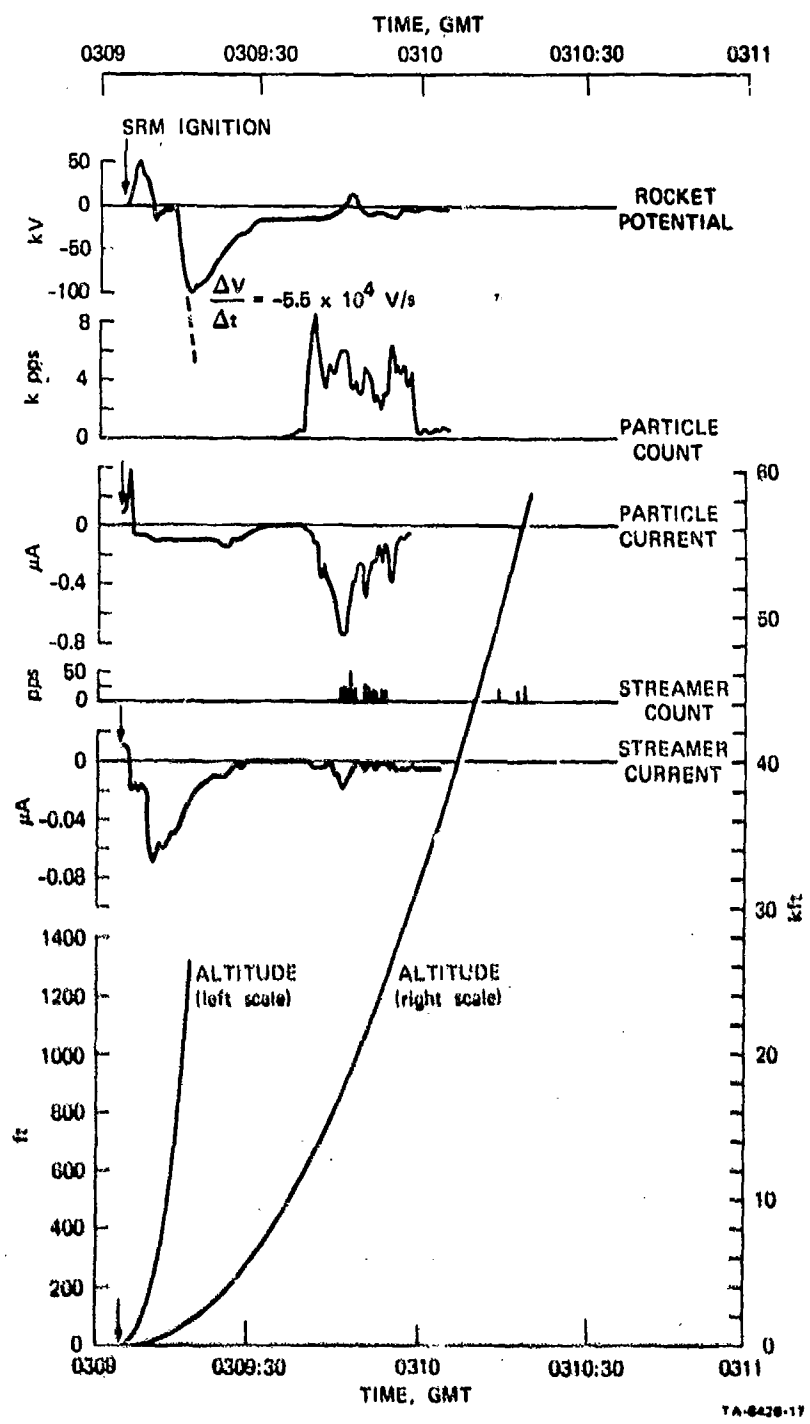
FIGURE 11 LAUNCH DATA FROM TITAN IIIC-21

far more activity than the C-20 data in Figure 10. Inspecting the rocket-potential record in Figure 11 we see that in the first two seconds after ignition, the field meter indicated a field change corresponding to a positive potential of 50 kV on the rocket. It is not clear what physical explanation should be offered for this initial positive potential excursion. The rocket has barely moved from the pad, so that the plume is certainly in good contact with the ground; thus, based on the C-20 experience, one would expect the rocket potential to be low. Seeking some transitory charging process involving the rain does not seem promising because the field meter was exposed to the rain and its reading was steady until SRM ignition.

Following the initial positive excursion, the potential assumed a low negative value and remained there until 0309:14 when the rocket reached 650 ft altitude. At this time the potential rapidly increased to a maximum of -100 kV. This rapid potential change again suggests that the conductive plume breaks contact with the ground when the rocket reaches 650 ft. The rate of potential increase is $\Delta V/\Delta t = -5.5 \times 10^4$ V/s. This corresponds to a charging current of $i_{chg} = -5.5 \times 10^4 (10^{-9}) = -55$ μA, which is roughly half the rocket-motor charging current observed during the launch of C-20. After reaching -100 kV, the rocket potential gradually decreased and remained within the range ± 15 kV for the rest of the flight through the atmosphere.

Both the particle- and streamer-counter channels indicate that negative charge is arriving on the sensor immediately after SRM ignition. It is very likely that these sensor currents do not represent actual charge arriving on the vehicle, but rather are electrochemical currents flowing in each probe system because the probes are wet from the rain. (The probes were uncovered prior to launch.) Although the sensors were made entirely of stainless steel, there is often sufficient difference in the metals that battery action can occur. This effect was often

34

observed on aircraft flights through rain where it was found that the current would gradually go to zero after the aircraft left the rain cloud and the probe dried.

True charging by precipitation begins unequivocally at 0309:36 GMT at an altitude of 10 kft when the particle counter first indicates particle impacts. Particle counting and particle current persist until 0310:00 when the rocket reaches 32 kft altitude. This occurrence of charging is in agreement with the available information regarding cloud structure at the time of launch. Figure 12 shows the AGC (Automatic Gain Control) record from the AFETR radar taken at 0130 GMT (roughly $1\frac{1}{2}$ hours prior to the launch). This record indicates that clouds existed from 10,000 ft to at least 40,000 ft. At the time the record of Figure 12 was made, there were altitudes in this range (17,000 ft and 24 to 30,000 ft) free of clouds. The weather was so variable, however, that at the time of launch it is quite possible that the cloud structure was solid from 10,000 ft to 32 kft. (Roughly two hours after launch all of the clouds over the pad had cleared and stars were visible.)

The particle-probe data indicate that negative charge is arriving on the rocket. This is in agreement with the charging polarity observed during aircraft flight in precipitation. Further comparisons with aircraft flight-test results are also interesting. For example, at 0309:45 GMT, when the particle current is maximum, $i_p = 0.8$ μA, the particle count N is 6×10^3 particles/s and the rocket velocity v is roughly 1000 ft/s = 305 m/s. Since the particle-probe area is A = 100 cm^2 ≈ 0.1 ft^2, this means that the frontal charging rate $i/A = 0.8/0.1 = 8$ $\mu A/ft^2$. This value is in excellent agreement with aircraft flight-test experience,[18] which indicates peak frontal charging of 5 to 10 $\mu A/ft^2$ in cirrus and 30 $\mu A/ft^2$ in frontal snow.

NOTE: AGC level is proportional to strength of radar return,
        which is related to cloud density.
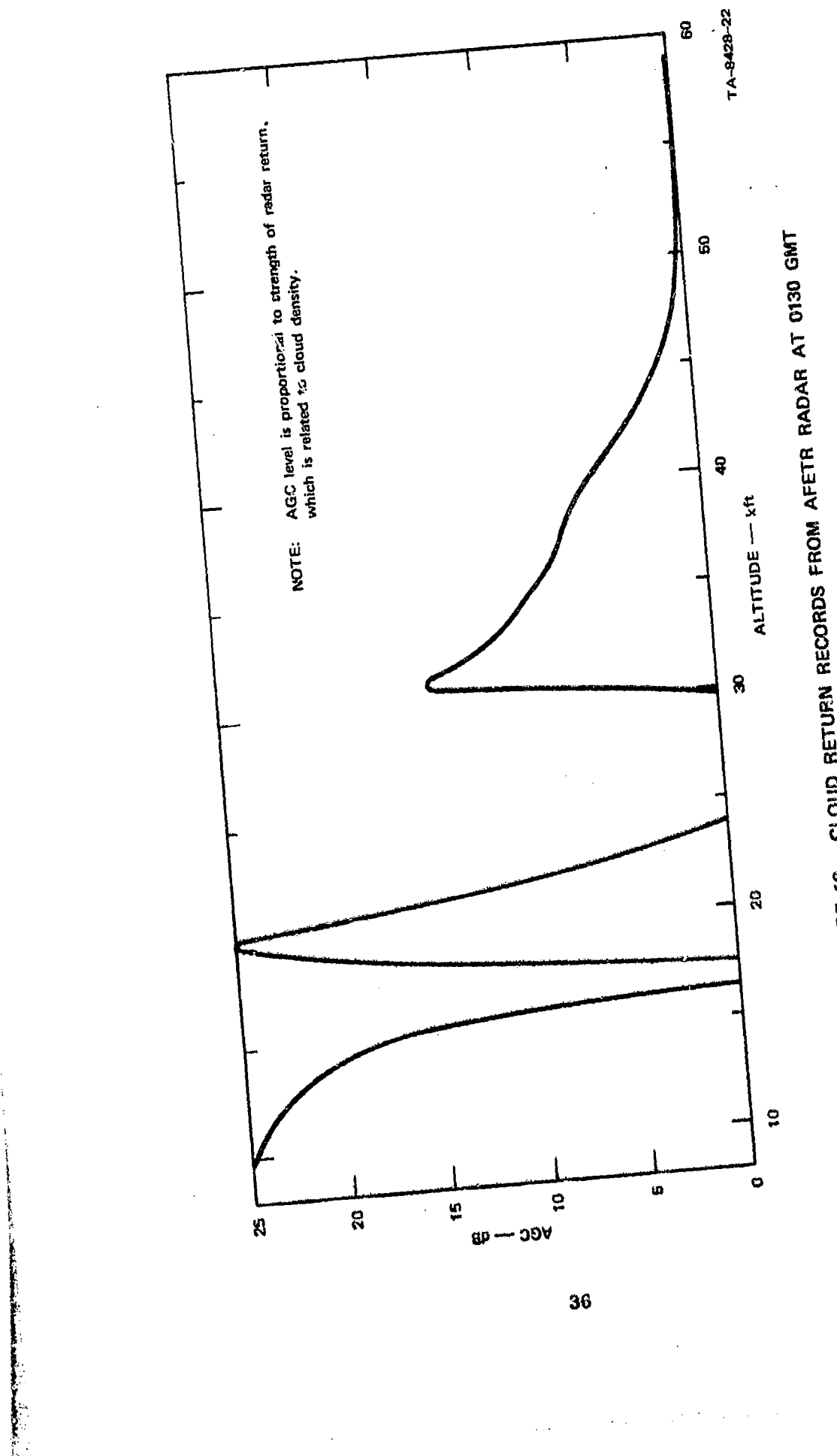
FIGURE 12   CLOUD RETURN RECORDS FROM AFETR RADAR AT 0130 GMT

TA-8428-22

The particle density ρ in the cloud can be found from

$$\rho = \frac{N}{Av}$$

$$= \frac{6 \times 10^3}{0.01(305)} \qquad (2)$$

$$= 2 \times 10^3 \text{ particles/m}^3 \quad .$$

Aircraft flight-test experience[18] indicates that typical maximum particle concentrations are, for cirrus-type clouds, 2×10^4 particles/m^3, and for a thunderhead, 6×10^4 particles/m^3. Thus, the Titan particle-density data are an order of magnitude below the maximum values measured in the aircraft flight-test programs.

The charge q_p acquired by each impinging particle can be found simply by dividing the particle current by the particle count

$$q_p = i_p/N$$

$$= \frac{0.8 \times 10^{-6}}{6 \times 10^3} = 1.3 \times 10^{-10} \qquad (3)$$

$$= 130 \ \mu\mu C \quad .$$

Charges of the order of 10 to 60 $\mu\mu C$ were measured during subsonic aircraft flight tests.[18,19] In more recent tests on an F-4 aircraft, particle charges of up to 100 $\mu\mu C$ were measured.*

The streamer study instrumentation also generated interesting data during the period of maximum precipitation charging. It should be noted that streamer counting does not start until 0309:45 GMT, almost 10 s after the onset of particle counting. This is reasonable because the plastic surface takes time to become charged before streamer discharges

---

*A report on these flight tests is currently under preparation at SRI as the Final Report on Project 7104.

37

can occur. It is also interesting that the streamer current is not steady, but there are peaks of current corresponding to bursts of streamer occurrence. The charge q_s transferred per streamer discharge can be estimated from the streamer current i_s and the streamer count N_s, using the relation

$$q_s = \frac{i_s}{N_s} . \qquad (4)$$

For the period of maximum streamer current at 0309:45 GMT, we find $i_s = 2 \times 10^{-8}$ A and $N_s = 20$, so that

$$q_s = \frac{2 \times 10^{-8}}{20}$$

$$= 10^{-9} \text{ C} .$$

This result is in perfect agreement with the results of ground- and flight-test studies of streamer processes, where it was found[19] that the charge transferred per streamer was 1 to 1.5 $\times 10^{-9}$ C.

3. Comparison with 707 Data

Although many aspects of the Titan IIIC-21 electrostatic behavior have been similar to that observed on large jet aircraft, there are important differences. Figure 13 shows plots of the potential of the Titan IIIC-20 and C-21, together with a typical record of the potential of a 707 aircraft during takeoff. In the case of the 707, engine charging causes the potential to rise to 100 to 150 kV (depending on whether water injection or dry engine operation is being used) immediately when the wheels leave the ground. In the case of the Titan IIIC, the conductivity of the exhaust plume in contact with the ground holds the potential down until contact is broken at an altitude of 650 ft. Then the potential rises to 100 to 200 kV.

38
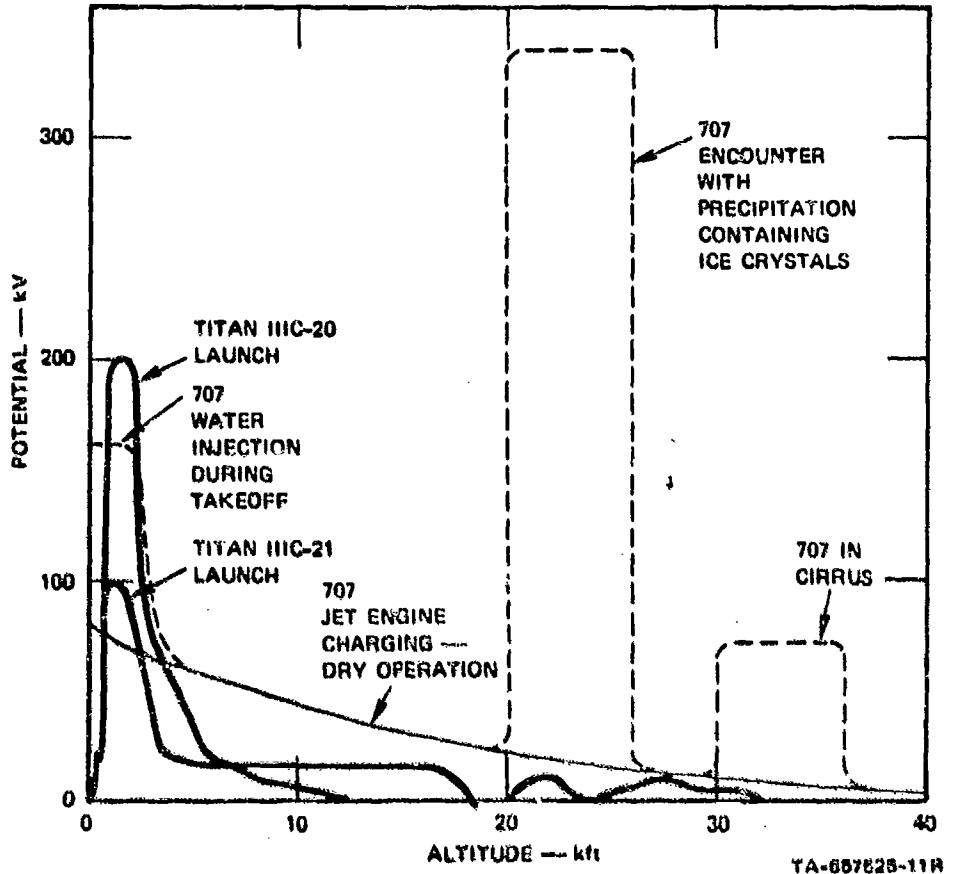
FIGURE 13 COMPARISON OF POTENTIAL OF 707 AIRCRAFT IN FLIGHT AND TITAN III IN LAUNCH

As the 707 climbs, in clear weather, its potential gradually decreases monotonically to zero. If the 707 encounters precipitation, its potential rises to 50 to 350 kV (the precise value depends on the density and type of cloud). The potential of Titan IIIC also decreases to zero as the rocket climbs. However, the Titan potential is only slightly affected by an encounter with precipitation. For example, in Figure 11 at time 0309:45 GMT we showed that the frontal charging current is 8 $\mu A/ft^2$. (At this charging rate, the 707 potential would reach 150 kV.) This insensitivity of rocket potential to charging undoubtedly stems from the high conductivity of the high-temperature rocket plume.

39

Similar behavior is observed on fighter aircraft equipped with after-
burners. For example, in flight tests on an F-4 at Eglin AFB[*], it was
observed that operating the afterburner on takeoff increased the engine
charging, thereby increasing the aircraft potential. On the other hand,
if the aircraft was at operational altitude, the activation of the after-
burners served to help discharge the aircraft and reduce its potential.

It is interesting to estimate the total precipitation charging
current to the Titan at the time at which charging rate was 8 $\mu A/ft^2$.
Referring to Figure 5, we note that the payload fairing has a hemispherical
nose followed by a conical section that transitions into a cylinder.
Let us assume that the 8-$\mu A/ft^2$ charging rate can be applied to the entire
hemispherical region, and that there is no charging aft of this point.
The diameter of the vehicle at the bottom of the hemispherical section
is roughly 7 ft. Thus the projected frontal area effective in charging
is 38.5 ft^2.

From this it follows that the total charging to Titan IIIC-21
at time 0309:45 GMT is $I_T = 38.5(8) = 308 \mu A$. This current was discharged
via the ionized engine exhausts at vehicle potentials substantially below
corona threshold level.

B. Ground Data

The Titan IIIC ground instrumentation array was described in
Section II-B. This instrumentation was used to record data during the
launches of C-20 and C-21. Good data were obtained on those instruments
on both launches. A detailed discussion of the ground data and its
interpretation is presented in Appendix B. Some of the essential details
will be discussed here for the sake of continuity.

---

[*] A report on these flight tests is currently under preparation at SRI
as the Final Report on Project 7104.

40

The purpose of these measurements was to investigate the degree to which information recorded from ground instrumentation can be used to infer the electrical characteristics of a vehicle during the early lift-off period. If it were shown that such ground measurements are indeed capable of generating useful data, considerable information regarding vehicle electrical parameters could be gained from a wide variety of vehicles at relatively little cost.

On the launches of both Titan IIIC-20 and C-21 it was found that in the immediate vicinity of the vehicle, large field variations were observed on the instruments located on the ground. It was argued that these field variations probably stemmed from the fact that a wide variety of exhaust, steam, and debris clouds exist near the launch tower and flame trench in the early stages of the launch. It is likely that these various clouds carry different amounts and polarities of charge. A field meter located near the launch tower will be affected by these clouds as they pass by and will indicate erratic field variations.

The field meters farther removed from the launch tower indicated that the launch generated a region of negative charge in the vicinity of the launch pad. The time history of the measured field variation was such that it could not be ascribed to a negatively charged vehicle climbing up from the region of the pad. The ground field variations were much too slow to be compatible with this physical picture. In general, it was concluded that the electric field measured on the ground stemmed from a large negative charge residing on the clouds generated during the launch. As the cloud drifted away and dissipated, the field in the vicinity of the pad gradually returned to its original level.

The above observations are in good general agreement with the results of ground field measurements made during the Apollo 13 and 14 launches.[9] During the Apollo launches, however, it was found that a

41

positive field excursion was generated by the launch at locations removed from the pad.

In addition to field meters emplaced around the launch pad, a field meter was installed on the launch tower for both Titan launches and for the launch of Apollo 14. Comparison of onboard Titan field-meter data with the readings of the launch-tower field meter indicate that the launch-tower data can be used to determine vehicle potential when the Titan is in the range 50 to 170 ft, nozzle height. In this altitude regime, charge on the vehicle couples strongly to the launch-tower field meter. When the nozzle height exceeds 170 ft the flame is viewed by the field meter and the readings are no longer related to vehicle charge. Unfortunately, the conductive flame keeps the rocket potential down until the vehicle reaches 650 ft altitude, so that the vehicle-potential measurement from the tower is not able to supply any information about the ultimate potential of the rocket once the plume breaks electrical contact with the ground.

An interesting result from the Apollo 14 launch-tower field-meter measurement is the observation that the engines charged the vehicle positively. (It will be recalled that both Titans charged negatively.) At the time the engines reached the field meter, the measured field magnitude indicates that the Apollo 14 potential was less than 6000 V. This is in agreement with the argument that the plume conductivity holds down the vehicle potential while the conductive part of the plume is in contact with the ground.

V FLIGHT DATA BELOW 500,000 FT ALTITUDE

A. Titan IIIC-20 Data

One of the interesting events observed during the time the rocket was below the ionosphere was associated with the principal period of particle-counter activity during the launch of Titan IIIC-20 shown in Figure 14. Here occasional bursts of counting at approximately 50 pps occurred at random times. There was no corresponding indication of either particle current or streamer current. A single streamer pulse is indicated at 0744:46.4 GMT. Interestingly, this is the altitude regime at which the computer anomalies on Titans IIIC-10 and C-14 occurred. (The altitudes of occurrence are shown in Figure 14.) Evidence of particle impact at this altitude was not expected when the experiment was being planned, since appreciable particulate matter does not usually occur at this altitude. Nacreous clouds do occur in the range 60 to 130 kft, however, and it is possible that they were present the night of the launch. An effort was made to obtain independent evidence for the existence of nacreous clouds over AFETR the night of the C-20 launch. Unfortunately, these clouds are quite rare, and no systematic procedure has been established for their detection and monitoring.

Evidence that the particle/streamer-current and field-meter systems were functioning at the 100-kft altitude regime and that the absence of current indications coincident with the counts is not due to instrument malfunction is given in Figure 15, which shows the records of these systems at the time of solid-rocket-motor (SRM) jettison. At this time, two rockets (exhausts directed toward the Titan I stage) are activated

43
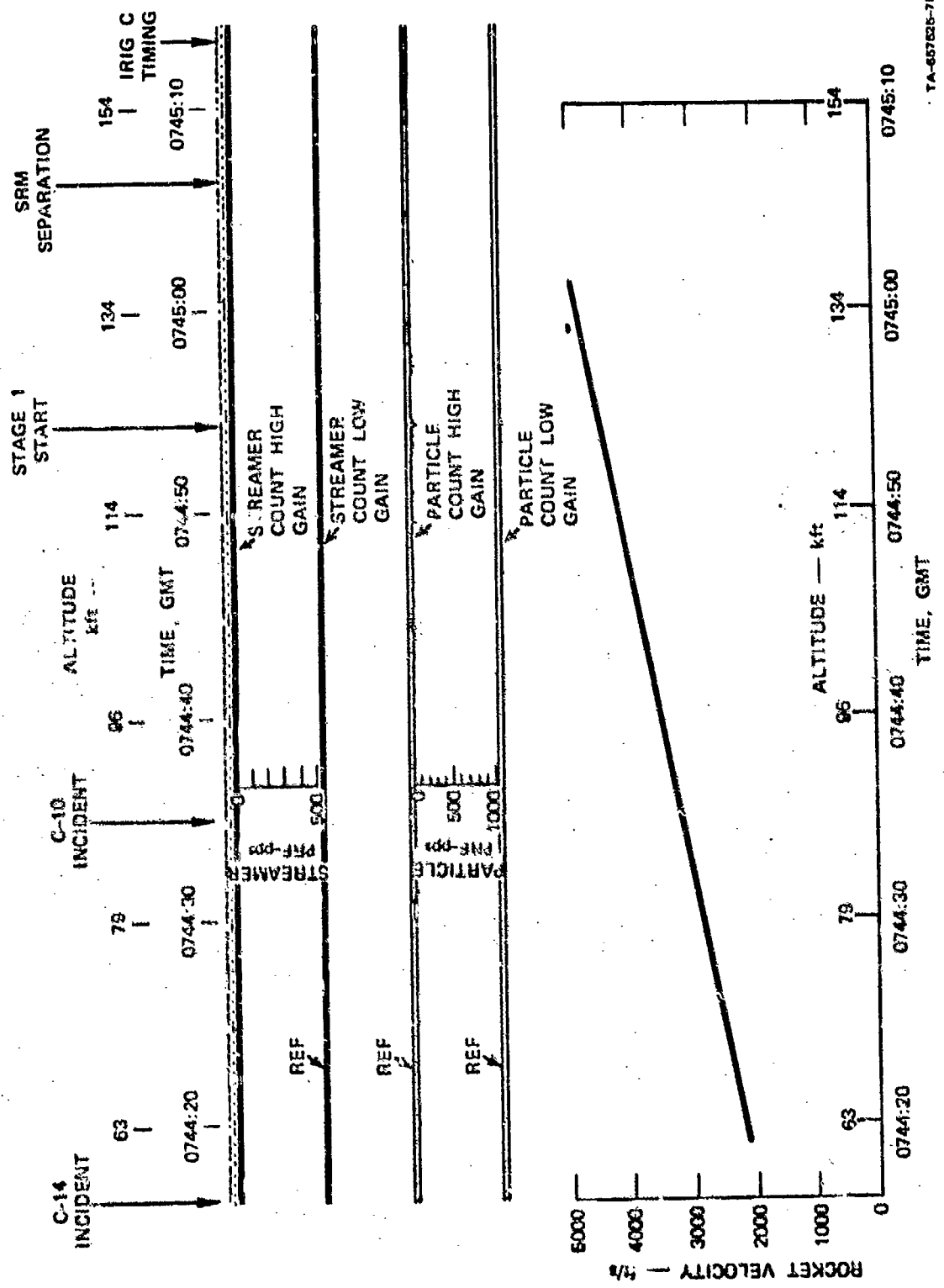
FIGURE 14 ILLUSTRATION OF PRINCIPAL PERIOD OF PARTICLE-COUNTER ACTIVITY DURING LAUNCH OF TITAN IIIC-20

TA-657625-7R

44
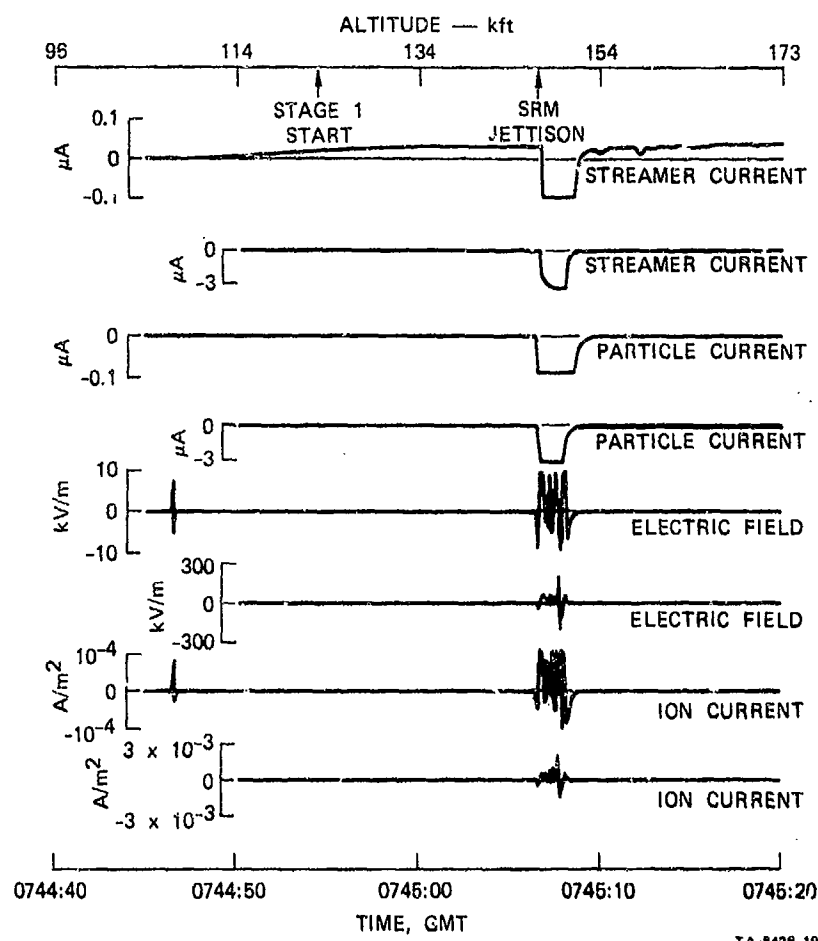
FIGURE 15 MEASUREMENTS DURING FIRST STAGING OF TITAN IIIC-20

to move the solid, strap-on rockets away from the main vehicle. The
operation of the jettison rockets bathes the vehicle (including the
transtage) in exhaust products. This exhaust striking the Langmuir ion-
probe sensors undoubtedly generates the charging currents that saturate
both channels of both the particle-current and streamer-current systems.
The same exhaust products impinging on the field-meter sensor produce
the noisy records shown. It must be concluded, therefore, that the
particle counts of Figure 14 were indeed not accompanied by appreciable
charging current.

45

In this regard, it is interesting to calculate the magnitude of particle-probe charging current that might be expected under these circumstances. Flight-test measurements of particle impact charging made on high-speed jet aircraft indicate that, following impact, atmospheric ice crystals acquire charges of up to 50 $\mu\mu$C. Let us assume that the particles of Figure 10 acquired the same charge upon impact. Since we have 50 particles per second striking the probe, depositing a charge of 5×10^{-11} C per impact, the current arriving on the probe will be

$$i_{probe} = 50 \times 5 \times 10^{-11} \text{ C/s}$$

$$= 0.0025 \ \mu\text{A}.$$

Unfortunately, the full-scale deflection of the sensitive-particle and streamer-current channels is 0.1 μA, so that a current of 0.0025 μA is right at the limit of detectability of the current-measuring system. Accordingly, it is not surprising that there is no indication of charging current accompanying the evidence of particle impact.

Before leaving the question of the encounter with particles at 100 kft altitude, it is interesting to invoke a further test. Experiments involving the firing of 5/32-inch-diameter steel balls through clouds of ice crystals and dust indicate that charging by impact with the ice crystals was zero at velocities 3500 ft/s and above, while impact with dust particles produces charging to velocities of 4000 to 5000 ft/s, depending upon the type of dust.[20] The velocity profile shown in the lower portion of Figure 14 indicates that, at this time, the rocket velocity is in the regime where particle impact charging is marginally possible. (It is not clear that the data obtained with 5/32-inch-diameter balls at sea level should be applied on a one-to-one basis to a 10-ft-diameter rocket at high altitude. Thus it is conceivable that charging could persist to the velocities shown in Figure 14.) It appears, therefore, that the evidence of particle impact of Figure 14 must be accepted as real.

An overall plot of particle data, streamer data, ion-probe data, and electric-field measurements on the Titan IIIC-20 rocket from launch to an altitude of 500,000 ft (approximately 80 nmi) about 8 minutes after liftoff is shown in Figure 16. Particle and streamer currents were measured from launch until the payload fairing (PLF) and the particle- and streamer-current probes were jettisoned. After PLF jettison the two ion probes were connected to the instrumentation and ion-probe current was recorded. Also shown in Figure 16 are times of occurrence of discrete events associated with the operation of the launch vehicle. From an inspection of the figure, it is evident that much of the activity is associated with these discrete events. The first such activity is associated with the jettisoning of the SRM at 0745:06 GMT and has been discussed in detail in connection with Figure 15.

The next sensor activity began at roughly 0747 and was associated with I-II staging. Starting at 0747, there was a 10-s period during which the particle-current sensor indicated current flow, and a noisy output was obtained from the field meter. These signals are consistent with a physical picture of engine-exhaust products striking the field meter and the No.2 ion probe (the No. 2 ion probe is electrically connected to the particle-current electronics--see Figure 3). It is interesting to note from Figure 5 that the field meter and the No. 2 ion probe are in close proximity on one side of the transtage, while ion probe No. 1, which did not record any current flow, is located on the opposite side of the transtage. Thus, during the last 10 s of the Stage-I burn, it appears that exhaust products impinged on one side of the transtage.

At the time of Stage-II ignition, a large transient signal appeared on all sensors. Following this transient, the sensor readings went to zero until the time of payload-fairing jettison. At this time again, a transient occurred on all sensors.

47
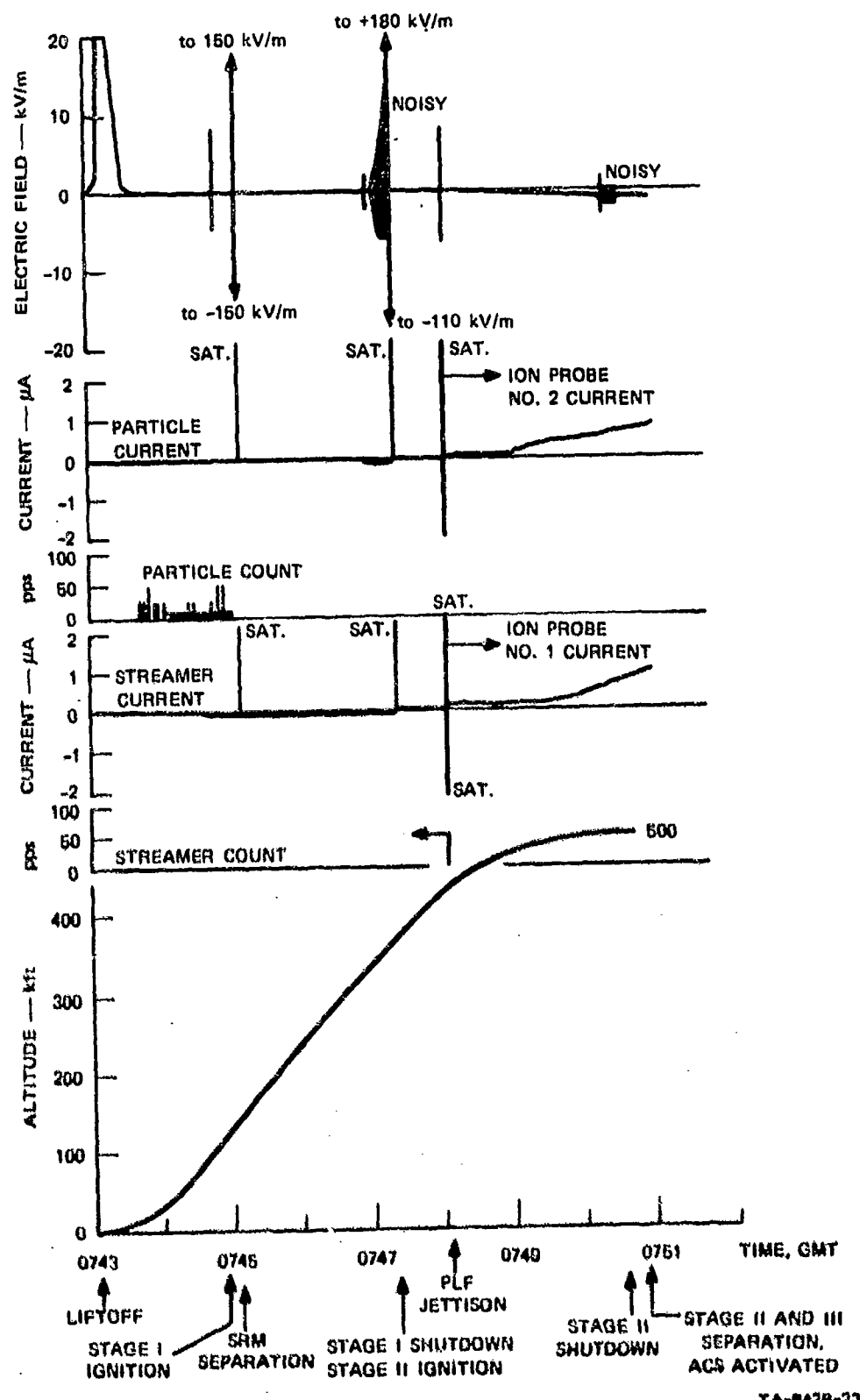
FIGURE 16   TITAN IIIC-20 FLIGHT TO 500,000 FT

48

Following PLF jettison, the Langmuir-ion-probe function was activated, and ion-probe current increased as the vehicle climbed. It is of interest to compare the value of electron density indicated by the Langmuir-ion-probe readings with published data and with the electron density inferred from an ionogram made in Grand Bahama at the time of launch. The analysis of Appendix C indicates that at 500 kft altitude, the electron density N_e

$$N_e \cong 4 \times 10^{10} \, I \quad el/cm^3 \tag{5}$$

where I is the ion-probe current in amperes. At the time of Stage-II shutdown, 0750:40 GMT at an altitude of 500 kft, both ion probes indicate a current of 0.7 μA. From Eq. (5), this means that $N_e = 2.8 \times 10^4$ el/cm^3. This result is in reasonable agreement with Figure 17, which shows repre-
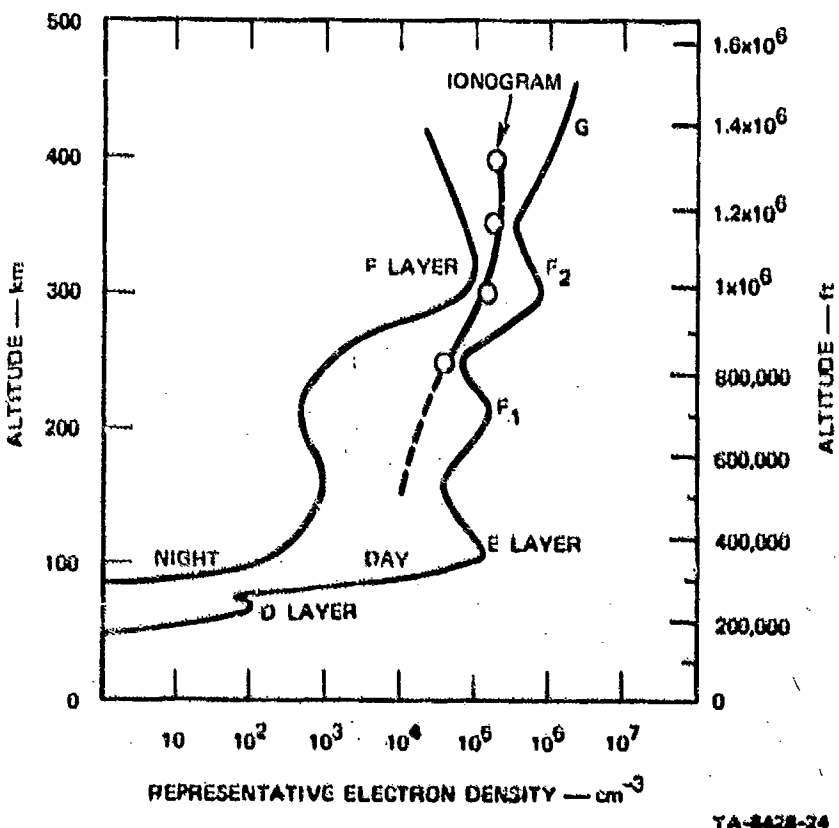
FIGURE 17   IONOSPHERIC ELECTRON DENSITY

49

sentative curves for ionospheric electron density as well as the data
from the ionogram recorded the night of the launch. The ionogram data
do not extend down to an altitude of 500 kft. The available data,
however, lie roughly midway between the representative day and night
curves in the figure. Thus it appears that, at 500 kft, an electron
density of 1 to 2 $\times$ 10^4 el/cm^3 would be in agreement with a judicious
extrapolation of the ionogram data as shown by the dashed lines in the
Figure 17.

Beginning shortly after PLF jettison, the field meter indicates a
progressively increasing negative field. According to the sign convention
adopted for the field-meter polarity, this means that the vehicle is
becoming positively charged with respect to its surroundings. No definite
physical argument for this charging is available. It is undoubtedly
connected with entry into the ionosphere, but the precise processes active
are complicated by the fact that the Stage-II engine is operating at
this time.

B.   Titan IIIC-21 Data

An overall plot of particle data, streamer data, ion-probe data,
and electric-field measurements on the Titan IIIC-21 rocket to an
altitude of 500 kft is shown in Figure 18. There are some similarities
with the C-20 flight data for this altitude regime, but the detailed
behavior is different. One of the obvious differences is the high level
of particle-counter activity during the C-21 flight. As was discussed
earlier, particle counts below 32,000 ft altitude coincide with frontal-
charging-current flow resulting from triboelectric charging during flight
through clouds of precipitation. Above 32 kft in Figure 18 the source
of the particle counts is not clear. On the actual strip-chart records
from the C-21 flight, the character of the particle-count record starting
at 0310 is very unusual. The counter output consists largely of a series
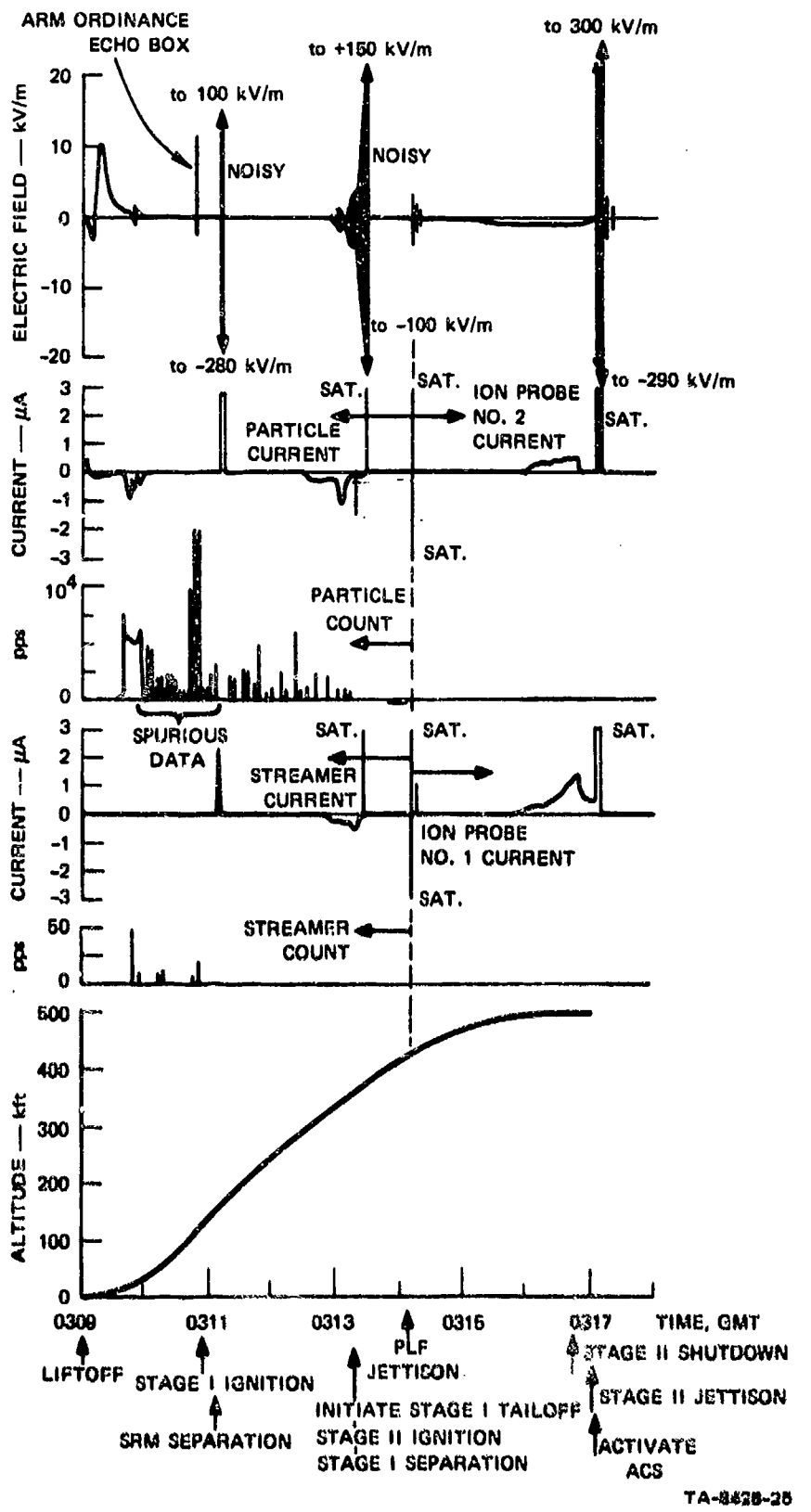
FIGURE 18   TITAN IIIC-21 FLIGHT TO 500,000 FT

TA-8426-25

of pulses with a very regular PRF of 10 pps. The pulse rise time of 0.02 s (two samples at a telemetry sampling rate of 100/s), indicating that all of the counting occurred in this brief period, and that, during the remaining 0.08 s, no counting occurred. Occasionally the rise of the pulse occupies 0.05 to 0.08 s (5 to 8 sample periods). Since each sample period in the rise of the pulse added an almost equal increment of amplitude to the pulse, the pulses with the 0.05-to-0.08-s rise time are from 2 to 4 times as high as the more usual 0.02-s-rise-time pulses. During this period of unusual counter output signal, the ratio of the high-gain and low-gain counter outputs is not consistent with the relative sensitivities of the two channels. In addition, the particle counts are not accompanied by charging current. It appears possible, therefore, that the signals activating the counter circuits were not generated by impinging particles, but were associated with some spurious process such as sensor microphonics. During the qualification testing of the Titan-III sensor system, for example, slight "hair" or noise was observed on the sensitive particle-count channel output during the application of the acoustic environment.[8] On the qualification test unit, it was possible to get a noise response from the system by sharply rapping the particle sensor with a screwdriver handle. It is possible, therefore, that the particle counts registered beginning at 32 kft altitude are spurious and result from a microphonic particle sensor. It should be recalled that the stage-zero or stage-one engine is operating throughout this time, so that the acoustic noise levels on the vehicle are high. Alternatively, it is possible that some electrical signal on the rocket was coupled into the counter. The source of such a signal is not known at this time.

The observed signals could be produced if the PLF door and particle-sensor structure were resonant at 10 Hz, and if the sensor microphonics generated bursts of noise signals of a substantially higher frequency

when excited by the 10-Hz vibration. The 10-Hz excitation would account for the regular 10-pps pulse rate. The character of the counter circuits is such that their response to a signal consisting of bursts of modulated high-frequency noise would cause both output channels to generate comparable signals. This anomalous behavior of the particle counter appears to end at 0311 GMT, so that the data after this time are probably more reliable. However, in view of the fact that anomalous behavior was observed during the period 0310 to 0311, the subsequent data are suspect, and have not been analyzed in detail.

Continuing with the review of Figure 18, we find that at the time of SRM separation at 0311:08.57, all of the sensors are affected, as they were during the launch of Titan IIIC-20.

Starting at 0312:30, current flow begins on the particle-current channel. A few seconds later, at 0312:50, current flow starts on the streamer-current channel, and noisy output signals are observed on the field-meter channel. This same general behavior was observed on the C-20 flight, except that on the C-20 flight the streamer-current channel was unaffected. There it was argued that the observed signals were consistent with the physical picture of engine-exhaust products striking the sensors on the transtage. It is not clear why such a flow of exhaust products should be associated with the end of the Stage-I burn, since all of these signals go to zero at Stage-II ignition, at 0313:24.01.

The sensor readings remained at zero until the time of PLF jettison. At this time a transient was observed on all sensor channels.

Starting at 0315:40 GMT, an increasing ion current is collected by both ion probes. By 0316:30, when the rocket has reached 500 kft altitude, the current in each probe is 0.7 μA, indicating an ambient electron density of 2.8×10^4 el/cm^3, in agreement with the value measured on the C-20 flight. Whereas, on C-20, neither ion-current channel was affected by

Stage-II shutdown, on C-21 the No. 2 ion current goes to zero at 0316:46.52 when the Stage-II engine is shut down, while the No. 2 ion-probe current drops to 1/3 of its previous level. This result means that engine operation can markedly affect the electron and ion density at the ion-probe location. Accordingly, electron-density data obtained during periods of engine operation are very likely not representative of the undisturbed electron density at that altitude.

The jettison of the C-21 Stage-II engine at 0317:02.58 generated a large transient on all sensors. It is interesting that the jettison of the C-20 Stage-II engine produced no effect on any of the sensors.

In Figure 18, the field-meter record after PLF jettison indicates that the vehicle gradually charges positively with respect to its surroundings. The magnitude of the field and its time structure are in good agreement with the experience on C-20.

VI   FLIGHT DATA IN UPPER IONOSPHERE

A.   General

During the upper-ionospheric portion of the Titan IIIC flights,
data were obtained from the field meter (electric field and ion current
density) and from the two ion probes. The readings of these instruments
were strongly affected by the operation of the attitude-control-system
(ACS) rockets. In the upper ionosphere, the orientation of the vehicle
with respect to the sun is of great importance in determining the sensor
signal. For example, when a sensor surface is illuminated by the sun,
photoelectric current is emitted from the sensor. Such current can be
misinterpreted as an incoming positive ion current. To assist in the
interpretation of the flight results, sun-orientation data were made
available to SRI for discrete times corresponding to the occurrence of
specific events on the rocket during ionospheric flight.

It is important to note that the rationale behind extending the
experiment to the ionosphere was not to obtain basic data regarding
ionospheric properties over the flight trajectories. Rather, the primary
purpose was to observe the ways in which the electrostatic and plasma
parameters vary during flight as a specific vehicle, the Titan IIIC,
passes through successive regions of the ionosphere and as various
operations of the vehicle are carried out. In planning a purely scientific
experiment, one adjusts the form of his vehicle including shape, materials,
outgassing, periods of engine operation, and so forth, to optimize the
accuracy of the projected measurements. For the present experiment, on
the other hand, it was important that the instrumentation modify the
physical characteristics of the flight vehicle as little as possible.

The form of the mission was not changed in any way to accomodate the electrostatic experiment. In spite of these limitations, it is important to compare what the present experiment indicates regarding the ionosphere, with accepted data to verify the general functioning of the instrumentation system.

A detailed review and analysis of the flight data from the ionosphere has been carried out and is presented in Appendix D. Only certain of the essential results will be discussed here.

B. Essential Results

As the flight vehicle climbs into the ionosphere, the ambient electron density gradually increases until the peak of the F layer of the ionosphere is reached. Above the F layer, the electron density decreases. These changes in electron density were evidenced on the Titan IIIC flights by systematic variations in ion-probe current as the vehicle climbed. In general, the electron-density values inferred from the ion-probe currents during the flights were in quite good agreement with published data throughout each flight.

Each ion probe consisted essentially of a stainless-steel plate 137 cm^2 in area positioned on the surface of the vehicle and biased 10 V negative with respect to the vehicle. This bias attracts positive ions from the plasma, and the resulting ion current can be interpreted in terms of an ambient ion/electron density. It is important to note, however, that a stainless-steel plate illuminated by the sun will emit photoelectrons. These photoelectrons will be repelled by the negative potential on the probe. The electronic system cannot distinguish this photoelectric current from true ion collection current, and under conditions of low ambient ion density, the photoelectron current can be almost an order of magnitude higher than the ion collection current.

By employing data regarding vehicle orientation with respect to the sun, it was possible to sort out ion current from photoelectron current. This process is assisted by the fact that two ion probes were used in the experiment, with one sensor on the opposite side of the vehicle from the other. In this way, when one probe is in the sunlight, the other is in the shadow of the vehicle.

Very good agreement was obtained between measured values of photoelectron current, and values predicted from recent laboratory experiments using stainless-steel electrodes illuminated by an ultraviolet source. The good agreement obtained between the measured ion-probe data and accepted values of electrical parameters indicated that the ion-probe system functioned properly throughout the flight.

Functioning of the field-meter systems was also checked by comparing their indication with the readings expected in the plasma existing at the vehicle altitude. In general, a body in the ionosphere collects negative charge from the ambient plasma, which tends to charge the vehicle to a negative potential. If the vehicle is illuminated by the sun, photoelectric emission from the vehicle generates a current tending to charge the vehicle to a positive potential. In the ionosphere, the ion/electron density is sufficiently high that electron collection dominates and the vehicle is negatively charged. As the vehicle climbs to an attitude of roughly an earth radius, the ambient ion/electron density becomes sufficiently low that photoelectron emission dominates and the vehicle becomes positively charged.

This behavior of vehicle polarity was observed on the field-meter E-field channel. When the field meter was pointed at the sun, the current density indicated on the field meter J-field channel was in good agreement with predicted photoemission current from a gold surface (the field-meter vanes were gold plated).

57

The charge flow to or from the vehicle results in an ion or electron sheath about the vehicle across which most of the voltage drop occurs. This voltage drop across the sheath generates an electric field at the surface of the vehicle. This sheath field provided another opportunity to verify the functioning of the field-meter system.

As was indicated above, the measured upper-ionosphere data are in agreement with published values. Operation of the main engines on the transtage engine produced large changes in both ion-probe and field-meter readings. The character of the field-meter readings was such that it appeared to indicate that exhaust products were being collected on the vehicle surfaces.

Following the first transtage burn, the vehicle attitude-control system (ACS) was activated. Operation of the ACS rocket motors could be detected on both the ion-probe and field-meter systems. At synchronous-orbit attitude, for example, the ion-probe current was increased by a factor of as much as 5 by the operation of the ACS jets.

These data indicate that the exhaust products from the ACS jets diffuse to the vicinity of the vehicle where they can deposit on vehicle surfaces. If the exhaust products are not benign, their deposition on the vehicle surfaces can cause degradation in the performance of sensors and optical surfaces.

Under some conditions, it was not possible to completely explain the measured data in terms of expected ambient environment and theory applicable to a completely conducting vehicle. It was argued there that the electrically insulating thermal-control coating applied to the surface of the transtage modifies the collection of current by the skin of the vehicle.

At orbit altitude, the electric field indicated by the field meter is higher than expected, strictly on the basis of predicted vehicle

58

potentials. It appears that the high field-meter reading was caused by charge residing on surface films near the field-meter sensor.

A particularly interesting development in the program was the detection of spinup-rocket-motor operation on the payload satellite after it had separated from the transtage and was 12 to 18 ft away. The spinup rocket activity was detected by SRI personnel as an unusual event occurring at a particular time without a priori knowledge of the spinup motor burn. The operation of this motor on the satellite caused a 5-to-1 change in the ion-current reading of ion probe No. 2 on the transtage. The time history of the ion-probe current was indicated to be in good agreement with the chamber-pressure variation normally observed in a motor of this type.

VII CONCLUSIONS

The Titan III experiments were successful in all respects. The
flight instrumentation worked throughout the entire flight from the
liftoff phase to payload ejection. The experiments also generated a
variety of significant results. Of great interest is the fact that the
rocket appears to be connected to earth until it reaches an altitude of
650 ft. This means that the rocket is trailed by a highly conducting
plume 650 ft long. The presence of this plume is significant in many
situations. It is important, for example, in making determinations of
the likelihood of lightning striking the rocket. A highly conducting
plume will also modify the way RF currents are distributed on a vehicle
immersed in an electromagnetic field. Such considerations are important
in determining vehicle susceptibility to noise and EMP signals.

The experiments indicate that, in the early stages of the launch,
the rocket motors charge the vehicle to potentials of 100 to 200 kilo-
volts. Accordingly, corona discharges can be expected from prominent
protrusions from the vehicle. At liftoff the engine-charging current
was 50 to 100 μA, with the vehicle charging negatively on both flights.

At higher altitudes, the rocket motors serve to discharge the
vehicle so that high vehicle potentials and corona discharges do not
occur during flight through precipitation. On the flight of Titan
IIIC-21, a precipitation charging current of roughly 300 μA was discharged
by the action of the engines at potentials substantially below vehicle
corona threshold.

Precipitation charging of the frontal surfaces does occur as in the
case of aircraft. The charging rates measured on the Titan are in good

61

agreement with aircraft data. For example, during flight through a cloud at 20,000 ft altitude, the frontal-charging rate measured on Titan IIIC-21 was 8 $\mu A/ft^2$. Aircraft measurements indicate peak charging currents of 5 to 10 $\mu A/ft^2$ in cirrus and 30 $\mu A/ft^2$ in heavy frontal snow. Evidence of frictional charging by particles was present to altitudes of 100 kft (where nacreous clouds occur).

Streamer discharges on dielectric frontal surfaces of the Titan were shown to occur. The characteristics of these discharges appear to be in good agreement with aircraft experience. (It should be noted that the frontal charging and the resulting streamers occur in spite of the fact that the vehicle as a whole is at low potential as the result of the rocket-motor discharging.)

The ground experiments conducted in connection with the launches indicate that the electric fields in the vicinity of the launch pad are so dominated by the charged clouds associated with the launch that relying solely on ground-field measurements to infer the rocket's behavior is not likely to be fruitful.

During the ionospheric portion of the flight, the Titan instrumentation provided data in good general agreement with accepted values of measured parameters such as ambient electron density and photoelectric emission. These measurements served to demonstrate the proper functioning of the instrumentation during this portion of the flight. The primary purpose of the instrumentation, however, was to measure electrostatic processes occurring during the flight of a large operational rocket. It was found that each time an ACS rocket was burned, ion current collected by the ion probes increased. This means that the rocket-exhaust constituents returned to the vicinity of the transtage skin where they were collected by the probes. One of the ACS motors appeared to produce a more pronounced effect than did the others. This result is

significant, since it means that rocket exhaust products do remain in the vicinity of the vehicle where they can settle out on sensitive instruments and optical surfaces.

The field-meter data indicate that at synchronous-orbit altitude, substantial electric fields exist at the surface of the vehicle. These fields can serve to alter the trajectories of charged particles in the vicinity of the vehicle, thereby modifying the rate at which surface contamination occurs. The presence of an electrically insulating thermal-control coating over the vehicle greatly complicate the interpretation of the interaction of the vehicle with the plasma environment.

An unexpected result of the tests was the demonstration that the instrumentation on the transtage was able to detect the operation of spinup rockets on the payload satellites after the two vehicles were separated by distance of at least 12 to 18 ft. Not only did the instrumentation detect the occurrence of the burn, but it provided a time signature of the spinup-rocket-chamber pressure. With suitable calibration procedures, it should also be possible to infer something about the size of remote engines being operated. This result is of interest in that it demonstrates that simple, passive instrumentation can be used for remote monitoring and study of synchronous-satellite activity.

Finally, the Titan III experiments demonstrated that piggyback experiments on operational vehicles can be conducted without in any way compromising the primary mission. Such experiments are capable of generating needed information available in no other way.

VIII RECOMMENDATIONS

The results of the flight experiments indicate that the Titan III rocket at low altitudes behaves very much like an aircraft, but that the detailed behavior is somewhat different. Operation of the engines at liftoff charges the rocket to potentials of hundreds of thousands of volts. Accordingly, the same precautions regarding corona-discharge interference applied to aircraft should also be observed on the Titan III, provided there are systems aboard the rocket susceptible to this sort of interference.

Once the Titan reaches an altitude of 4000 ft, the engines no longer charge the vehicle, but begin to act as dischargers. On Titan IIIC-21, the engines discharged precipitation charging currents of 300 µA while holding the vehicle potential substantially below corona threshold. This result means that, except for the flight period up to 4000 ft altitude, corona discharge noise will not be a problem on the Titan IIIC.

Although the engines keep the vehicle potential down to low values, precipitation charging of frontal surfaces will still occur. This means that many of the same precautions observed in aircraft design should be applied to rockets. In particular, care should be exercised to avoid unbonded metal frontal surfaces, since these will lead to highly noisy spark discharges from the unbonded member to the adjacent airframe. If sensitive systems are carried on the vehicle, provisions, such as the use of conductive surface coatings, should be made to eliminate streamering on dielectric frontal surfaces.

Liftoff data indicate that the vehicle behaves as if it were electrically connected to ground until it reaches an altitude of 650 ft.

65

This result was interpreted to mean that the electrically conducting portion of the exhaust plume is 650 ft long. This result is significant in connection with the establishment of launch rules for electrically disturbed weather conditions. In estimating the likelihood that the Titan III will trigger a lightning stroke, the 650-ft conducting-plume length should be added to the length of the vehicle in defining the dimensions of the triggering conductor inserted into the region of high electric field.

Flight experiments on other vehicle types should be conducted to determine plume lengths on other vehicle types. In particular, measurements would be desirable on liquid-fueled vehicles and on solid-fueled vehicles having compositions differing greatly from that of the Titan III strap-on motors.

Additional experiments to define the RF characteristics of the plume would be desirable because the presence of the plume can markedly affect the distribution of RF current on the vehicle and modify susceptibility to EMP and other interfering electromagnetic signals.

The flight tests demonstrate that in the ionosphere a portion of the plasma generated by rocket operation remains in the vicinity of the vehicle, since rocket-motor activity caused pronounced changes in ion-probe current. This means that operation of sensitive sensors or optical surfaces aboard the vehicle can be altered by the deposition of engine-exhaust products. If such sensitive devices are aboard, care should be taken either to control the character of the engine effluent or to carefully direct it away from the sensitive regions.

The ionospheric measurements also indicate that substantial electric fields exist in the vicinity of the skin at orbital altitude. Such fields can modify the flow of charged particles in the vicinity of the skin and cause them to deposit in undesireable locations on the

66

vehicle. The presence of such fields should be considered in the design of sensitive long-life systems capable of being adversely affected by the deposition of charged particles.

At the time of satellite ejection, it was observed that the Titan III instrumentation detected the operation of the spinup rocket motors on the satellites when they were at least 14 ft away, and provided a record similar to the time history of spinup-rocket chamber pressure. This capability should be investigated and developed further since it provides a scheme for passive remote monitoring of engine activity on synchronous-orbit satellites. The Titan III experiments already demonstrate that the time history of the engine burn can readily be obtained. It should also be possible to infer information regarding probable engine size from the measured electron-density change and the distance to the satellite under observation.

Finally, it is recommended that the possibility of piggyback experiments be considered on future operational launches. Although there are many scientific experiments conducted on satellites and sounding rockets, specifically dedicated to the experiment, it is also necessary to perform measurements on operational vehicles. The work on operational vehicles is necessary to obtain engineering data appropriate to that vehicle type or class. Such information is generally not generated in purely scientific experiments.

In planning a piggyback experiment, it is necessary to make clear at the outset that the installation of the experiment must in no way compromise the primary mission of the vehicle. This means that the instrumentation must be designed and qualified to the same levels as the prime payload. It also means that the experimenter will be restricted regarding acceptable sensor designs and locations. These restrictions can generally be met with a modest additional effort devoted to the experiment design.

Appendix A

SIGN CONVENTIONS FOR POLARITIES OF CURRENTS AND FIELDS

Appendix A

SIGN CONVENTIONS FOR POLARITIES OF CURRENTS AND FIELDS

The sign conventions used in this report are those generally observed by atmospheric electricians in describing currents and fields observed at the surface of the earth in response to charges in the atmosphere. The reason for adopting this convention here is that in this program, field meters were used to measure fields observed on the ground and on flight vehicles. Certain calibration procedures and ways of thinking about the data have been developed in connection with the use of field meters, and it was felt that it would be safer to continue these conventions here rather than risk the confusion that might result from instituting a new convention.

Basically, the field convention is as illustrated in Figure A-1(a). Here, if a positive charge exists above the earth, the atmospheric electrician says that the earth's field is positive. This enables him to associate a positive field with positive charge overhead. The convention of Figure A-1(a) is opposite to the normal convention in which a field is taken to be positive in the direction in which a positive charge would move if immersed in the field.

Extending this convention to the case of a field meter mounted on a charged rocket, we find that we get a positive-field indication if the outside world looks positive to the field meter. This happens when the rocket is negatively charged as shown in Figure A-1(b)

The sign convention regarding currents is the normal one illustrated in Figure A-1(c). Here a current is said to be positive if positive charge is arriving on the sensor.

71

(a) FIELD METER ON GROUND

(b) FIELD METER ON CHARGED ROCKET

(c) CURRENT FLOWING TO PROBE

TA-8428-28
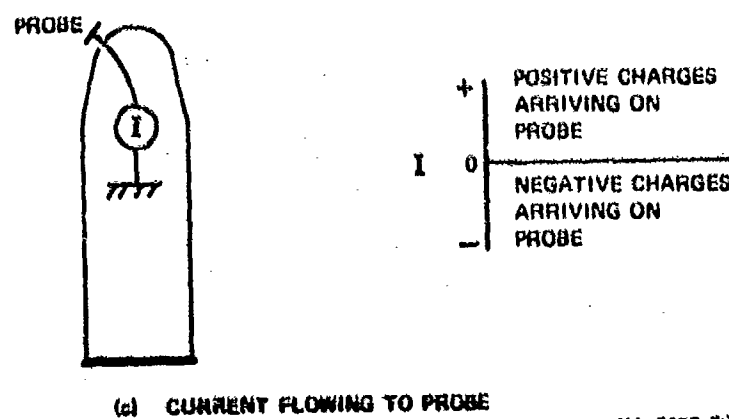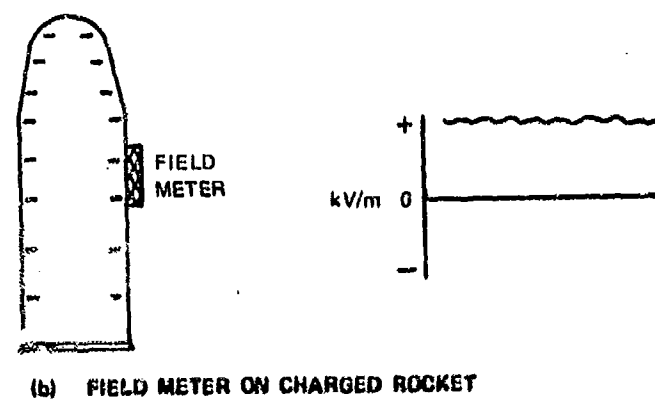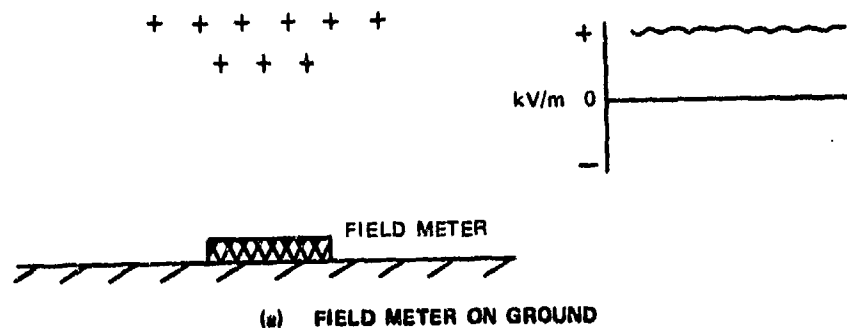
FIGURE A-1   SIGN CONVENTIONS FOR CURRENTS AND FIELDS

Appendix B

DETAILS OF GROUND FIELD-MEASUREMENT DATA

Appendix B

DETAILS OF GROUND FIELD-MEASUREMENT DATA

1.   Titan IIIC-20

The Titan IIIC ground instrumentation array was described in Section
II-B.

Data generated by the array during the launch of Titan IIIC-20 are
shown in Figure B-1. Good data were obtained at all sites except for
10-to-15-s intervals of signal saturation at the flame-trench site, D,
and the track by tower site, A. It is of interest to analyze the ground-
based data to understand electrification processes occurring during
launch and in particular to determine the degree to which the ground
fields are produced by the presence of the charged rocket in the launch
area or by charges in the launch-associated exhaust clouds.

Buildup of exhaust clouds up the umbilical tower, along the flame
trench, and at right angles to the flame trench during the C-20 launch
is illustrated in Figure B-2. During liftoff, the central exhaust
cloud along the umbilical tower varies in height from below the rocket
nose to near the top of the tower. The cloud extending eastward along
the flame trench is nearly as high. After the tops of the solid, strap-on
motors pass the top of the tower at SRM + 3.4 s, launch-associated
clouds diffuse from the central cloud in a southerly direction toward
field-meter sites A, B, and C (see Figure B-1), and also in the northerly
direction. At SRM + 6.1 s (0743:07.34 GMT), exhaust clouds extend
throughout the ground area viewed by the camera. Peak fields occur
after this time at all sites except for initial peaks at the flame-trench
site and on the umbilical tower.

75
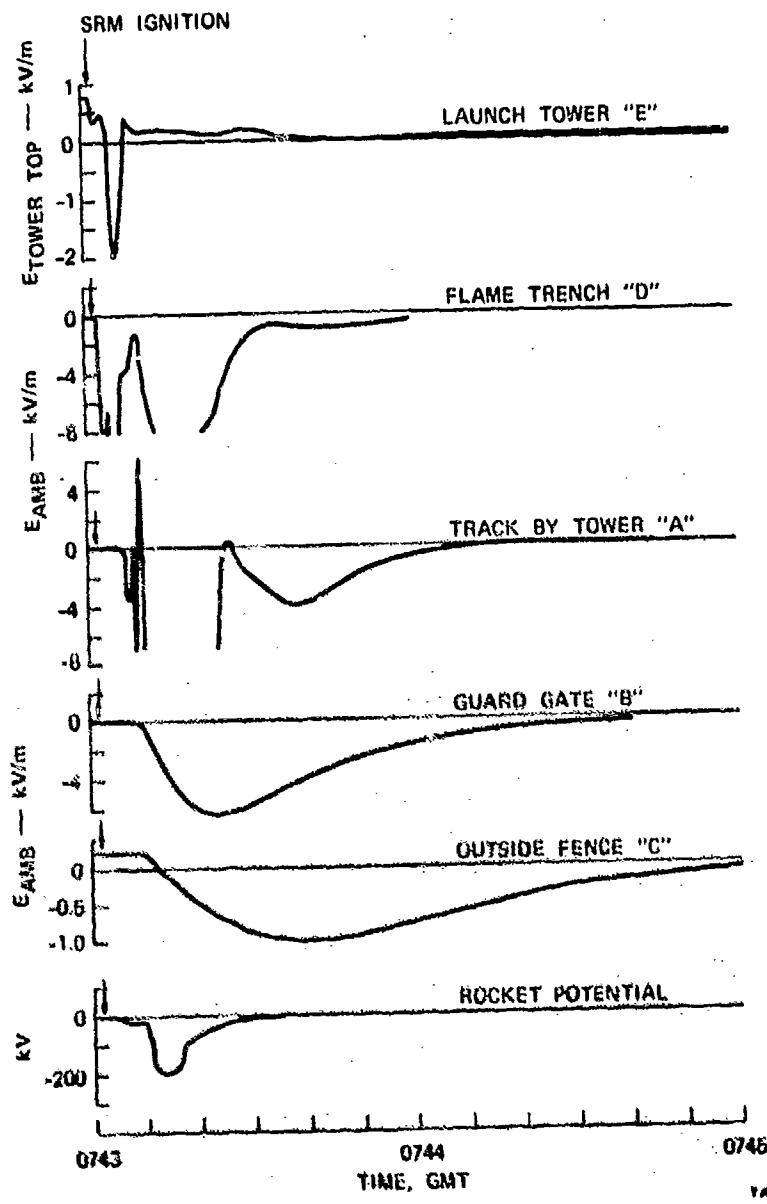
FIGURE B-1   GROUND INSTRUMENTATION DATA FROM TITAN IIIC-20 LAUNCH
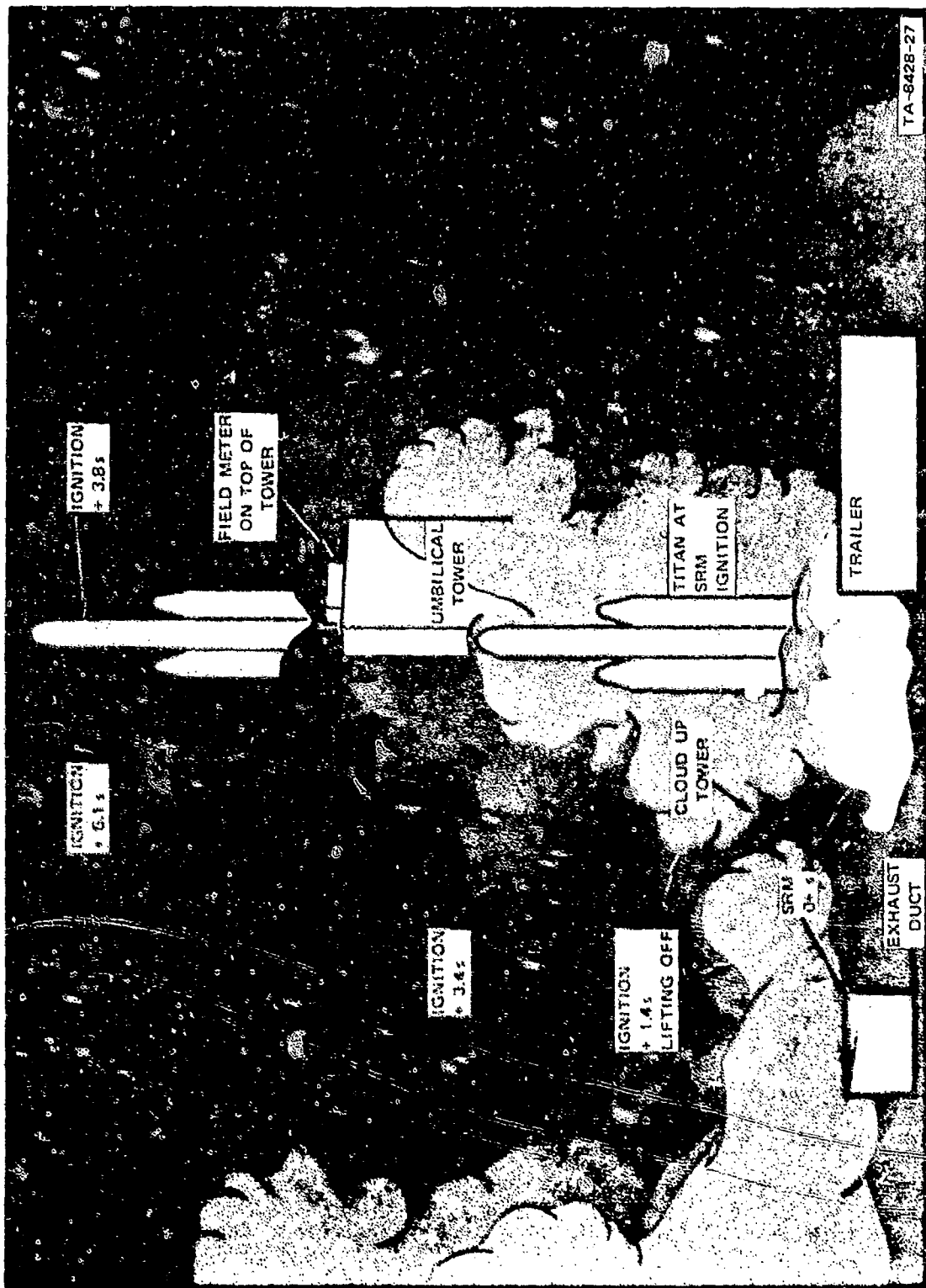
FIGURE B-2   TITAN IIIC-20 EXHAUST CLOUD BUILDUP DURING LAUNCH

The launch-tower field-meter data (to the time the motors reached the top of the tower) can be interpreted to indicate that a negatively charged body passed the top of the tower. This is in agreement with the onboard instrumentation, which indicated that the rocket acquired negative charge at liftoff. The peak field of -2 kV/m at 0743:06 GMT occurs when the rocket passes the top of the tower and the rocket motors emerge from the launch-associated cloud at the tower. Unfortunately, the central exhaust cloud, which is probably charged, extends to the field-meter height at this time and could also contribute to the measured electric field. It will be interesting, therefore, to compare rocket potential inferred from the launch-tower field with the potential inferred from the onboard-field-meter readings.

The relationship between vehicle potential V and electric field E at the launch-tower field-meter position was determined using the setup of Figure B-3(a). Here a model of the tower is placed on the floor of the laboratory, and provisions are made to charge a model of the Titan III, which can be positioned at various heights above ground along the trajectory followed during liftoff. Charge-transfer measurements of E at the scaled launch-tower field-meter location and at the onboard field-meter location are made as the rocket model is moved past the tower. The results of this measurement are shown in Figure B-3(b). Combining the data of Figure B-3(b) with the launch-tower field measurements of Figure B-1 yields the inferred rocket potential shown in Figure B-4. Also shown for comparison in Figure B-4 is the rocket potential measured by the onboard field meter (replotted from Figure 10). From an inspection of Figure B-4, one must conclude that the launch-tower field-meter record is representative of the rocket potential, but that it is modified by the presence of the launch clouds. In particular, the apparent peak in rocket potential at 0743:02.3 probably is caused by charge on the exhaust cloud that rises up along the launch tower during the early part

78

(b) MEASURED RESULTS

TA-8428-28

(a) TEST SETUP
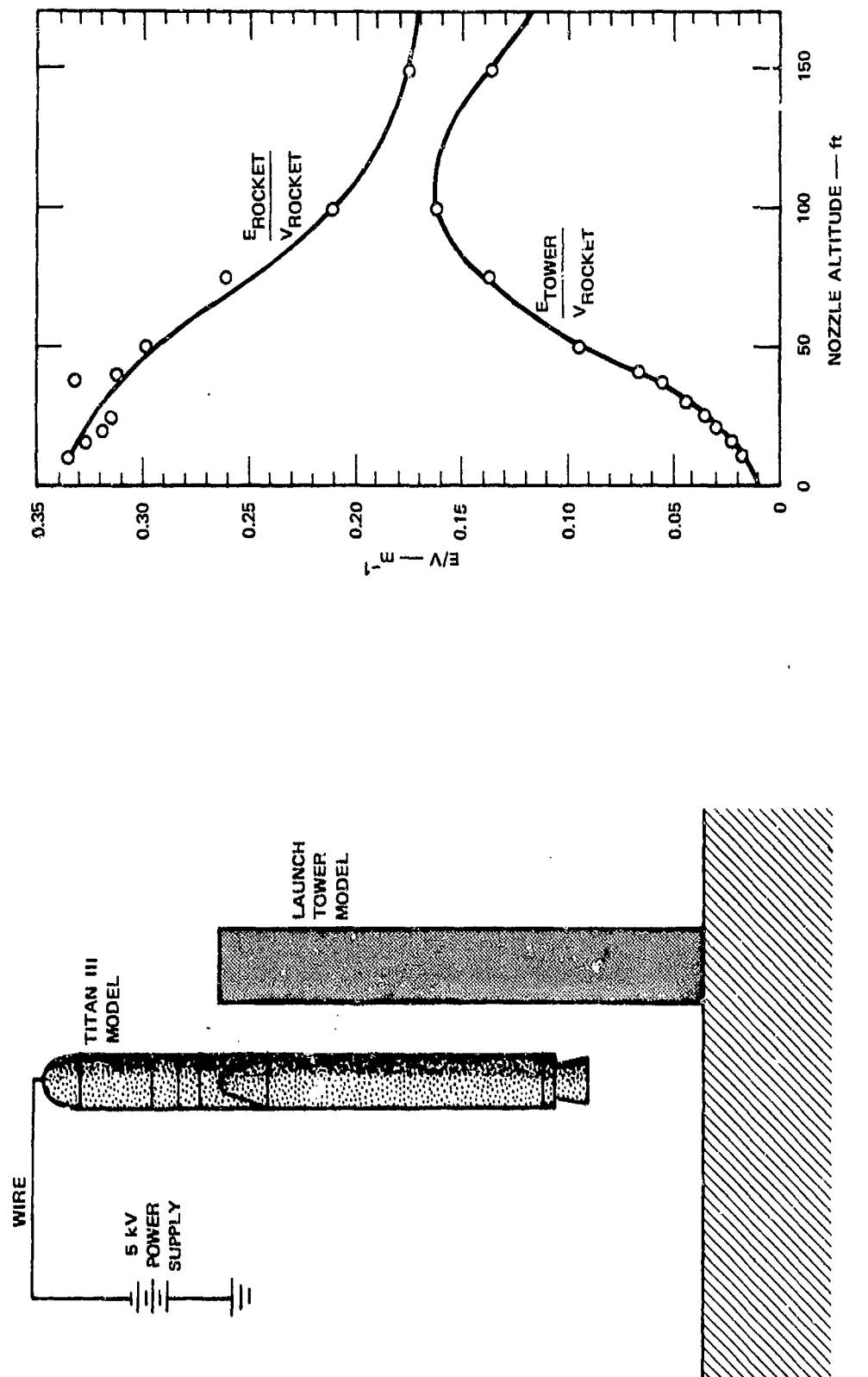
FIGURE B-3   MODEL MEASUREMENTS TO DETERMINE RELATIONSHIP BETWEEN ELECTRIC-FIELD INTENSITY
AND ROCKET POTENTIAL
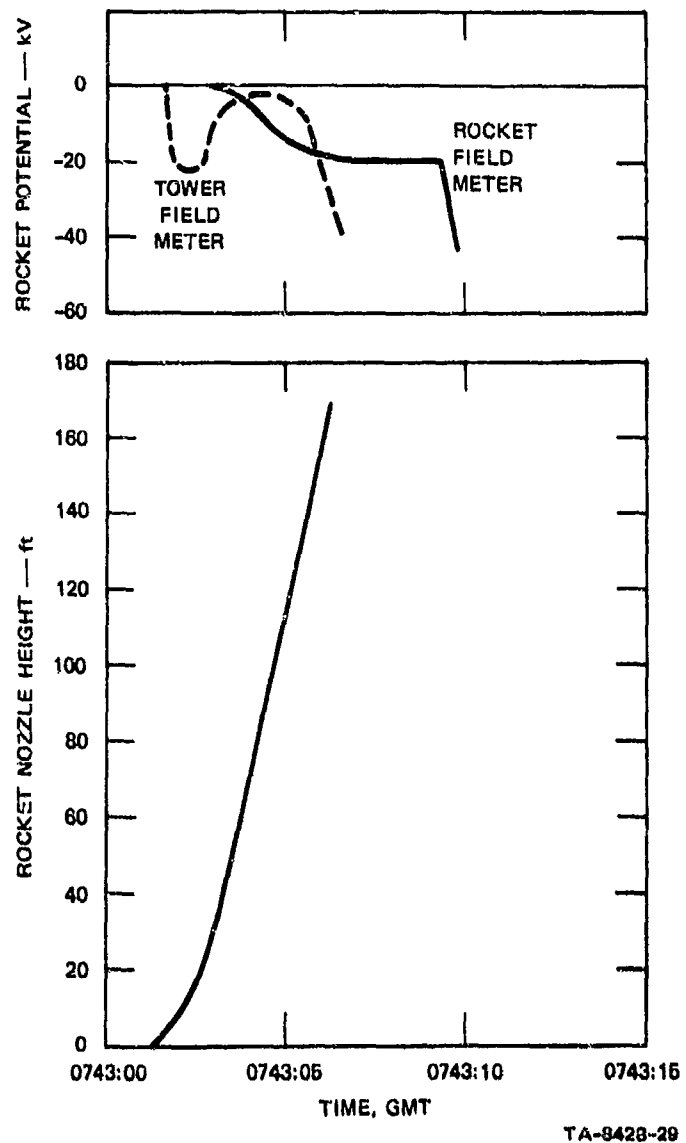
FIGURE B-4   TITAN IIIC-20 POTENTIAL INFERRED FROM LAUNCH-TOWER FIELD
MEASUREMENTS AND FROM ROCKET-BORNE FIELD METER

of the launch. Any field generated by such a cloud early in the launch is highly weighted in terms of equivalent rocket potential, since at this time E/V is low [E/V $\leq$ 0.02 m^{-1} for nozzle heights up to 20 ft--see Figure B-3(b)], so that a small field is interpreted as a large potential. Once the rocket nozzles reach an altitude of 50 ft or more, the tower field meter couples more strongly to charge on the rocket, and the tower field-meter data are more representative of the true rocket potential. Once the nozzles reach the top of the tower, the tower mill data become unreliable because the exhaust products envelop the top of the tower. In view of the above arguments, it appears that the tower-top measurement of rocket potential is most reliable in the range 50 to 170 ft, rocket nozzle height. From Figure B-4 we see that, in this range, the potential inferred from the tower data is in best agreement with the potential inferred from the onboard field meter. From these arguments we may also conclude that in the case of a rocket such as the Saturn, which does not produce clouds rising along the tower, a launch-tower field measurement should provide a good estimate of vehicle potential as the rocket is passing the tower.

The flame trench data of Figure B-1 indicate that negatively charged exhaust products reached the vicinity of the field meter immediately after SRM ignition. Some consideration should be given to the fact that although the rocket charged negatively, indicating that the exhaust gases leaving the rocket were positively charged, the flame-trench effluent is negatively charged. The most plausible explanation is that although the exhaust as it leaves the rocket may be slightly positively charged, it subsequently strikes the exhaust trench where it erodes the concrete surface causing electrification to occur. The exhaust also can pick up charge by interacting with water from the deluge in the exhaust trench. This interaction with material in the trench evidently

81

produces negative charging that completely overwhelms the initial positive charge in the rocket exhaust.

The time history of the records at the remaining ground field-meter locations argues that the fields in the vicinity of the launch pad are generated by charge on the exhaust clouds rather than by charge on the rocket. For example, the field at Site C does not reach its maximum until the rocket potential shown in the bottom of Figure B-1 for reference has reached zero. A more detailed examination of the electric-field behavior in relation to vehicle charge is also of interest. To estimate the fields a charged rocket would produce along the ground, one can consider the field E produced at the surface of a ground plane by a charged body located a distance h above the ground plane as given by

$$E = \frac{2Q}{4\pi\epsilon_0} \frac{h}{(h^2 + r^2)^{3/2}} \qquad (B\text{-}1)$$

where

Q = Charge on body

ϵ_0 = 8.85×10^{-12} F/m

r = Distance from launch point to measurement point.

For a body carrying constant charge, the field E is maximum when $\frac{\partial E}{\partial h} = 0$. Carrying out the differentiation gives E_{max} when $h = r/\sqrt{2}$. For this value of h, the maximum value of the field is

$$E_{max} = \frac{Q}{\pi\epsilon_0 r^2} \frac{1}{3\sqrt{3}} \qquad (B\text{-}2)$$

If fields along the ground are induced by the charged rocket and Eq. (B-1) is applied, peak fields should occur at approximately the following times:

Site	Time (GMT)
Track by tower (A)	0743:06
Guard gate (B)	0743:08
Outside fence (C)	0743:10
Flame trench (D)	0743:07

Initial peaks in the Site D (Flame trench) field between 0743:03 and 0743:06.5 and the Site A (Track by tower) field at 0743:08 could possibly be induced by the charged rocket. However, peak fields at the ground sites for times exceeding 0743:09.5 are not consistent with the physical picture. The source of initial peaks in the Site-D field and in the Site-A field is further complicated in that exhaust clouds that are probably charged exist in the flame trench and up the tower at liftoff.

Because launch-associated exhaust clouds, which are probably charged, extend past the top of the tower and throughout the immediate area after about 0743:05 (see Figure B-1 for SRM + 6.1 s), following this time the umbilical-tower field, and the fields along ground, are probably induced by charge distributions residing in these high-rising exhaust clouds. Although it would be intellectually satisfying to be able to account for all of the details of the variations in the various field-meter readings, such a calculation would be time-consuming and of marginal utility. It would be necessary to follow the development and motion of each of the clouds and to assign charge densities to the various regions. Physical arguments would have to be devised to account for variations in polarity and charge magnitude. The result would be an extremely detailed picture of the electrification of a highly specialized cloud system. Accordingly, such an analysis was not undertaken.

Disregarding the inconsistencies between the time history of the field records and the simple model of a highly charged rocket climbing

out of the launch area, it is interesting to estimate the charge the vehicle would have to carry to generate such fields. For example, at Site B (610 ft from the pad) a maximum field of 6.4 kV/m occurs roughly 20 s after SRM ignition. At this time the rocket altitude is roughly 3,000 ft. Rewriting Eq. (B-1) as

$$Q = 4\pi\epsilon_0 E \frac{(h^2 + r^2)^{3/2}}{h} \qquad \text{(B-3)}$$

on substituting numerical values we find $Q = 0.625$ coulomb. Since the vehicle capacitance C is 1000 pF, this value of charge implies a vehicle potential of $V = Q/C \leq 625 \times 10^6$ V. This potential is several orders of magnitude higher than the highest potential measured on the vehicle.

Ignoring time history even further, and arguing that the vehicle is at $h = r/\sqrt{2}$ when E_{max} occurs, so that Eq. (B-2) applies, it is interesting to calculate the implied vehicle potential. Solving Eq. (B-2) for Q we obtain

$$Q = 3\sqrt{3}\,\pi\epsilon_0 r^2 E_{max} . \qquad \text{(B-4)}$$

Substituting values applying to the Site B field meter we find $Q = 3.2 \times 10^{-2}$ coulomb. This charge implies a vehicle potential of 32×10^6 V. This potential also is several orders of magnitude higher than the highest potential measured on the vehicle. It appears, therefore, that there is no way in which the charged vehicle could have generated by itself the electric field variations measured in the vicinity of the pad during the launch of Titan IIIC-20.

2. Titan IIIC-21

The ground data from the Titan IIIC-21 launch are shown in Figure B-5. Good data were obtained at all sites except Site C (outside of
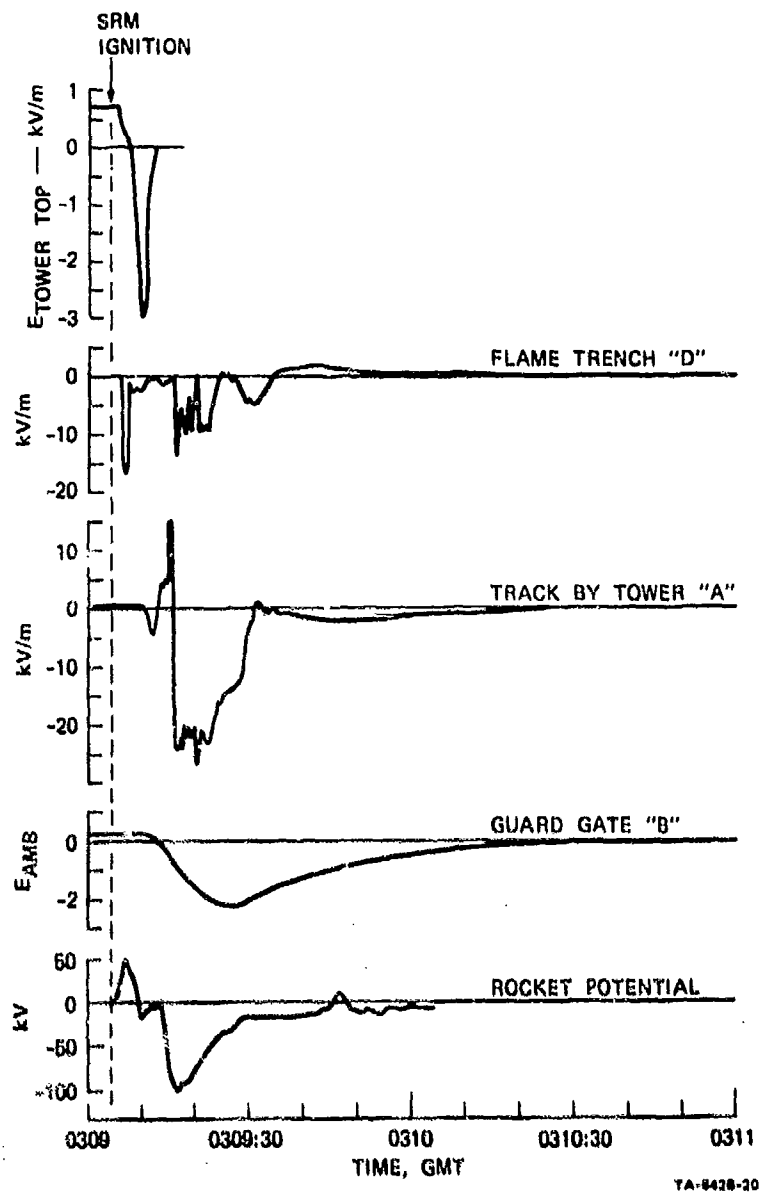
FIGURE 6-3   GROUND INSTRUMENTATION DATA FROM TITAN IIIC-21 LAUNCH

fence), where the strip-chart recorder malfunctioned. Charging is seen
to be similar to that obtained during the C-20 launch. Again the launch-
tower field-meter record up to 6 s after SRM ignition is consistent with
a negatively charged body moving by. The behavior of the rest of the
field meters indicates that again the exhaust clouds were negatively
charged. The fields associated with the launch of C-21 are roughly
half those observed on C-20. Again, the time history of the ground records

argues that they are not generated by charge on the rocket vehicle, since the field at Site B, for example, reaches its peak considerably after the rocket potential has peaked.

Figure B-6 shows the rocket potential as inferred from the launch tower compared with the rocket potential inferred from the onboard field meter. As was indicated in connection with the discussion of Figure 11 in the main text, there is no obvious physical explanation for the initial positive excursion in rocket potential indicated by the rocket-borne field-meter data. It is very likely, therefore, that the rocket potential in Figure B-6 inferred from the launch-tower field-meter record is more nearly correct (for the 50-to-170-ft altitude regime) and that the rocket potential remained less than -20 kV while the rocket passed the tower.

Launch-cloud buildup during the C-21 launch is shown in Figure B-7. Clouds are seen to envelop the launch tower 4 s after SRM ignition (about 0309:09). At SRM + 7 s, clouds in the area are comparable to the height of the umbilical tower. Comparing Figures B-2 and B-7, launch cloud structure during the C-21 launch is seen to be similar to cloud structure during the C-20 launch.

For the electric field along the ground to be induced by the C-21 rocket charged to a constant potential, peak fields would be observed at

Site	Time (GMT)
Track by tower (A)	0309:10
Guard gate (B)	0309:12
Flame trench (D)	0309:11

Since peak fields do not occur at these times one must assume that this simple model is incorrect, and that charges in the exhaust clouds are the source of fields as was argued for the C-20 launch.
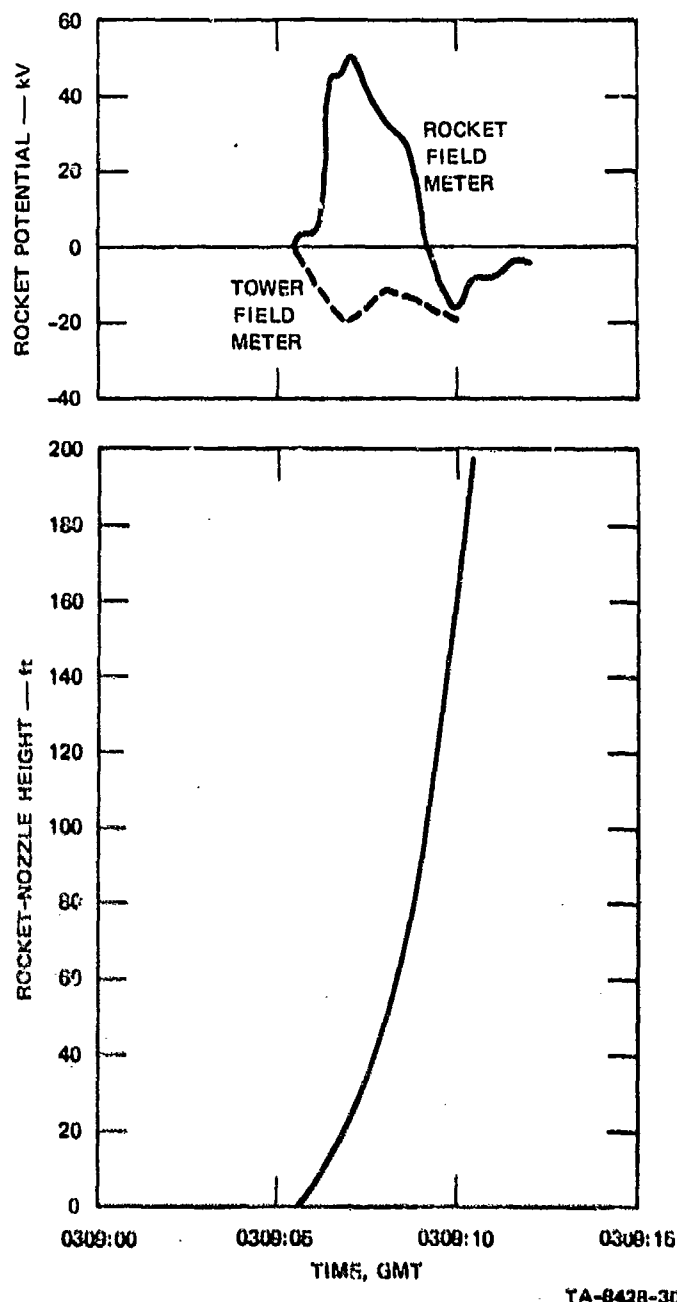
FIGURE B-6   TITAN IIIC-21 POTENTIAL INFERRED FROM LAUNCH-TOWER FIELD
MEASUREMENTS AND FROM ROCKET-BORNE FIELD METER

87
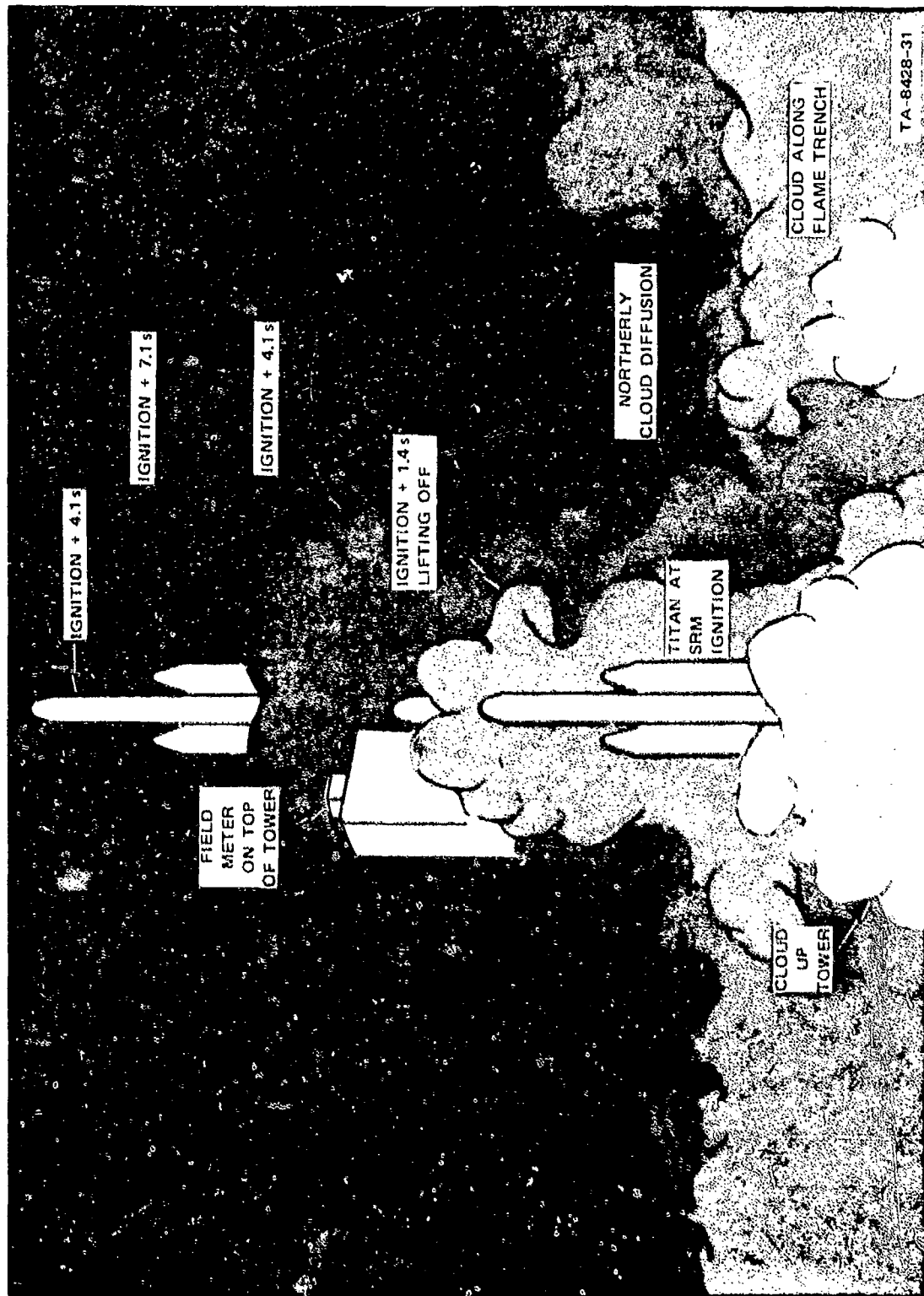
FIGURE B-7 TITAN IIIC-21 EXHAUST-CLOUD BUILDUP DURING LAUNCH

Comparison of ground fields for the two launches is easiest at the guard-gate site (B). Similar and smooth field variations were recorded for both launches. During the C-20 launch a peak field of -6 kV/m was obtained about 22 s after SRM ignition. During the C-21 launch, a peak field of -2 kV/m was obtained also at about 22 s after SRM ignition. Additionally, the 90% decay times of the two fields are about 70 s after SRM ignition.

Peak electric fields at Site A also occurred at approximately the same times after SRM ignition--e.g., 10 to 22 s for both the C-20 launch and the C-21 launch. Momentary reversals of charging occurred on both launches 26 s after SRM ignition. Erratic variations in field intensity occurred during the period of peak electric field during the C-21 launch. (This data period was saturated for the C-20 launch.) These erratic field variations indicate erratic charge structure in the clouds generated during the launch.

Peaks in the data at Site D (Flame trench) also occurred at about the same times after SRM ignition for both launches--e.g., between 2 and 6 s and between 12 and 20 s for the C-20 launch and at about 2 s and between 11 and 17 s for the C-21 launch. The erratic field behavior at the flame-trench site also reflects erratic charge structure in exhaust clouds, probably the cloud in the flame trench. Bipolar charging seen at 0309:34 for the C-21 launch was not measured for the C-20 launch.

3. Comparison with Apollo Data

For comparison, the results of SRI ground field measurements during the launches of Apollo 13 and 14 are reproduced from Ref. 9 in Figures B-8 and B-9. The Apollo ground field-meter arrangement was similar to that employed for the Titan experiments and is shown in Figure 9.
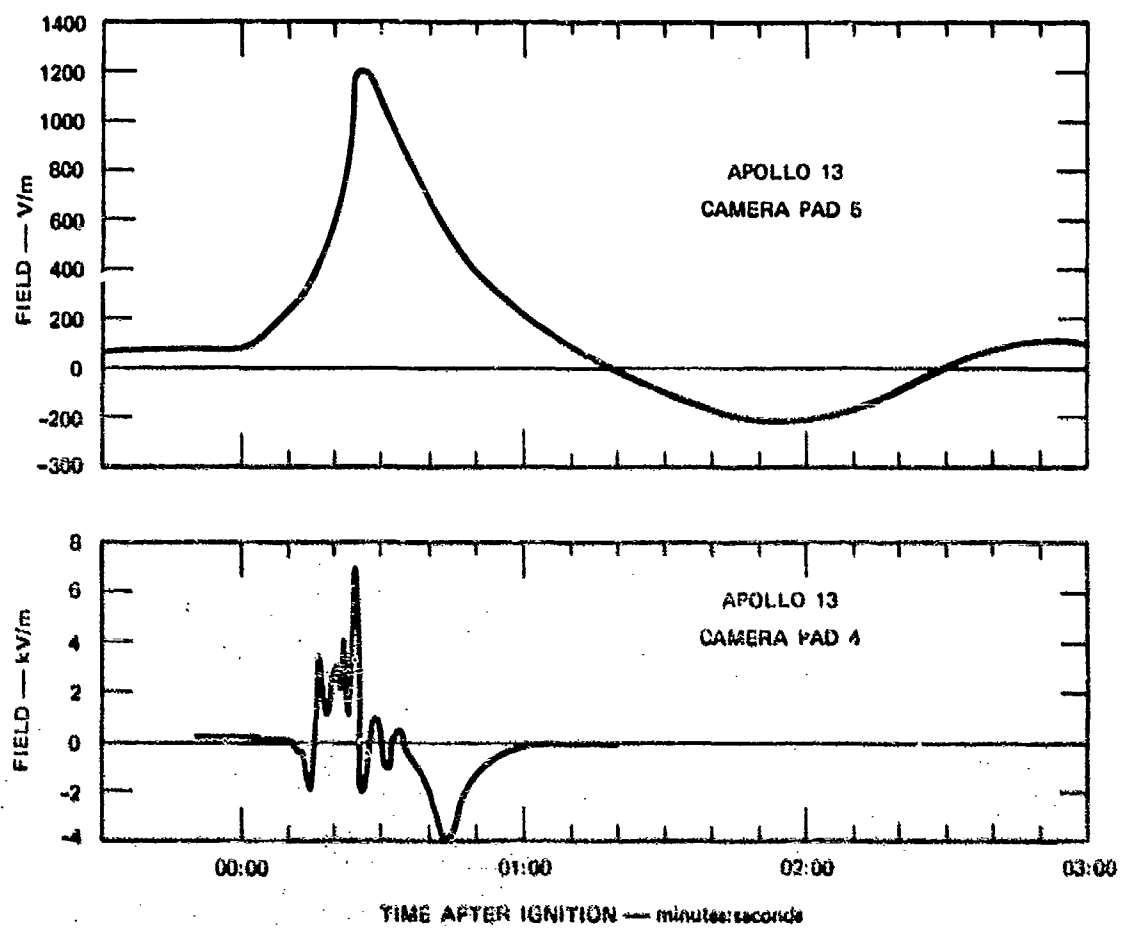
FIGURE B-8   GROUND-BASED FIELD-METER DATA FROM APOLLO 13 LAUNCH

Three exhaust clouds were observed during the Apollo 13 and 14 launches; one along the south flame trench, another along the north flame trench, and the third associated with the water spray along the umbilical tower. As with the Titan field data, the Apollo data after the Saturn leaves the tower area is attributed to launch-cloud charge distributions. A comparison of the Apollo and Titan data is useful because no in-flight rocket-potential-measuring instruments were carried on the Apollo vehicles, and because the Apollo (liquid-fueled) and Titan (solid-fueled) may exhibit different charging characteristics on the vehicles themselves as well as on the ground and on the umbilical towers.
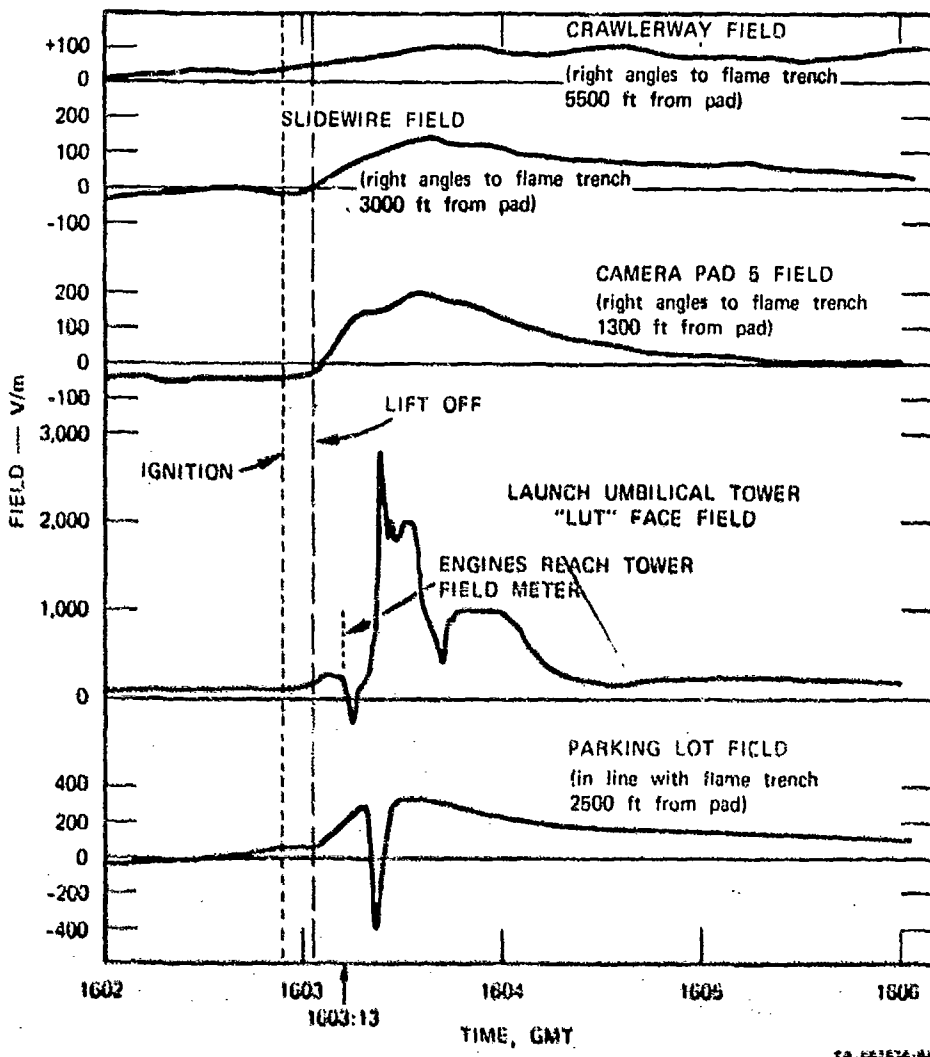
FIGURE B-9   SRI GROUND-BASED FIELD-METER DATA FROM APOLLO 14 LAUNCH

The electrostatic-field records for the Apollo 13 launch are shown in Figure B-8. (This launch occurred on a clear day.) The field at camera pad 5 (intended to not coupled strongly to the flame-trench effluent) smoothly rises to a peak of 1.2 kV/m, 25 s after ignition. The polarity reverses 80 s after ignition, then the field reaches a peak negative potential of 210 V/m 120 s after ignition. The field at camera pad 4 (intended to coupled strongly to the south flame trench effluent) is seen to be erratic with a peak positive value of 7 kV/m, 24 s after ignition. Both fields before ignition are comparable to the earth's

static electric field, normally +100 to +300 V/m on a fair day. Charging activity is seen to be affecting the camera pad 5 field data, 2 minutes after ignition.

Electrostatic-field data for the Apollo 14 launch are shown in Figure B-9 (the launch occurred on a cloudy day). Fairly smooth positive field changes occur after liftoff at the crawlerway, slidewire, and camera pad 5 sites. Positive field changes indicate that predominantly positive exhaust clouds were generated by the launch, whereas, negatively charged clouds were observed in the Titan experiments. There is evidence in the Apollo ground data (discussed in Ref. 9) for the existence of different charge polarities.

The launch-umbilical-tower (LUT) field meter indicates a positive field change accompanying liftoff, indicating that the engines charged the Apollo 14 vehicle positively. (It will be recalled that both Titans charged negatively.) At the time the engines reach the field meter, the measured field magnitude indicates that the rocket potential is less than 6000 V. This result is in good agreement with the Titan experiments in which it was argued that the rocket potential remained relatively low until the rocket plume broke contact with the ground. As stated earlier, Uman's work[15] indicates that the Apollo rocket plume is a good conductor to a length of 625 ft.

For comparison of Apollo 13 and 14 data, the field-meter records obtained at camera pad 5 on the two launches are shown in Figure B-10. The peak field on Apollo 14 is one-sixth that obtained during the Apollo 13 launch. The Apollo 13 field is bipolar while the Apollo 14 field is positive. Data from the New Mexico Institute of Mining and Technology (NMI) field-meter installation at the air intake near camera pad 5 is also shown in Figure B-10 for the Apollo 14 launch. The NMI intake and the SRI campera pad 5 records are in reasonable agreement.
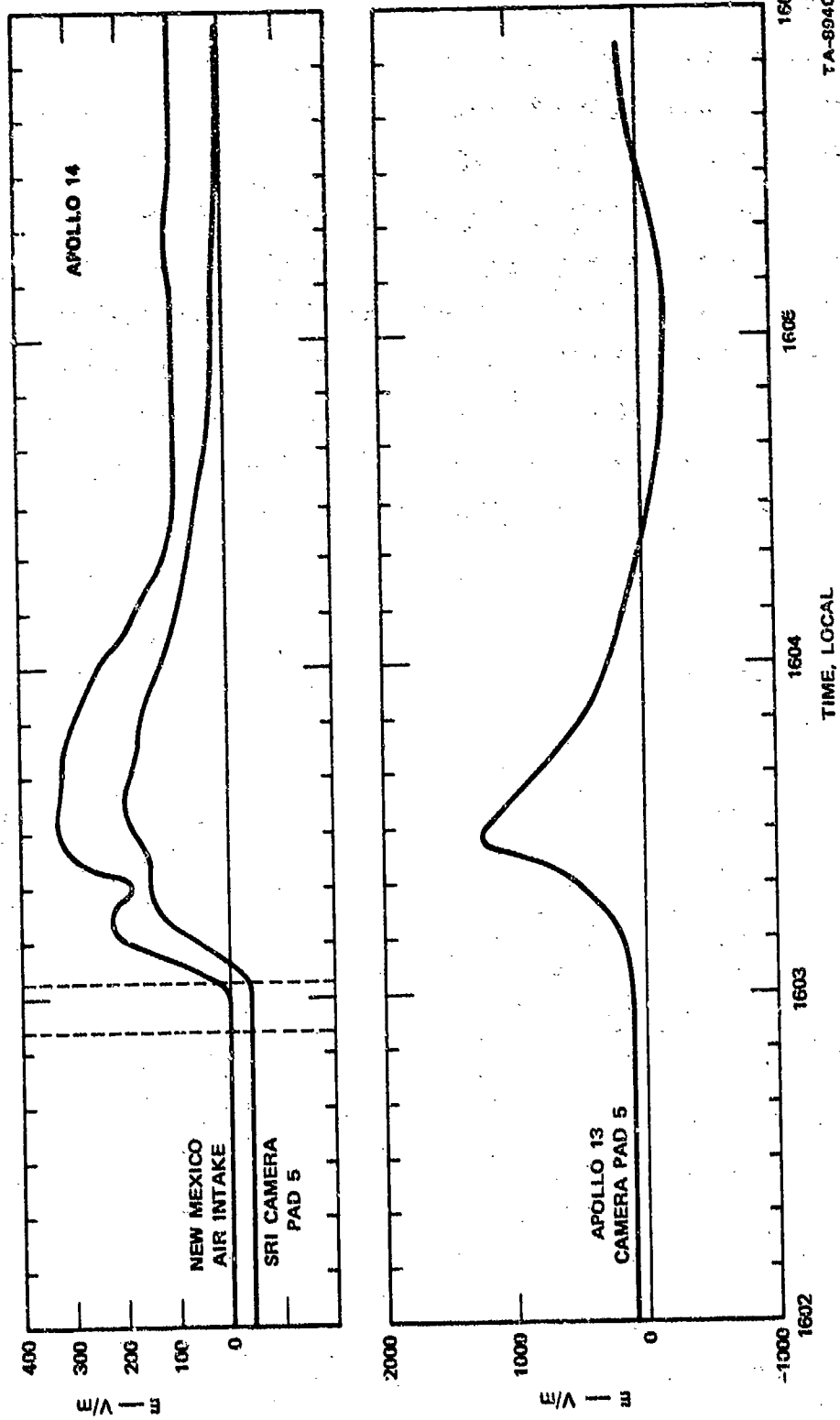
FIGURE B-10 COMPARISON OF APOLLO 13 AND 14 FIELD-METER DATA

93

In comparing Titan and Apollo data, the liquid-fueled Saturn booster used in the Apollo launches is seen to generate essentially positive charging and positive electric fields, while the Titan booster generates essentially negative charging and negative electric fields. Peak field changes for Titan and Apollo launches are plotted in Figure B-11 as a function of distance from the launch pad. Also shown in the figure are lines showing $1/r^3$ and $1/r$ variations of field. It is difficult to generalize from these data beyond observing that, far from the pad, the fields fall off with distance more slowly than they do near the pad. Also, it is apparent that the differences in the data obtained from successive launches of the same vehicle are as great as the differences among data obtained from vehicles of different types.
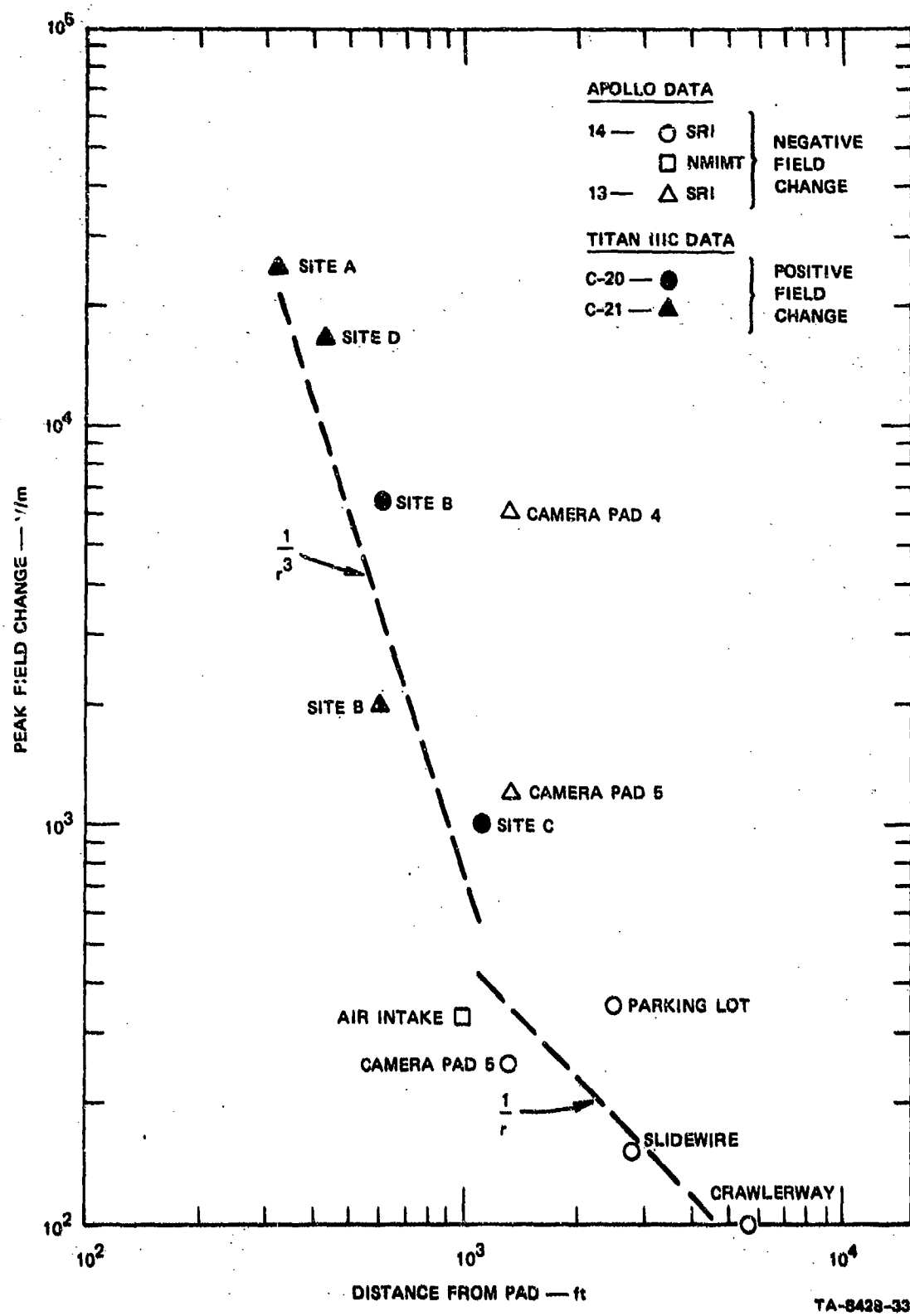
FIGURE B-11   COMPARISON OF MAXIMUM FIELD CHANGES FOR APOLLO AND TITAN
LAUNCHES

95

Appendix C

LANGMUIR-ION-PROBE ANALYSIS

Appendix C

LANGMUIR-ION-PROBE ANALYSIS

An order-of-magnitude estimate of ion density can be obtained by
observing that during C-20 and C-21 flights the principal flow-field
velocity is parallel to the probe surfaces. The flow-field velocity into
ion probe No. 1 and away from probe No. 2 at synchronous-orbit altitude
is a few hundred feet per second. This velocity is much less than the
flow-field ion velocities of about 25,000 ft/s. Since the body size is
less than the mean free path for all altitudes following the brief
period when the probe is first exposed, the analysis can ignore
collisions.

The geometry of the analysis is shown in Figure C-1.

TA-8428-34
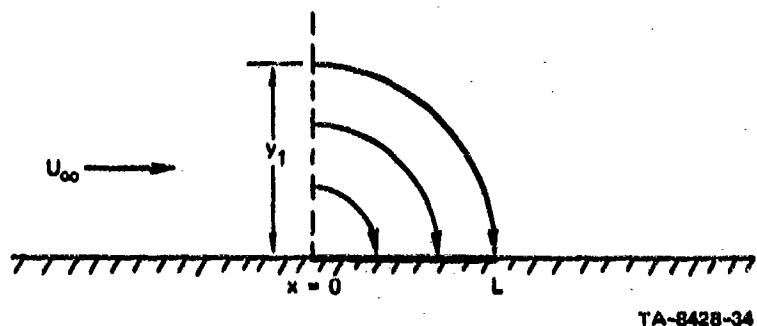
FIGURE C-1   ION-PROBE GEOMETRY

Particles are assumed to enter the field of the probe abruptly at
$x = 0$. They are pulled into the probe by the normal field. All particles
are collected that enter below a dimension y_1 such that the particles
that enter at y_1 reach the probe surface at L, the probe length. At
distance greater than y_1, particles miss the probe and are not collected.

99

The probe current is thus

$$I = \int_0^{y_1} eNU \ dy \ dz \qquad\qquad (C-1)$$

where

N = Ion density

U = Parallel velocity

z = Transverse dimension.

We assume that N and U are constant with y and z are are equal to their free-stream values so that we can write

$$I = eN_\infty U_\infty \ y_1 z_1 \quad . \qquad\qquad (C-2)$$

To estimate y_1 we assume that the Debye length and probe potential are such that the potential is unaffected by space charge out to y_1. This is consistent with the inferred values of charge density. An ion falling through a potential drop of V volts will have a terminal velocity v_a of about $1.4 \times 10^4 \ \sqrt{V}$ m/s for H^+ ions. y_1 can be found by taking this velocity and multiplying it by the time it takes a particle to flow across the probe due to the flow-field velocity. This time is

$$\tau_T = \frac{L}{U_\infty} \qquad\qquad (C-3)$$

so that

$$y_1 = \frac{L v_a}{U_\infty} \qquad\qquad (C-4)$$

The potential drop from y_1 to the probe surface may not be the full probe potential, but for purposes of estimation we shall take it as V. Therefore,

100

$$I = eN_\infty L \, v_a \, z_1 \quad . \tag{C-5}$$

Note that the free-stream velocity cancels out. Since Lz_1 = probe area (A_p), we may write

$$I = eN_\infty \, v_a \, A_p \tag{C-6}$$

where

N_∞ = Free-stream charge density

e = electron charge

$v_a = 1.4 \times 10^4 \, v_p^{\frac{1}{2}}$ = Ion velocity for extremum particles entering at y_1

A_p = Probe area.

For a probe area of 137 cm^2 the charged-particle density is related to ion current as

$$N \approx 10^{10} \, I \text{ el/cm}^3 \qquad (I \text{ in amperes}) \tag{C-7}$$

assuming that the measurement is made at an altitude when H^+ is the dominant ion. Johnson[21] indicates the altitude regimes in which ion composition changes. This information has been used to calculate v_a for the dominant species and to modify Eq. (C-7) appropriately. The results of these calculations are shown in Table C-1, which shows the electron-density equation appropriate for each altitude regime.

Table C-1

ELECTRON DENSITY EXPRESSIONS FOR VARIOUS ALTITUDES

Altitude (ft)	Altitude (nmi)	Ion Type	Mass	N_e (cm^{-3})
$> 6.2 \times 10^6$	> 1020	H^+	1	$10^{10} I^*$
3×10^6 to 6.2×10^6	493 to 1020	He^+	4	$2 \times 10^{10} I$
$< 3 \times 10^6$	< 493	0^+	16	$4 \times 10^{10} I$

$I^* = $ probe current

Appendix D

DETAILS OF FLIGHT DATA IN UPPER IONOSPHERE

Appendix D

DETAILS OF FLIGHT DATA IN UPPER IONOSPHERE

1. General

During the upper-ionospheric portion of the Titan IIIC flights, data
were obtained from the field meter (electric field and ion current density)
and from the two ion probes. The readings of these instruments were
strongly affected by the operation of the attitude-control-system (ACS)
rockets. The locations of the static-electrification instrumentation
sensors and the ACS rockets on the rocket transtage are shown in Figure
D-1. It is evident from the figure that there is a great difference in
the positioning of the various rocket motors with respect to a particular
sensor. Also, the exhausts of some of the rockets are directed along the
vehicle roll axis, whereas the exhausts of others are directed along the
circumference of the vehicle. Accordingly, it is reasonable to expect
that there will be a great variation in the degree to which different
ACS motors affect a particular sensor.

In the upper ionosphere, the orientation of the vehicle with respect
to the sun is of great importance in determining the sensor signal. For
example, when a sensor surface is illuminated by the sun, photoelectric
current is emitted from the sensor. Such current can be misinterpreted
as an incoming positive ion current. To assist in the interpretation of
the flight results, sun-orientation data were made available to SRI for
discrete times corresponding to the occurrence of specific events on
the rocket during ionospheric flight. The orientation is given in terms
of a cone angle and a clock angle. The cone angle is the angle the
insolation vector (the vector from the vehicle to the sun) makes with the

105
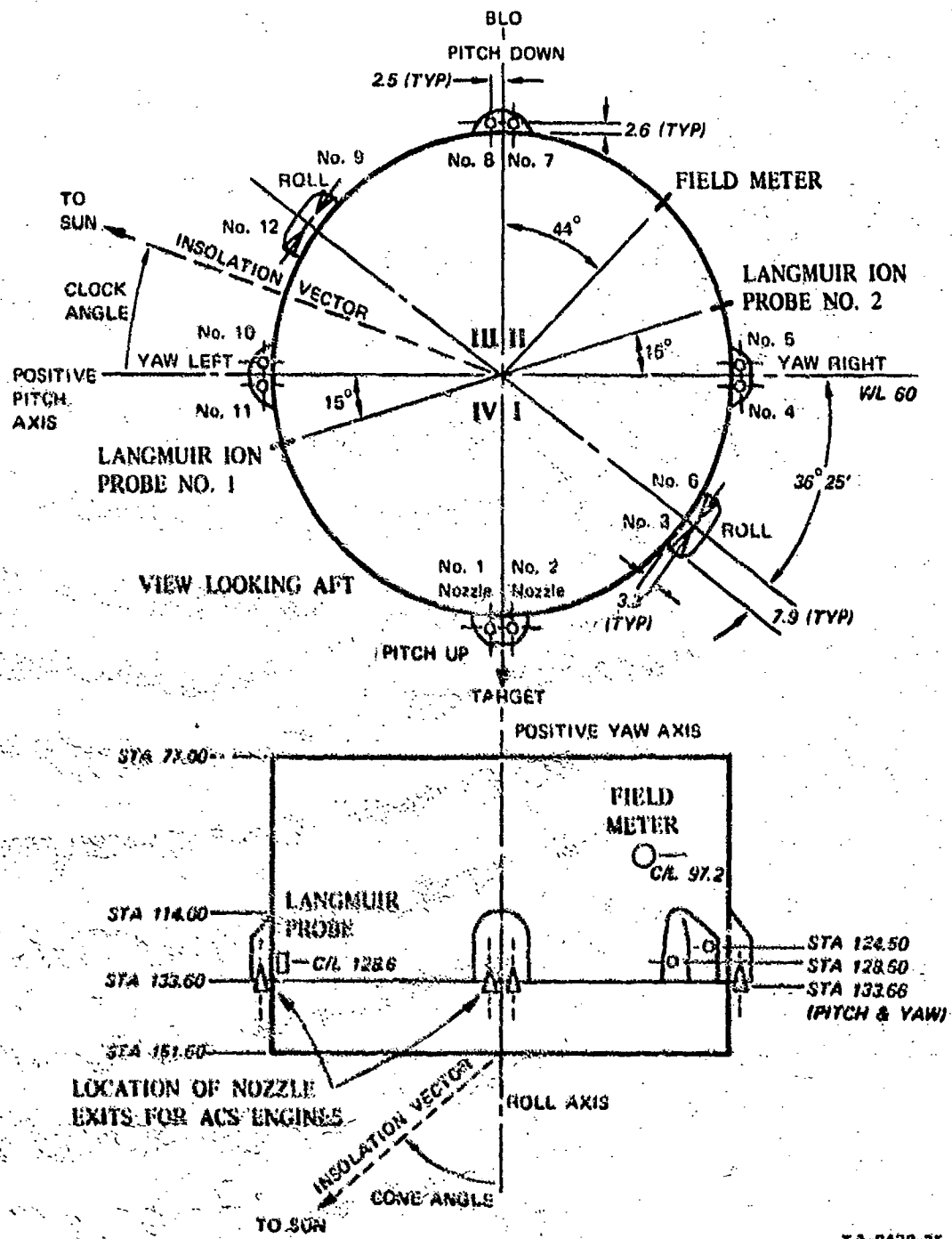
FIGURE D-1 PLACEMENT OF SENSORS AND ALTITUDE-CONTROL ROCKETS ON
TITAN IIIC TRANSTAGE

TA-8428-35

vehicle negative (aft) roll axis as shown at the bottom of Figure D-1. The clock angle is the roll angle between the projection of the insolation vector in the roll plane and the positive pitch axis. Positive is measured clockwise from the positive pitch axis looking aft (see Figure D-1).

Following the above convention, probe No. 1 is within the hemisphere illuminated by the sun for clock angles between -105° and 75°. Ion probe No. 2 is within the sun-illuminated hemisphere for clock angles from 75° to 255°. However when the insolation vector approaches normal incidence to the roll axis (cone angles about 75° to 105°), ion probe No. 1 will be shaded by the yaw-left ACS jets 10 and 11 for clock angles between about 55° and 75°, and ion probe No. 2 will be shadded by the yaw-right ACS jets 4 and 5 for clock angles between 235° and 255°. The field meter will be illuminated by the sun for all clock angles in the hemisphere between 44° and 224°.

In reviewing and interpreting the field-meter data from the upper-ionosphere portion of the flight, it is important to recall that the field-meter design was dictated largely by the requirement that the field-meter function during the liftoff phase of the flight. To minimize supersonic airflow loading of the field-meter vanes, the entire vane assembly was recessed below the surface of the skin. This recessed design means that the magnitude of the electric field existing on the sensor vane is only a small fraction of the ambient field at the vehicle skin (of the order of 1/10 the skin field). For normal operation of the field meter in an un-ionized medium, the actual value of the field at the sensor vane is immaterial (because of fringing effects, the field is not constant over the vane). This is so, because the field meter is calibrated by generating a known field intensity over the vehicle skin and measuring the field-meter output. When the field meter is operated in a plasma, however, the plasma sheath (the region of nonzero

electric field) conforms generally to the shape of the conductor about which it exists. Thus, the sheath penetrates into the recessed portion of the field meter, with the result that, particularly for a thin sheath, the magnitude of the field on the sensor vane is more nearly equal to the magnitude of the field over the skin. Thus, if one uses the normal sea-level field calibration to interpret plasma-sheath fields, the inferred field will be considerably higher than the actual sheath field. The sheath thickness and the degree to which the sheath penetrates into the field-meter recess depends on the plasma characteristics, and must be determined experimentally for a geometry as complex as that of the field-meter vane structure.

It was not possible to carry out plasma simulations on the present program, so that the degree to which inferred fields differ from the true sheath field is not known. It is planned, however, that, as part of the satellite experiment discussed in Appendix E, the satellite field-meter will be operated and calibrated in a laboratory plasma of known characteristics.

2. Titan IIIC-20 Data

a. 80 to 150 nmi Altitude

As was indicated in Section III-A, telemetered flight data were received in real time during six telemetry windows, each roughly 10 minutes long, occurring at critical times during the flight. Data from such a window when the vehicle is in the altitude regime 80 to 150 nmi are shown in Figure D-2. It is evident from the activity log in the figure that considerable engine activity occurred during most of this window, so that the electron density in the vicinity of the vehicle may be expected to be perturbed by the presence of the exhaust products. It is interesting, however, to compare the measured electron densities at the beginning of the window (before appreciable rocket-motor activity
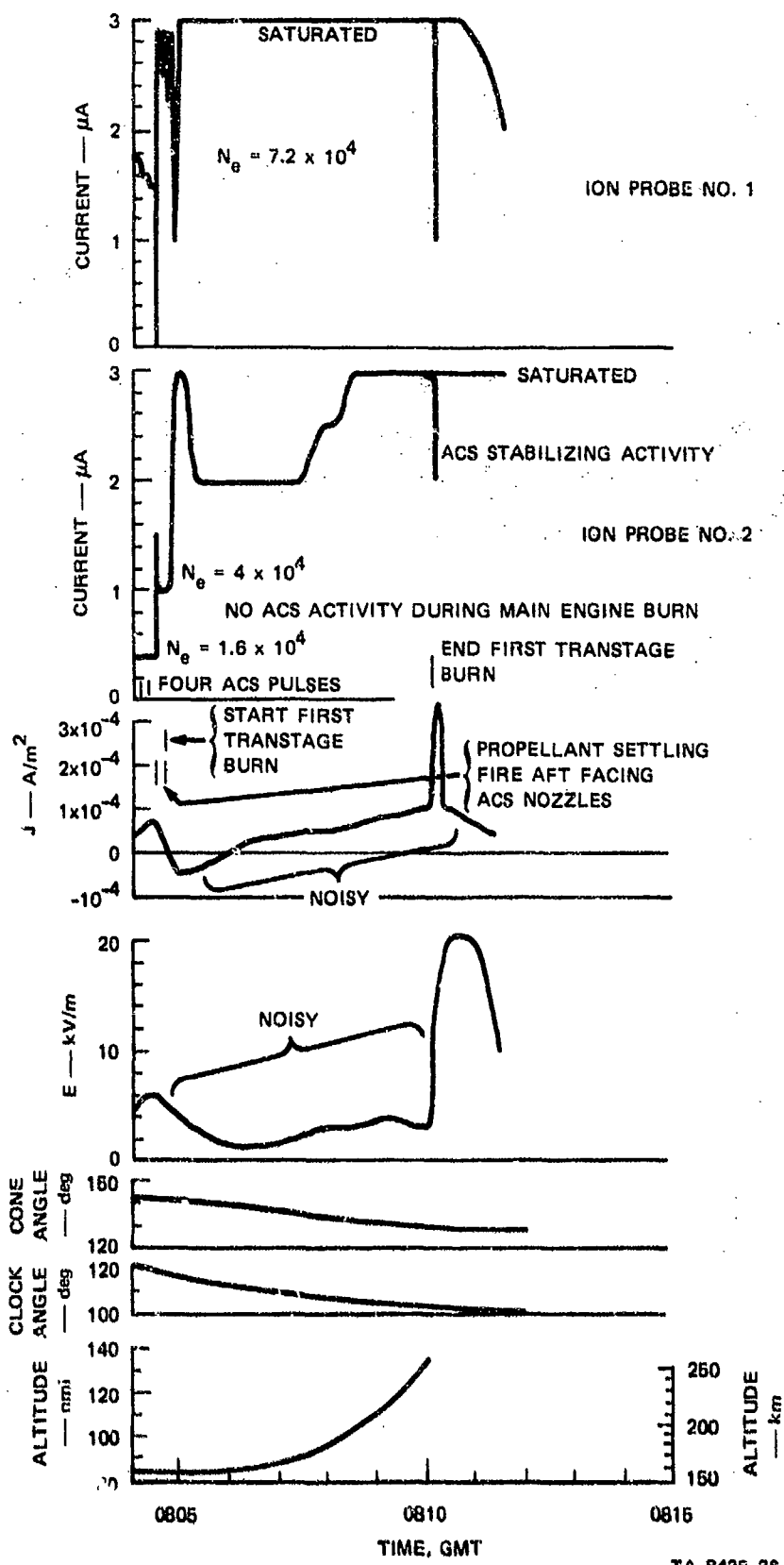
FIGURE D-2   TITAN IIIC-20 DATA FROM 80 TO 150 nmi ALTITUDE

occurred) with nominal values of electron density at this altitude. For example, at 0804, the No. 2 ion-probe current is 4×10^{-7} A. From Appendix C, for this altitude we find that Eq. (5) still applies, which means that the electron density is 1.6×10^4 el/cm^3. At this same time, the No. 1 ion probe indicates an electron density of 7.2×10^4. From Figure 17, we find that the nominal electron density at an altitude of 80 nmi ranges from 10^3 for night conditions to 3×10^4 for daylight conditions. Thus the electron density measured on the Titan IIIC is in reasonable agreement with nominal values.

With these verifications of the functioning of the instrumentation out of the way, it is interesting to return to the data of Figure D-2. Operation of the ACS rockets and burning of the transtage engine both have a pronounced effect on the ion-probe current. The ionized engine exhaust increases the electron and ion density in the vicinity of the vehicle, with the result that the current in both probe channels reaches saturation by the end of the burn. The reason for the difference in the detailed behavior of probes 1 and 2 during the transtage burn is not clear. The field meter is also affected by the rocket-motor activity during this telemetry window. It is interesting to note in passing that terminating the transtage burn produced a greater effect on the field meter than did the actual burn. Although these results are interesting, it was not felt that any effort to make an analysis of the detailed interrelationships during periods of engine operation would be worthwhile.

b. 310 to 450 nmi Altitude

Data from the 310-to-450-nmi flight regime are shown in Figure D-3. A striking feature of this record is the constant, 0.5 μA, ion probe No. 2 current. Since this probe is in the sun-illuminated hemisphere throughout the period of this record, it is interesting to investigate whether the measured current can be ascribed to photoemission from the
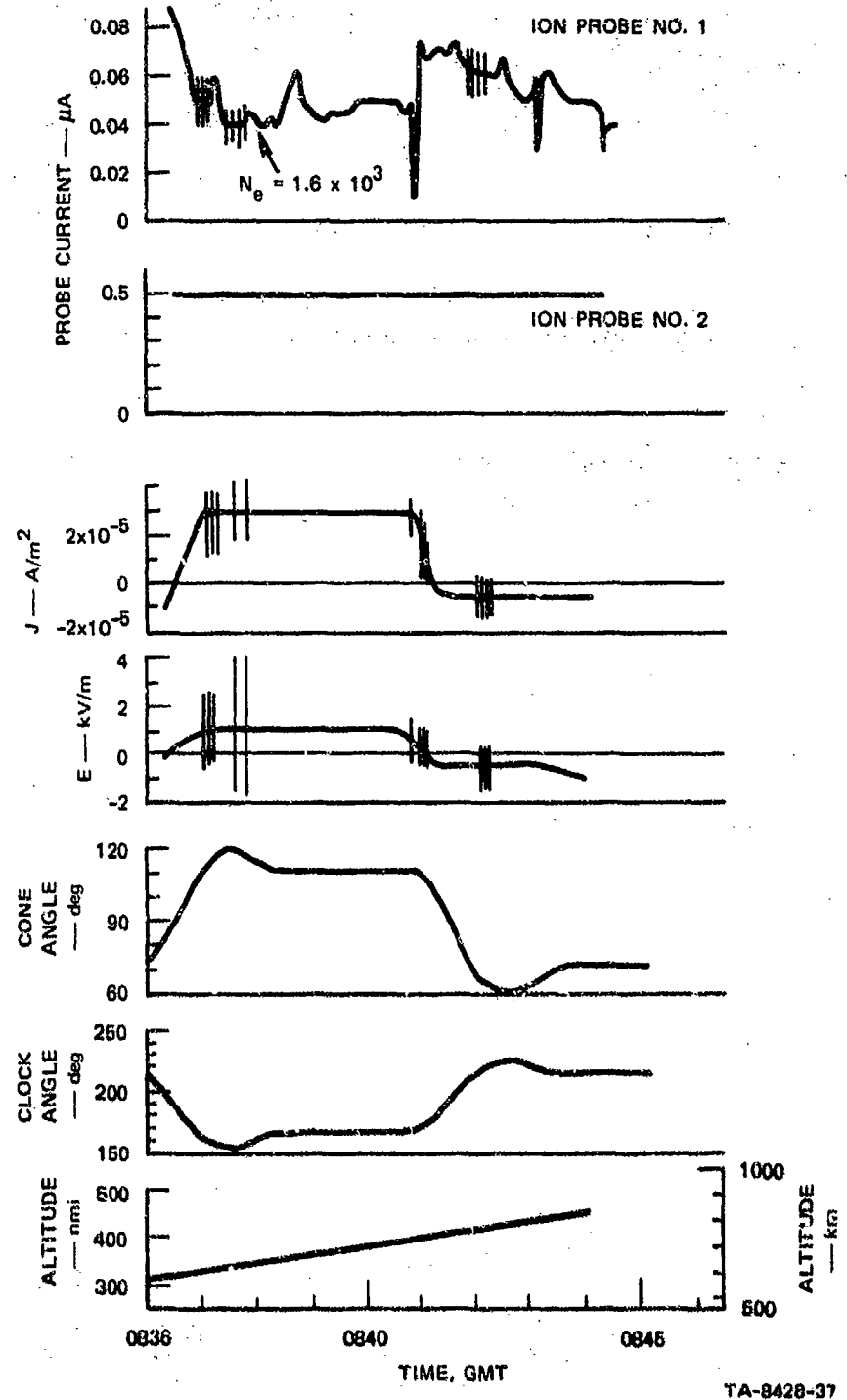
FIGURE D-3   TITAN IIIC-20 DATA FROM 310 TO 460 nmi ALTITUDE

TA-8428-37

111

probe element. From Ref. 22 we find, for stainless steel, that the integrated photoelectron flux under solar irradiation is 2.4×10^{-9} A/cm^2. Since the area of the Langmuir-probe electrode was 137 cm^2, the probe current one would predict on the basis of photoelectric emission is $137 (2.4 \times 10^{-9}) = 0.33$ μA. Thus, although the measured probe current is somewhat higher than the predicted photoelectric current, the agreement is sufficiently good that it is reasonable to conclude that the ion probe No. 2 current resulted from photoelectric emission.

The ion-current-density "J-field" channel field-meter data can also be interpreted as being indicative of photoelectric current emission from the field-meter vanes. Prior to the beginning of the record, the clock angle of the insolation vector is greater than 224° so that the field meter is in the hemisphere shaded from the sun. As the clock angle decreases below 224°, the field meter becomes progressively more exposed to the sun, and the field-meter current-density channel indicates progressively increasing positive charge arriving on the stator vanes (or negative charge leaving). The current density increases to a maximum value of 3×10^{-5} A/m^2 = 3×10^{-9} A/cm^2 at time 0837. From Ref. 22 we find that for gold (the field-meter vanes were gold-plated) the integrated photoelectron flux for solar irradiation is 2.9×10^{-9} A/cm^2. Since the measured current density is in agreement with the predicted photoelectron flux, it appears that the J-field reading from 0837 to 0841 GMT can be attributed to photoelectric emission from the field-meter stator vanes. At 0841 the vehicle is maneuvered to shield the field meter from the sun and the photoelectric current decreases.

Next, it is interesting to compare the electron density inferred from the ion probe No. 3 current with other electron-density measurements at this altitude. The probe current varies from a maximum of 0.09 μA at the beginning of the window to a minimum of 0.04 μA during the period 0837 to 0838 GMT. From Appendix C, we find that Eq. (5) for electron

112

density is valid at this altitude, which means that the electron density varies from 1.6×10^3 to 3.6×10^3 el/cm^3. This range of densities compares well with the data of Ref. 23 where electron densities at this altitude range from 1 to 5×10^3 el/cm^3 depending on the particular orbit chosen for consideration.

The electric field during the telemetry window of Figure D-3 varies both in magnitude and polarity. At the beginning of the record at 0836:20 the field is zero, indicating zero potential on the vehicle. By 0837 the field has increased to 1 kV/m, with the vehicle negative. At 0841 the field changes sign following vehicle reorientation. Since the E-field variation is similar to the J-field variation, it is tempting to attribute the E-field readings to imperfect isolation between the E- and J-field channels. Later on in the flight, however, the two channels of the field meter do not change in unison, so that this crosstalk explanation is not valid. Accordingly, it must be assumed that the indications of true electric field at the surface of the vehicle must be accepted as real.

Returning again to the data in Figure D-3, it is evident that there are numerous transient changes in ion probe No. 1 current coincident with transient changes in field-meter indications (both E- and J-field). These transients are undoubtedly associated with ACS rocket activity connected with vehicle maneuvering to achieve proper orientation during the telemetry window. Unfortunately, no record of ACS chamber pressure was made available for the Titan IIIC-20 flight, so it is not possible to identify individual transients with individual rocket firings.

c. 1350 to 1420 nmi Altitude

The data in Figure D-4 are from the 1350-to-1420 nmi altitude regime. Starting at 1020 in this record, the ion probe No. 2 current remains virtually constant and sufficiently high in magnitude that it is
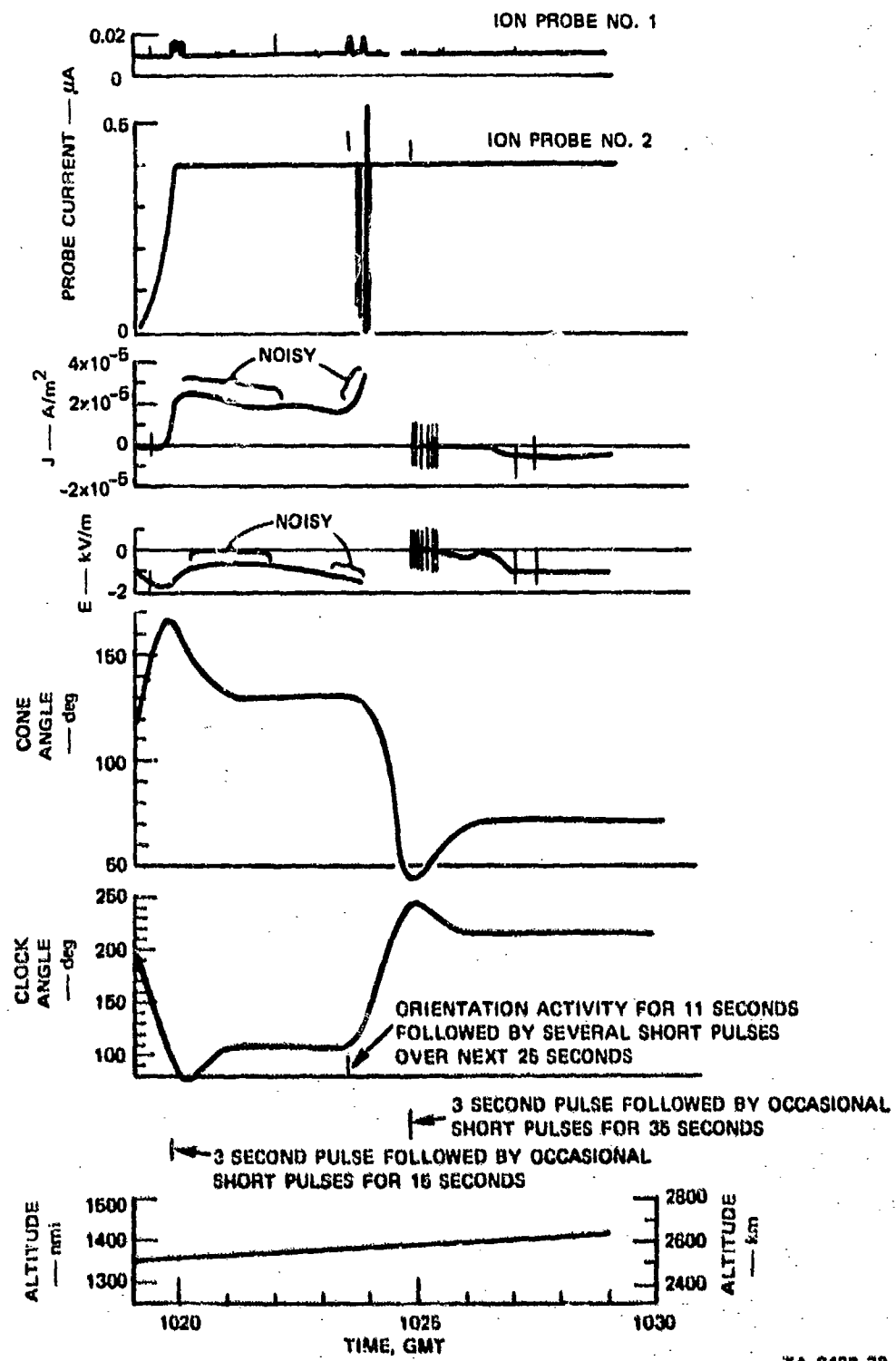
FIGURE 1-4   TITAN IIIC-20 DATA FROM 1350 TO 1420 nmi ALTITUDE

114

not affected by the changes in ambient ionization caused by ACS motor activity. The value of the current, 0.4 µA, is in good agreement with the 0.33-µA photoelectric current predicted for a stainless-steel sheet 137 cm^2 in area (see discussion in connection with Figure D-3). Ion probe No. 2 is illuminated by the sun throughout this period.

The $\approx 2.5 \times 10^{-5}$ A/m^2 value of the "J-field" channel indication starting at 1020 (when the field meter was exposed to the sun) is also in reasonable agreement with the 2.9×10^{-9} A/cm^2 photoelectron flux predicted for old under solar irradiation (see discussion in connection with Figure D-3). This current is zero from 1025 on, when the field meter is shielded from the sun.

During the portion of the flight illustrated in Figure D-4, ion probe No. 1 is shielded from the sun so that it indicates ambient ion density. From Appendix C, we find that, for this altitude regime, ion density N is related to the ion-probe current I by

$$N = 10^{10} I \ el/cm^3 . \qquad (D-4)$$

Applying this relationship to the ion probe No. 1 current, $I = 10^{-8}$ A, in Figure D-4, we obtain $N = 10^{10} (10^{-8}) = 100$ el/cm^3. This number is an order of magnitude smaller than the values commonly expected at this altitude in the equatorial plane.[21] Matuura and Ondoh do report electron densities as low as ≈ 200 el/cm^3 at this altitude, but their low densities were measured at latitudes above 60°.[24] Why the measured electron density should be lower than expected is not evident. It should be observed in this regard that the field meter indicates that the vehicle polarity is positive throughout the period of time covered by Figure D-4. (This change in vehicle polarity is consistent with the increased importance of photoelectron emission at the higher altitudes.)[25] Positive charge on the vehicle could tend to drive positive ions away from the vehicle

115

and reduce ion-probe current. Aside from periods of ACS activity, however, the probe No. 1 current remains constant irrespective of changes in field-meter reading. It is possible, of course, that some of the variation in indicated electric-field magnitude may stem from changes in details of the plasma structure in the vicinity of the field-meter sensor as the vehicle maneuvers, and not result from actual changes in vehicle potential.

Ion probe No. 1 current exhibits pulse excursions to values roughly twice that of the normal current. At the time of the probe-current pulses there are accompanying pulses in readings of both field-meter channels. These pulses are associated with the operation of ACS rockets on the Titan vehicle. This result means that the efflux from the ACS rockets generates an electron density of roughly 100 el/cm^3 at the ion-probe location.

Reviewing the "E-field" record in Figure D-4, we observe that for insolation vector clock angles greater than roughly 220°, when the field meter is shielded from the sun, the electric field is 100 V/m or less. (The field-meter system used on the Titan vehicles was deliberately made insensitive to make certain that it did not overload under tribo-electric charging conditions during flight precipitation.[8] Accordingly, fields less than $\approx$ 500 V/m cannot be read with great accuracy.) At other times, when the field meter is illuminated by the sun, the E-field indication is roughly 1 kV/m with the vehicle positive.

d. 1835 nmi Altitude

Data obtained from the Titan IIIC-20 rocket at an altitude of 1835 nmi are shown in Figure D-5. The records of sensor output and sun direction are very similar to those observed in Figure D-4. Throughout the period of the telemetry window, ion probe No. 2 is exposed to the sun
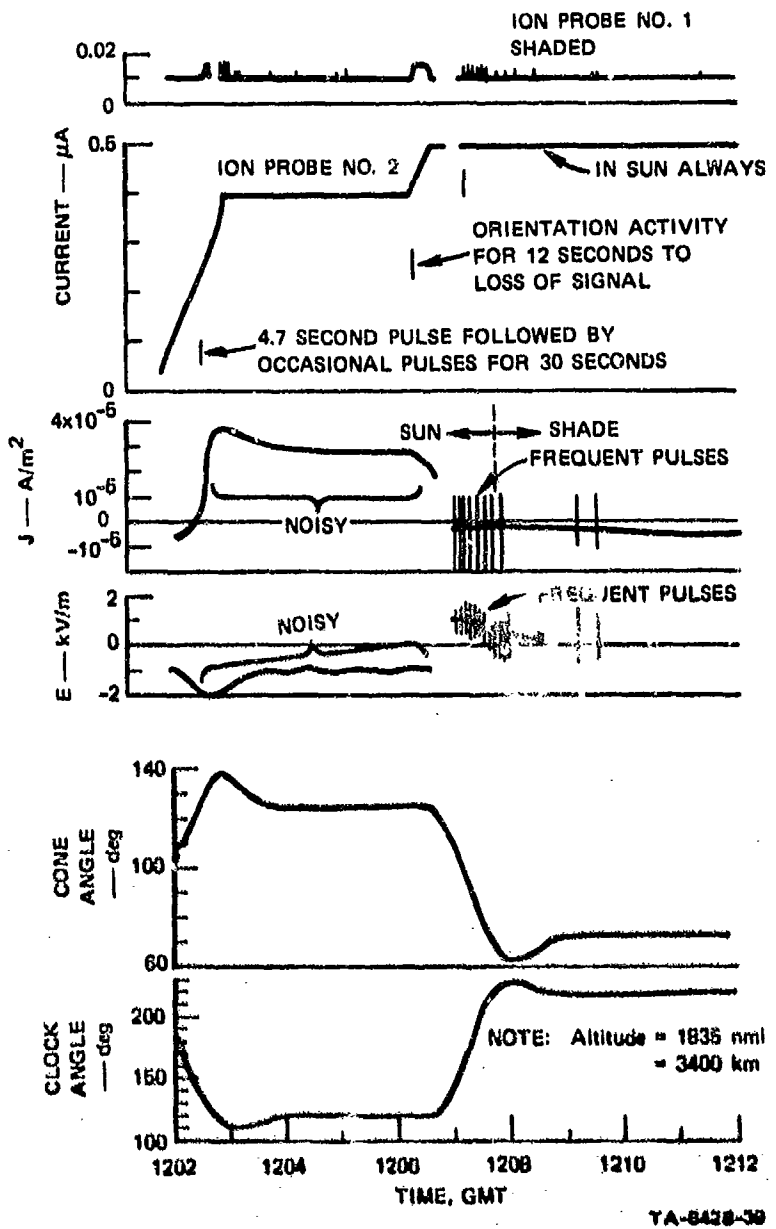
FIGURE D-5   TITAN IIIC-20 DATA FROM 1835 nmi ALTITUDE

and indicates photoelectron current during most of the period. Why the current increased by 25% at 1206, is not clear. From the ion probe No. 1 record, it is evident that a long ACS burn occurred at this time, and may have deposited material on the No. 2 ion probe sensor that changed its photoemission characteristics. Ion probe No. 1 is shielded from the sun throughout the telemetry window and indicates an ion current of 0.01 μA with occasional pulses of up to 0.008 μA superimposed at times of ACS engine operation. The 0.01-μA ion current corresponds to an electron density of 100 el/cm^3, which is roughly an order of magnitude lower than the normally accepted values for this altitude.[21]

The field meter is exposed to the sun at the beginning of the telemetry window and remains illuminated by the sun until 1207:45. Throughout the period of illumination, the J-field channel indicates a current of roughly 3×10^{-5} A/m^2 which is in excellent agreement with the 2.9×10^{-9} A/cm^2 photoelectron current predicted for gold under solar irradation[22] (see discussion in connection with Figure D-3).

Both field-meter channels are noisy during the period of sun illumination. After 1207:45, when the field meter is shaded, the field-meter readings are markedly affected by ACS engine operation coincident with pulses on the ion probe No. 1 current channel. At 1206:40 there is a pronounced change in the reading of both field-meter channels. This change coincides with the end of the long ACS burn, which coincided with the 25% change in ion probe No. 2 current. There is so much ACS activity during this telemetry window, and the ACS engine activity has such a pronounced affect on the instrumentation in this window, that one should not expect conformity of the data with accepted satellite behavior.

It should be noted that at 1208:40, after ACS activity has diminished and the field meter is shaded from the sun, the E-field

channel indicates essentially zero field. Starting at this same time, the J-field channel indicates a current density that increases to -5×10^{-6} A/m^2 arriving at the field-meter location. This could represent the electron current returning to the shaded side of the vehicle as the result of photoemissions from the sunlit side.

e. 19,320 nmi Altitude

Data from the telemetry window at an altitude of 19,320 nmi are shown in Figure D-6. Much activity on the rocket occurred during this time. Shortly after the beginning of the window, the ACS system was operated to settle the propellant in the transtage tanks. Starting at 1322:10, the second burning of the transtage motor began and continued until 1323:35. The vehicle was then oriented for payload release. Payload separation occurred at 1326:52. After release, the transtage was reoriented and driven away from the payload by operation of the ACS rockets.

Throughout this window, ion probe No. 1 was shaded from the sun and indicated a nominal ion current of 0.01 μA with occasional pulses of up to 0.005 μA superimposed at times of ACS operation. During the second transtage burn, the ion probe No. 1 current increased up to 0.05 μA. The 0.01-μA ion-probe current corresponds to an ambient electron density of 100 el/cm^3. This value is in the range of normally accepted values of electron density for this altitude.[21] The 0.05-μA ion-probe current during transtage-engine burn indicates that an electron-density increase of 400 el/cm^3 was generated at the ion probe No. 1 location by the ionization associated with the operation of this engine.

Ion probe No. 2 is illuminated by the sun throughout the telemetry window. At the beginning of the record, the 0.3-to-0.4-μA magnitude of the current is appropriate for photoelectric emission from

119
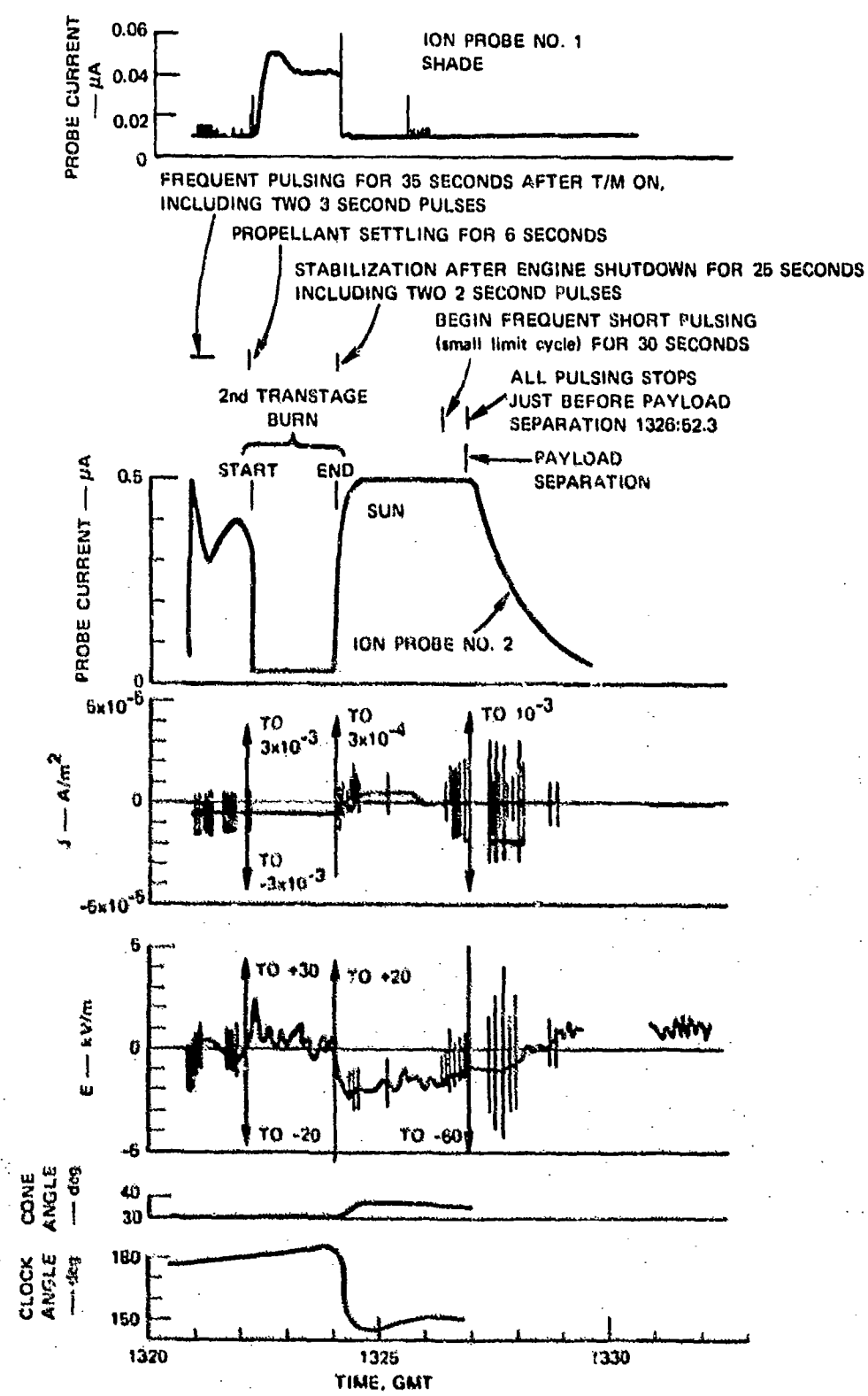
FIGURE D-6   TITAN IIIC-20 DATA FROM 19,320 nmi ALTITUDE

the probe. (It should be noted that the cone angle of the insolation vector during this window is only $\approx 30°$ so that one might expect the photoelectron current to be lower than it was in the previous records.) During the period of the second transtage burn, ion probe No. 2 current is reduced to 0.03 μA (roughly the same as the ion probe No. 1 current during the burn). Why such an ion-probe current reduction should occur during engine burn is not clear. It appears as though the photoelectric current to probe No. 2 has been reduced to zero and both ion probes are reading the electron density generated by the transtage-engine efflux. One might argue that the engine exhaust obscures the sun. Since the cone angle of the insolation vector at this time is 30°, the sun is off the tail of the vehicle (see Figure D-1) and the transtage engine exhausts out the back. At these altitudes, furthermore, the engine exhaust expands as soon as it leaves the nozzle and forms a broad cloud behind and around the vehicle. It is possible that the gas density of this cloud is adequate to reduce the photoemission from the No. 2 ion probe by an order of magnitude. At the same time, the ionized constituents in the effluent raise the electron/ion density in the vicinity of the probe to $\approx$ 300 to 400 el/cm^3.

At the end of the 2nd transtage burn, at 1324 the readings of both ion probes return to the values they had prior to the burn. After payload release, ion probe No. 2 current gradually decreases until it reaches the 0.01-μA value indicated by probe No.1. This change in No. 2 probe current probably stems from shielding of probe No. 2 from the sun as the vehicle is maneuvered after payload release. (Unfortunately no data were made available to SRI regarding sun orientation following payload release, so that the argument regarding No. 2 probe shielding is speculative.) With both probes shaded from the sun, both would read the same current corresponding to the ambient electron density.

Throughout the telemetry window, the field meter is in the sunlit hemisphere. The recessed design of the field meter, however, is such that the stator is largely shielded from the sun when the cone angle of the insolation vector is 30°. Thus, at the beginning of the record, one should not expect photoelectron emission from the field meter. This is in agreement with the measured data, which indicate a "J-field" current density of -5×10^{-6} A/m^2 arriving at the field-meter location. As was indicated in the discussion of the 1835-nmi data, this could represent the electron current returning to this portion of the vehicle as the result of photoemission from the sunlit portions. The J-field channel reading is affected momentarily by each operation of the ACS rockets, and by the start and end of the transtage motor burn, but immediately returns to -5×10^{-6} A/m^2 after each transient deflection—even during the period of the transtage motor burn.

At 1324:30 when the insolation-cone angle is increased to 38°, the J-field current density changes sign, becoming $+5 \times 10^{-6}$ A/m^2, possibly because now the field-meter stator is slightly illuminated by the sun and some photoelectric emission occurs. At 1325:40 the current density goes to zero possibly because vehicle orientation is now such that the photoelectric current emitted from the stator vanes equals the return electron current.

The E-field channel remains near zero during the early portion of the record when the insolation vector cone angle is 30° and the stator vanes are almost completely shaded from the sun. Operation of the ACS rockets generates large transient pulses in the E-field record throughout this portion of the flight. Start and stop of the transtage motor produced large transients, but there was no gross change in field-meter indication during the period of the burn. Starting at 1324:30 as the field meter enters the sun-illuminated hemisphere, the E-field channel reads -2 kV/m. This reading is probably generated by a photo-

122

electron sheath about the sunlit portion of the vehicle. Payload separation produced a large transient in the E-field channel, but no obvious permanent change in the reading. Attitude data following payload separation are not available, so that it is not possible to speculate on the reasons for the E-field-record behavior past this time.

As an illustration of the detailed way in which the measured parameters are affected by ACS system activity, the actual telemetry records obtained at about the time of payload release are shown in Figure D-7. As was explained earlier, ion probe No. 2 is illuminated by the sun and indicates photoelectron emission current that is over an order of magnitude higher than the ion current extracted from the ionospheric plasma at this altitude. The photoelectric current evidently also dominates any plasma generated by ACS operation, since ion probe No. 2 current is constant throughout the period of Figure D-7.

Ion probe No. 1, on the other hand, is shaded from the sun during this period and indicates ambient ion density. This probe current is markedly affected by ACS motor operation in general, and most of the thrustor pulses are short and result in a peak probe current roughly twice the steady-state value. The thrustor burn starting at 1326:27.4, however, persisted for approximately 5 s and raised the probe current to three times its steady-state value. It is interesting to observe that the payload-separation process did not affect the ion probe No. 1 current. This should be encouraging to the designers of the separation hardware because it means that all of the combustion products of the pyrotechnics used to accomplish the separation were so well contained that their effects were well below the effects produced by the ACS system.

Each time the ACS system is activated, the J-field channel of the field motor indicates a burst of negative charge arriving on the vehicle skin. This result is consistent with the physical picture of a

123
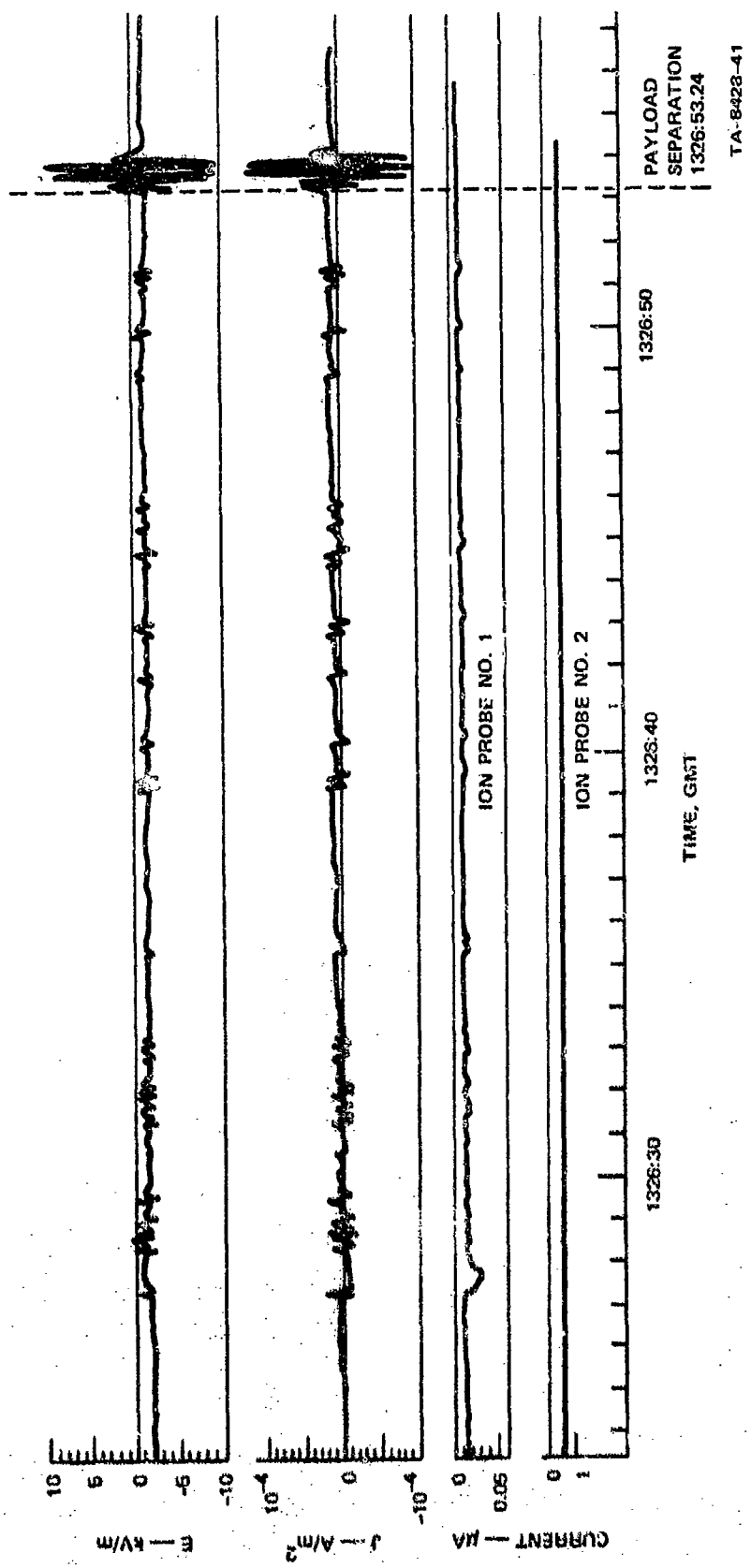
FIGURE D-7   TITAN IIIC-20 AT TIME OF PAYLOAD SEPARATION

PAYLOAD
SEPARATION
1326:53.24

TA-8428-41

burst of increased ion/electron density being associated with the operation of an ACS thruster. Since the electrons in the cloud are more mobile than the positive ions, the electrons will diffuse out of the cloud more rapidly than the positive ions, and this net diffusion to the skin of the rocket will be read as a negative current density at the field-meter location. At the time of payload separation, there is a pronounced transient persisting for roughly 1 s on the J-field record. The details of the transient are undoubtedly associated with details of the separation process.

The E-field channel in Figure D-7 is also evidently affected by the operation of the ACS thrustors. Each time a rocket fires, the field indication is reduced momentarily. Physical explanations for the details of this behavior have not been devised. At the time of payload separation, a transient signal lasting about 1 s occurs on the E-field record. The details of this signal stem from details of the separation process plus the response of the field meter to fast transient signals (this can be quite complicated because of the combination of signal chopping by the rotating vanes and the action of the synchronous detectors).

3. Titan IIIC-21 Data

a. General

There are many similarities between the C-21 data and those obtained from the C-20 vehicle. Since details of the two flights were not identical, however, there are differences in the measured results. In view of the detail with which the C-20 data have been discussed, an effort will be made to simplify the treatment of the C-21 data by referring whenever possible to the C-20 results. Where unique situations arise in the C-21 data, they will be considered in somewhat more detail.

b. **80 nmi Altitude**

Data obtained when the C-21 vehicle was at 80 nmi altitude
are shown in Figure D-8. Comparing Figure D-8 with Figure D-2, we note
that the first transtage engine burn occurred at this altitude during
the launch of C-20, thereby complicating the interpretation of the record.
No such transtage-engine activity occurred during the period covered by
Figure D-8. During this period, ion probe No. 1 was shaded from the sun
and indicated a current of 1 μA, which corresponds to an ambient electron
density $n_e = 4 \times 10^4$ el/cm^3, in agreement with the published data used in
Figure 17 for this altitude. No ionograms from the launch area were
provided to SRI for the Titan C-21 launch.

Ion probe No. 2 is sunlit during this period and is saturated
at a current level of $\geq 3\mu$A. Since the probe area is 137 cm^2,
this means that the measured current density is $\geq 2.2 \times 10^{-8}$ A/cm^2. This
is an order of magnitude higher than the photoelectric current density
of 2.4×10^{-9} A/cm^2 predicted for stainless steel under solar illumination.[22]
It appears, therefore, that the probe No. 2 current is primarily the
result of ion collection from the ambient plasma. Applying this inter-
pretation we find that the required electron density is $n_e \geq 1.2 \times 10^5$ el/cm^3.
Referring to Figure 17, we find that such a value of electron density is
possible (although it is somewhat high for this altitude). It remains
therefore to explain the difference between the readings of ion probe
No. 1 and ion probe No.2. If ion probe No. 1 in addition to being
shielded from the sun, were located in the wake of the vehicle, one
would expect its reading to be substantially lower than that of ion
probe No. 2. Velocity data made available to SRI indicate that during
this time interval, the component of vehicle velocity along the pitch
axis is -3846 ft/s = 1172 m/s, which means that ion probe No. 1 is
indeed in a wake region. (Normally the velocity vector is almost entirely
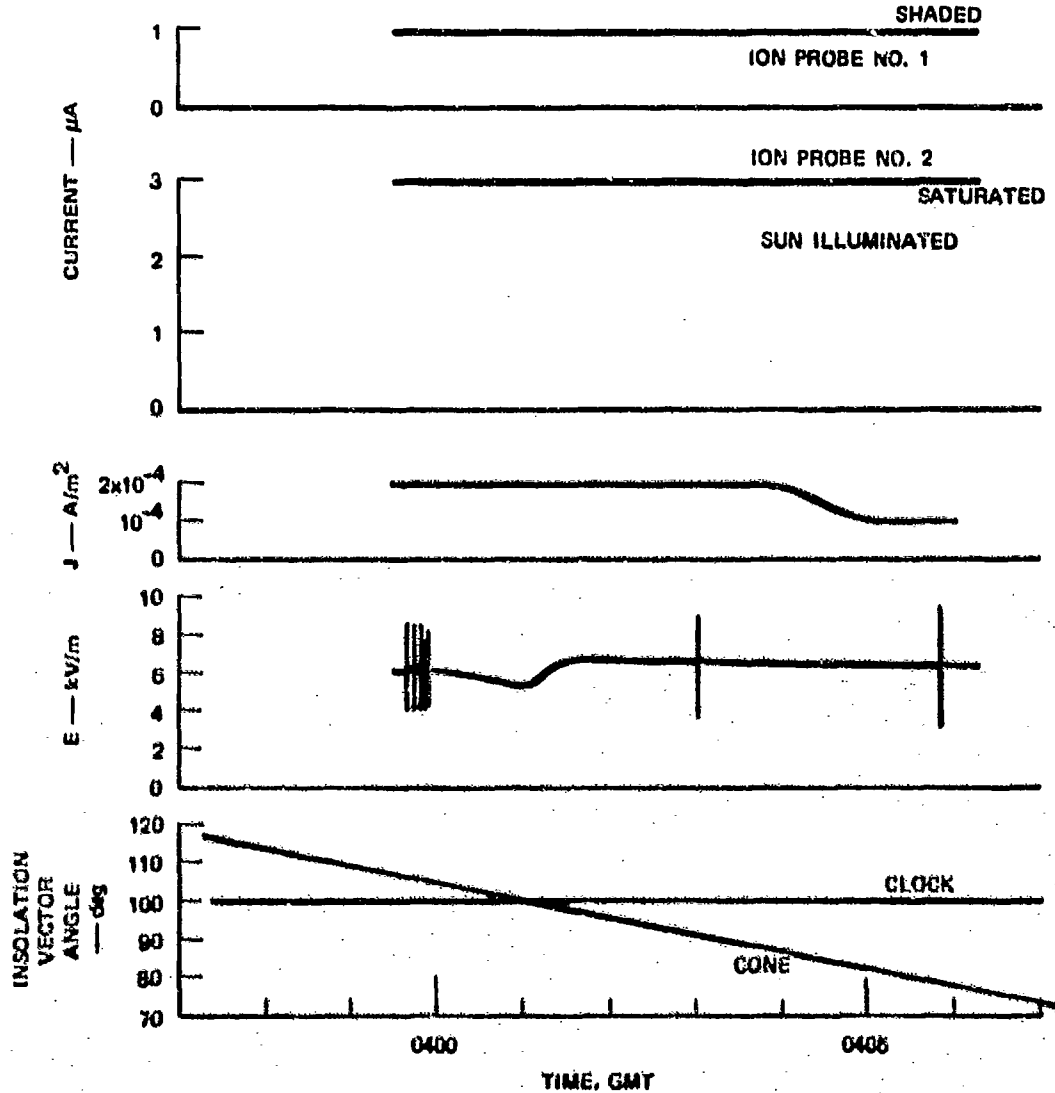
NOTE: Altitude = 82 nmi
= 152 km

TA-6428-43

FIGURE D-8   TITAN IIIC-21 DATA FROM 80 nmi ALTITUDE

along the roll axis.) Assuming a temperature of 600°K for this altitude (see Ref. 26 for 150 km altitude) the positive ions will have a thermal velocity of 425 m/s. This is substantially below the component of vehicle velocity along the pitch axis, so that a region of reduced ion density can be expected at the location of ion probe No. 1 which lies slightly in the wake of the vehicle.[27] The ion density in such a location can readily be one-third the ambient ion density (see Figure 1, Ref. 27). In this series of arguments we have been led to conclude that the ion probe No. 2 indication $n_e \geq 1.2 \times 10^5$ el/cm^3 is most representative of the ambient electron density.

It will be interesting to investigate the degree to which the field-meter J-field reading of 2×10^{-4} A/m^2 (this is essentially the same as the 2.2×10^{-8} A/cm^2 ion probe No. 2 current density) can be explained. Let us assume that the vehicle is slightly negatively charged and that the field meter collects all of the ram ion current arriving on the field-meter vanes as the result of the 1172-m/s component of velocity directed into the field meter.[28] The ram ion current is given by

$$I_{ram} = n \, e \, v \, A \qquad (D-5)$$

where n is the ion/electron density, e is the electronic charge (1.6×10^{-19} coulombs), v is the component of velocity directed into the field meter, and A is the intercepting area. The current density for our case will be

$$\frac{I_{ram}}{A} = n \, e \, v$$

$$= 1.2 \times 10^{11} \, (1.6 \times 10^{-19}) \, (1172)$$

$$= 2.25 \times 10^{-5} \text{ A/m}^2$$

which is roughly an order of magnitude lower than the measured ion current density arriving on the field meter. The calculated ram ion current can be brought into agreement with the measured field-meter current density by assuming that the ram ion velocity is v = 10,400 m/s, but this is greater than the total vehicle velocity of 7700 m/s at this altitude so that this argument is not tenable. Finally, we can observe that most of the transtage is covered with a thick layer of thermal-control material. This material is an excellent insulator, and its presence can greatly modify the normal flow of charged particles to the skin of the vehicle (ram ion current being collected on the frontal surfaces, and an equal electron current being collected in the wake region). It appears therefore that the No. 2 ion-probe current and the field-meter current density are both higher than they would be on a metallic vehicle. This situation, however, is representative of what occurs on a typical operational vehicle that includes insulating surfaces--the surfaces can become electrically charged and modify the collection of charged particles in their vicinity.

c. 100 to 200 nmi Altitude

Data obtained from the C-21 vehicle at 100 to 200 nmi altitude are shown in Figure D-9. Much of the period shown in the figure was occupied by the first burn of the transtage engine (0414:43.57 to 0420:04.67). It will be interesting to consider first the data prior to the start of the burn. At this time ion probe No. 1 is shaded from the sun while ion probe No. 2 and the field meter are both illuminated by the sun. The velocity vector is predominantly along the roll axis. The component along the roll axis is 7600 m/s, with 1200 m/s directed into the field meter and ion probe No. 2.

The readings of both ion probes prior to the burn are almost identical to their readings in Figure D-8. Since the orientation of the
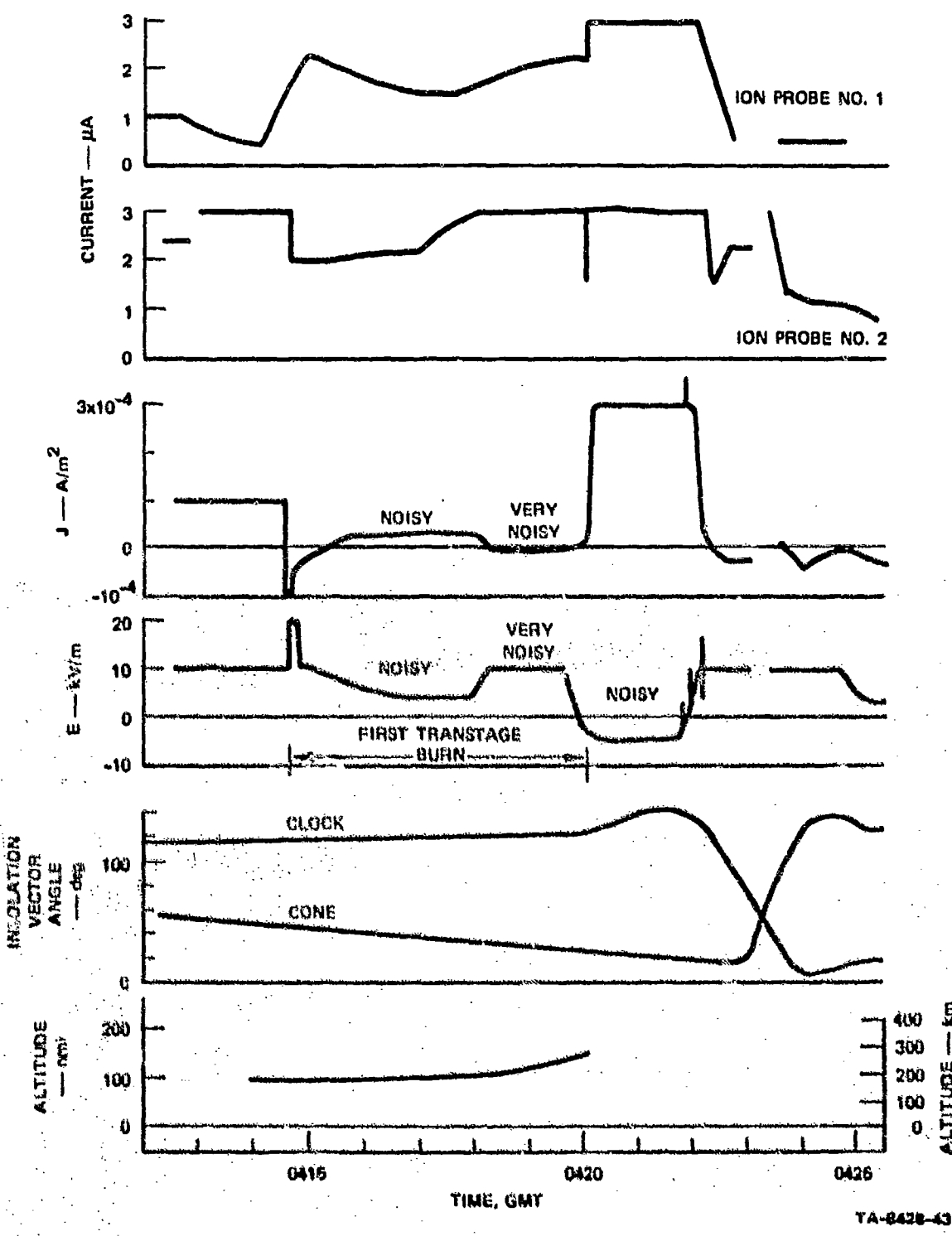
FIGURE D-8   TITAN IIIC-21 DATA FROM 100 TO 200 nmi ALTITUDE

TA-8428-43

130

vehicle is the same, and since the altitude change involved does not carry the vehicle into a radically different plasma regime, the arguments regarding interpretation of probe readings presented above in Section 3-b apply here.

The field-meter readings prior to the burn are also similar to the values in Figure D-8. The E-field reading is somewhat higher, and the J-field reading is somewhat lower, but the arguments of Section 3-b of this Appendix still apply.

During the period of the transtage-engine burn, the field-meter records are noisy, and there are pronounced changes in the values of the readings. It is interesting to note, however, that the engine burn did not produce a definite unipolar change in vehicle potential of the sort one would expect if the engine were expelling charged particles of a single polarity. Rather, the field-meter record is consistent with a physical picture of a turbulent flow of charged particles past the field meter or striking the field meter.

The ion-probe readings also are affected by the transtage-engine burn. Here too, there is no systematic increase or decrease in the probe current. Instead, the current varies considerably during the period of the burn as did the field-meter records.

To explain in detail the behavior of the instruments during the engine burn would require detailed description of the plasma flow during the burn, together with information on the way the sensors respond to a turbulent plasma. Such an analysis is beyond the scope of this report.

At the conclusion of the burn, the vehicle is reoriented so that the velocity vector no longer has a component into the field meter and ion probe No. 2. At 0420:13 (the last velocity-vector data for this telemetry window provided to SRI) the velocity-vector clock angle was

70° and getting smaller. These changes in orientation are undoubtedly
responsible for the changes in sensor outputs starting at roughly 0420:13.
Starting at 0422 there are additional changes in vehicle orientation, as
evidenced by pronounced changes in insolation vector cone and clock
angles in Figure D-9. The lack of data on the precise vehicle orien-
tations with respect to the velocity vector places arguments regarding
the details in instrumentation outputs into the realm of pure speculation.
Accordingly, no effort will be made to attempt to account for all of
these details.

d.   3500 to 4200 nmi Altitude

Data obtained from the C-21 vehicle in the flight regime from
3500 to 4200 nmi altitude are shown in Figure D-10. Throughout this
period (except for a brief interval at 0454:40) the orientation of the
vehicle with respect to the sun is such that ion probe No. 1 is illumin-
ated while ion probe No. 2 and the field meter are both shaded from the
sun. For this altitude regime we find from Appendix D that the electron
density is given by Eq. (D-4). Since ion probe No. 1 current is
$\approx 1.5 \times 10^{-8}$ A the corresponding electron density is $(1.5 \times 10^{-8}) (10^{10})$
$= 150$ el/cm^3. Ion probe No. 2 current of roughly 4×10^{-8} A corresponds
to an electron density of 400 el/cm^3. These electron densities are in
reasonable agreement with published values for this altitude regime.[25]
Ion probe No. 1 current is equivalent to a current density of 1.1×10^{-9}
A/cm^2, which is slightly less than half the photoelectric current density
of 2.4×15^{-9} A/cm^2 for stainless steel under solar illumination.[22]

The only explanation that can be offered for the difference
between the readings of ion probes No. 1 and No. 2 is the effect of
velocity. Probe No. 1 may be located in the wake of the vehicle where
ion density is low, so that probe No. 1 is indicating photoelectron
current while ion probe No. 2 is indicating ion density.[25] Unfortunately,

132
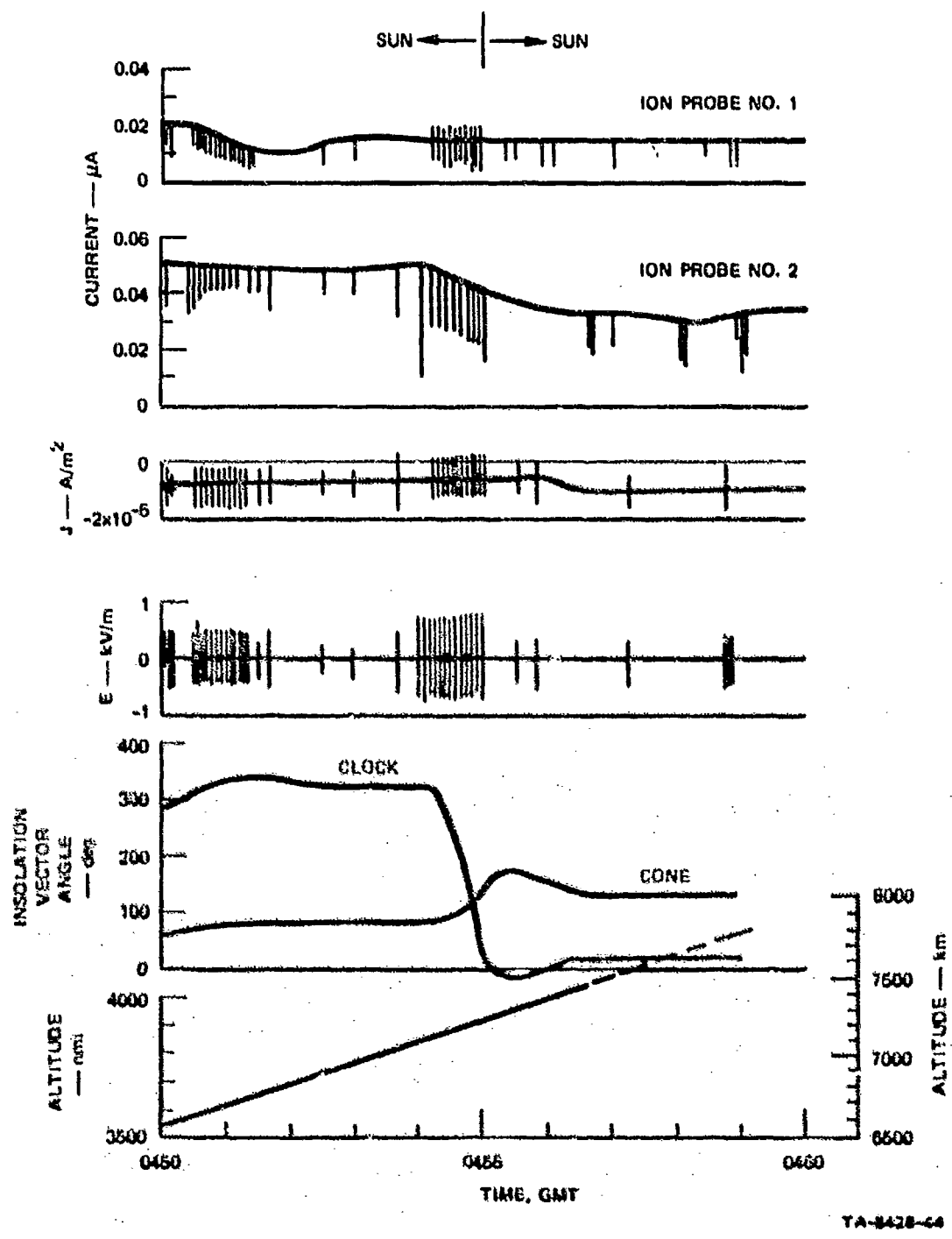
FIGURE D-10 TITAN IIIC-21 DATA FROM 3500 TO 4200 nmi ALTITUDE

TA-8428-64

no velocity-vector data were provided to SRI for this time period, so that this argument is speculative.

Throughout the period of Figure D-10, the E-field channel indicates zero. This can be interpreted to mean that, at this altitude, photoelectric emission is beginning to dominate in determining vehicle potential.

The J-field channel of the field meter indicates that a current density of roughly -10^{-5} A/m^2 is arriving at the field-meter location on the vehicle. Since the field meter is shaded from the sun throughout this period, the current arriving on the field meter probably represents the return current from the photoelectric emission on the sunlit side of the vehicle.

Activation of the ACS rockets produces the transient pulses evident in all of the records of Figure D-10. Most of the activations generate a pulse on each of the records. The magnitude of the disturbance produced in a particular sensor depends on the relative location of the sensor and the thrustor. Some of the thrustors couple poorly into certain of the sensors. In these cases pulses may appear on two or three of the channels but not on the others. The way in which the disturbance manifests itself on the record varies according to the sensor being considered. The ion probes, for example, generally indicate a reduction of electron density at the time of ACS rocket motor firing. The two field-meter channels, on the other hand, indicate a bipolar disturbance. In general, the connection between ACS rocket activity and sensor disturbance remained very clear-cut for the remainder of the flight. A typical electrostatic-data record will be examined in greater detail and compared to the thrustor activity record in a later section of this report.

134

e.   14,200 nmi Altitude

Data obtained when the C-21 vehicle was at an altitude of
14,200 nmi are shown in Figure D-11. At the beginning of the record,
both ion probes are shadowed from the sun. As the insolation-vector
clock angle changes, ion probe No. 2 becomes illuminated by the sun, and
the current to it increases until it reaches a maximum value of 0.2 μA.
This corresponds to a current density of 1.5×15^{-9} A/cm^2. This is
somewhat lower than the 2.4×10^{-9} A/cm^2 photoelectric current measured
in the laboratory for simulated solar illumination.[21] We must observe,
however, that ion probe No. 2 is positioned on the vehicle at a clock
angle of 165°, whereas the insolation-vector clock angle is 220°. Thus
the insolation vector makes an angle of 55° with respect to the normal
ion probe No. 2. Correcting for this deviation from normal incidence,
we obtain for the predicted photoelectric current $i_p = 2.4 \times 10^{-9}$ cos
$55° = 1.4 \times 10^{-9}$ A/cm^2, which is in excellent agreement with the
measured value.

At 0638:35 the insolation-vector clock angle reaches 235° and
ion probe No. 2 is shielded from the sun by the housing for yaw-right
ACS jets 4 and 5. The ion probe No. 2 current drops rapidly at this
time. As the insolation-vector clock angle increases further, ion probe
No. 2 enters the shaded hemisphere while ion probe No. 1 becomes illum-
inated by the sun.

When they are shaded from the sun, both ion probes No. 1 and
No. 2 indicate a current of 0.01 μA. From Eq. (D-4) we find that this
corresponds to an electron density of 100 el/cm^3. This is in good
agreement with published values of electron density at this altitude
along the equator.[21]

Throughout the period of Figure D-11 the field meter is in
the sun-illuminated alf of the vehicle, but the recessed design of the
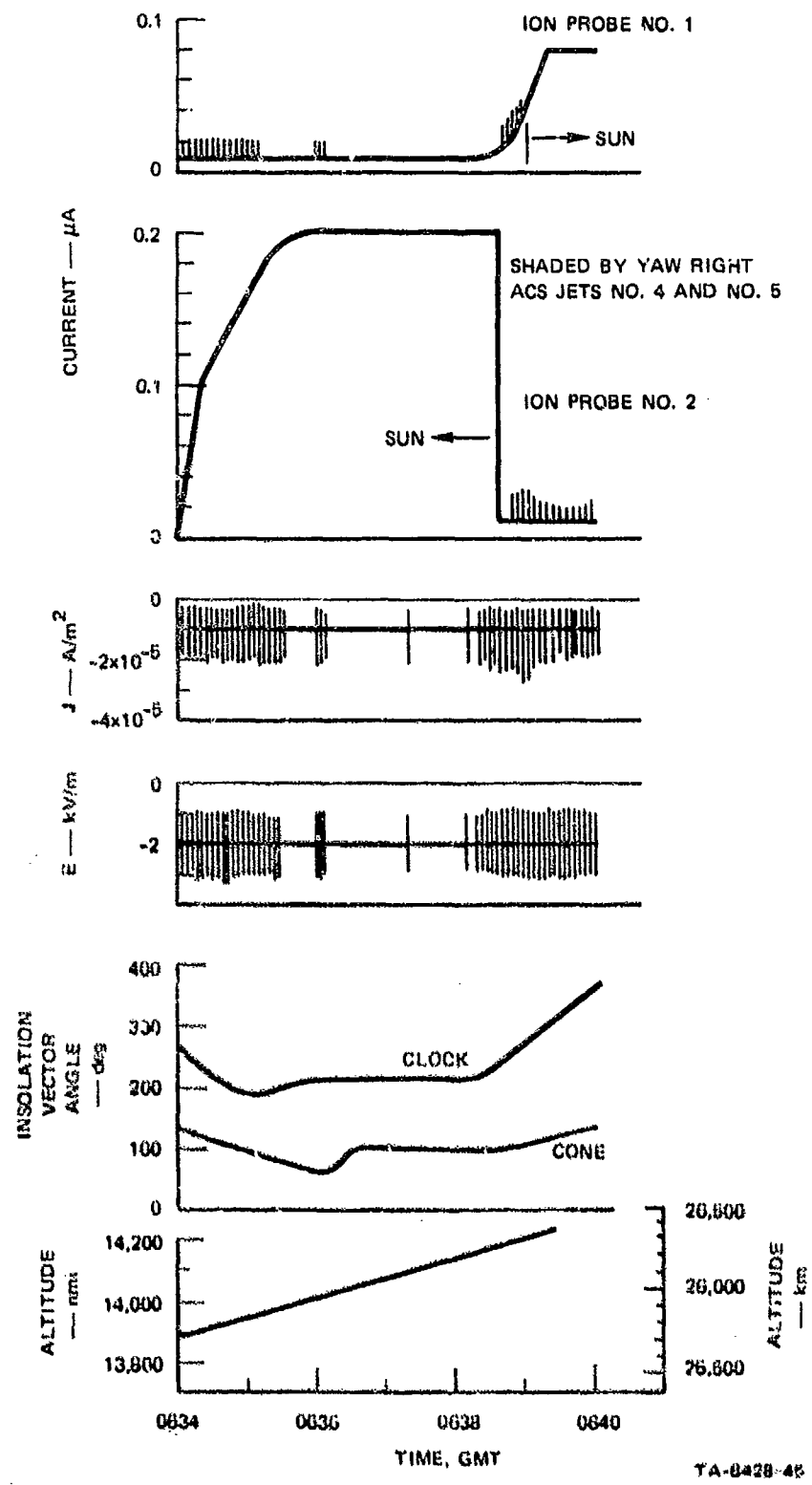
FIGURE D-11   TITAN IIIC-21 DATA FROM 14,200 nmi ALTITUDE

136

field meter is such that the stator is largely shielded from the sun when the insolation vector makes an angle of more than 60° with respect to the normal to the field meter. Since the field meter is positioned at a clock angle of 134° on the vehicle and since the insolation-vector clock angle is never less than 190° in Figure D-11, the angle between the field meter normal and the insolation vector never is less than 56°. Thus the field-meter stator vanes are shielded from the sun essentially throughout this record.

The J-field current of -10^{-5} A/m^2 probably represents the return current stemming from photoelectron emission from other parts of the vehicle.

Throughout this period, the E-field reading remains at -2 kV/m, which indicates that the vehicle is positive with respect to its surroundings. This is in agreement with the argument that, as ambient plasma density is reduced, the competition between negative charge accretion from the plasma and negative charge loss by photoemission becomes dominated by photoelectron emission, and the vehicle acquires a net positive charge.[25,29]

f.   18,600 nmi Altitude

Data obtained at 18,600 nmi altitude during the flight of the Titan IIIC-21 are shown in Figure D-12. In all respects this record is almost identical with that of Figure D-11. Thus all of the observations made in Section 3-e above regarding the significance of the Figure D-11 data also apply to Figure D-12.

g.   19,400 nmi (Synchronous Orbit) Altitude

Data from the C-21 vehicle after it reached synchronous orbit are shown in Figure D-13. The maneuvering associated with payload ejection
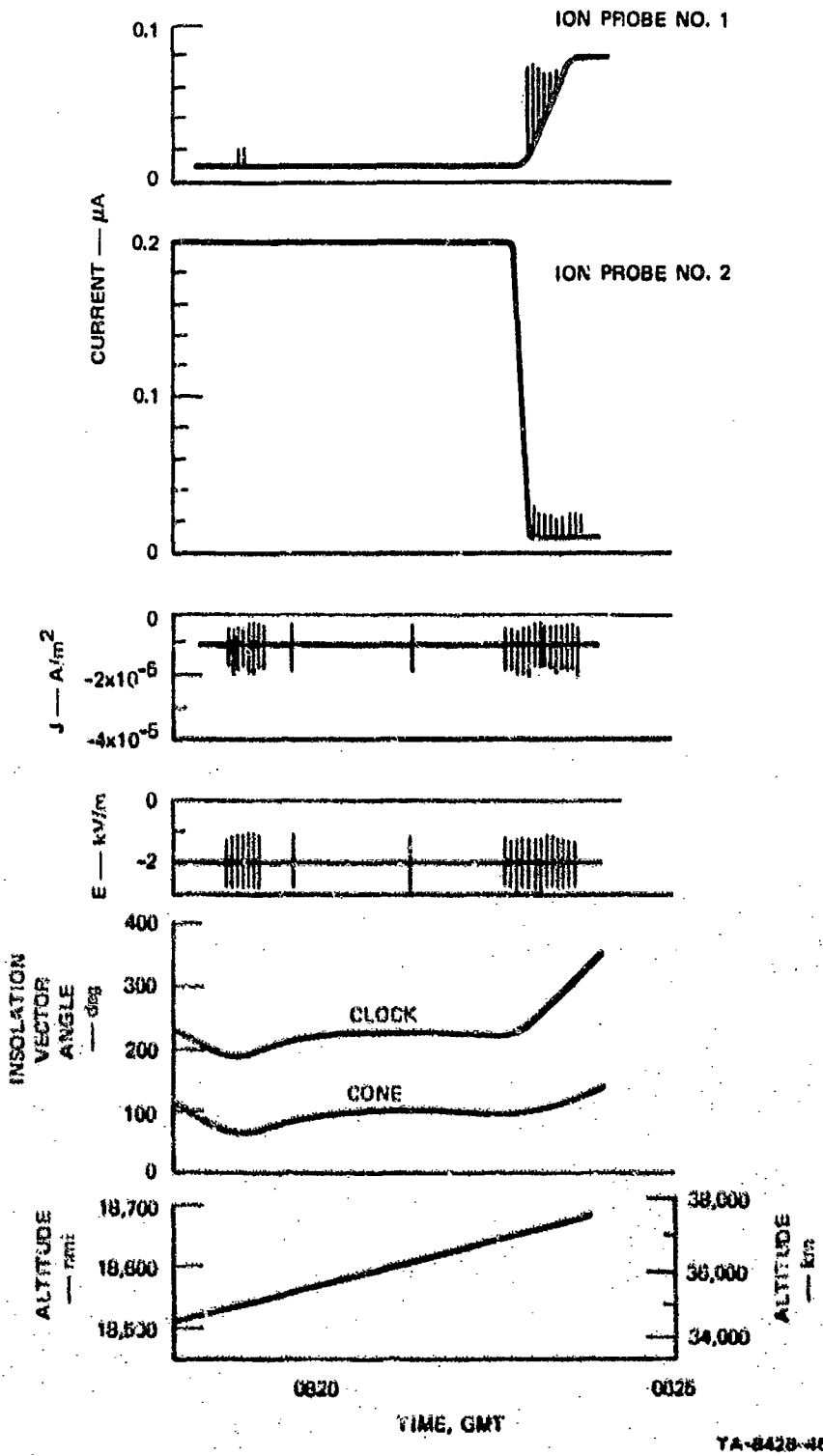
FIGURE D-12   TITAN IIIC-21 DATA FROM 18,600 nmi ALTITUDE

138
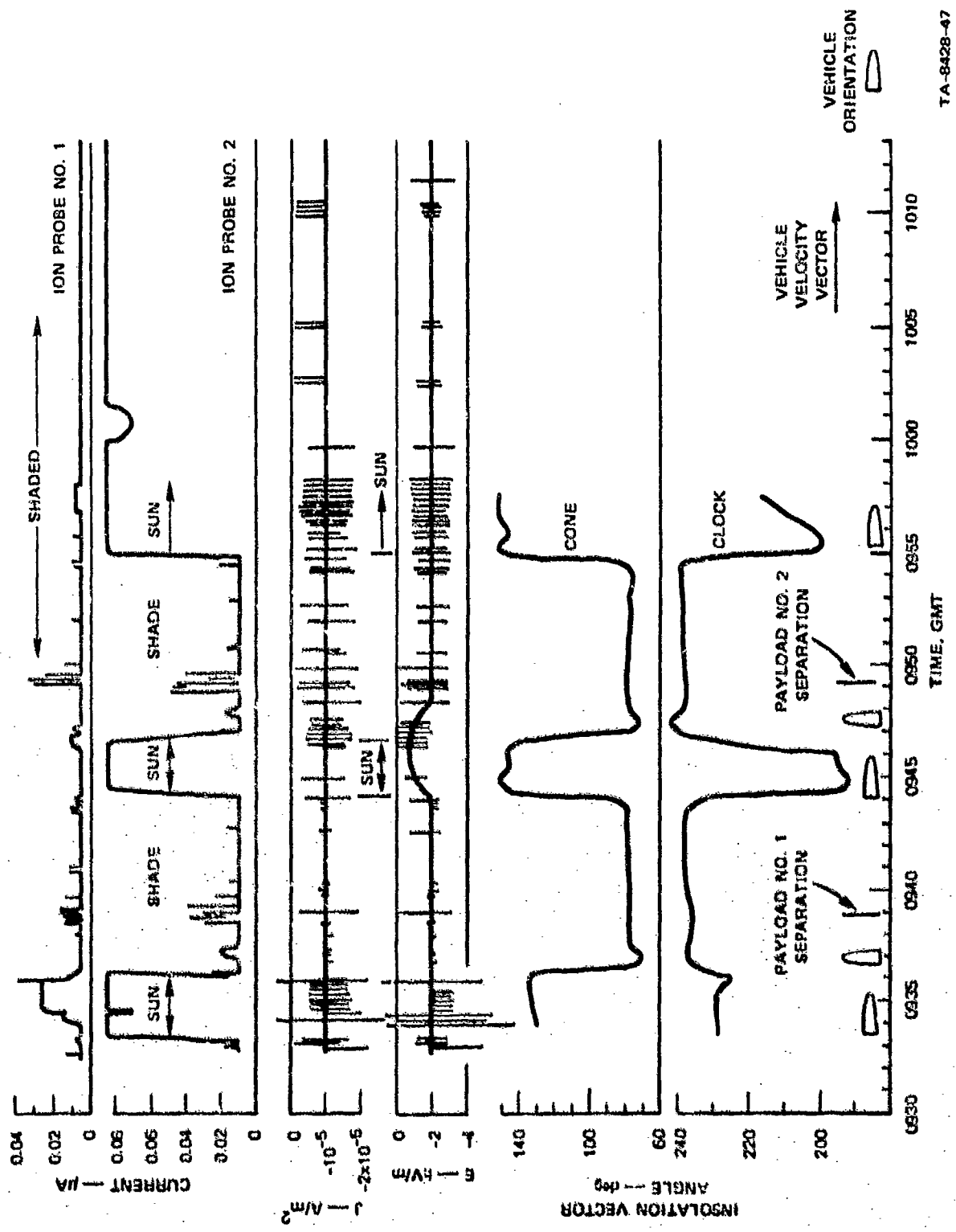
FIGURE D-13   TITAN IIIC-21 DATA FROM 19,400 nmi ALTITUDE

TA-8428-47

139

is evident in the insolation-vector plots, and in the sketch at the
bottom of the figure showing transtage orientation. In spite of the
maneuvering, ion probe No. 1 was shaded from the sun throughout this
period and indicated a nominal resting current of 0.005 μA (full-scale
deflection on this channel is 0.1 μA, so that this reading is approaching
the detection limit and is not overly precise). This reading corresponds
to an electron density of 50 el/cm^3, in agreement with the published
range of densities for this altitude.[21] The record of ion probe No. 1
is markedly affected by ACS rocket operation during this period.

The record of ion probe No. 2 shows the effects of vehicle
maneuvering. During parts of the period, the probe was illuminated by
the sun. When the vehicle was oriented for payload ejection, on the
other hand, the orientation was such that ion probe No. 2 was shielded
from the sun by the housing for the yaw-right ACS rockets 4 and 5.
During the shaded portions of the record, a current of 0.01 μA was
measured, corresponding to an electron density of 100 el/cm^3, in
agreement with the published range of densities for this altitude.[21]
The 2-to-1 disparity between the readings of ion probes No. 1 and No. 2
should not be taken too seriously because, as was indicated earlier, the
probe current is so low here that the detection limit of the system is
approached. The data should simply be interpreted to indicate that
an electron density of roughly 75 el/cm^3 (the average of the two probe
readings) was measured. During shaded periods, the activity of the ACS
system had a pronounced effect in the ion probe No. 2 record.

When ion probe No. 2 was illuminated by the sun, the probe
current was 0.08 μA. This corresponds to a current density of roughly
6×10^{-10} A/cm^2. This is $\frac{1}{4}$ of the 2.4×19^{-9} A/cm^2 measured in the
laboratory from stainless steel under simulated normally incident solar
illumination.[22] We must observe, however, that the insolation vector
is far from normal to the No. 2 ion probe. For example, at 0935 the

insolation vector clock angle is 230°, which is 65° from the clock position of the probe. At this same time, the insolation vector cone angle is 135°. The angle the insolation vector makes, with respect to the normal, to ion probe No. 2 is therefore 73°, and the flux density intercepted by the probe is cos 73° = 0.29 the flux at normal incidence.

The field meter is largely shielded from the sun throughout this period, since the insolation-vector clock angle is always greater than 224° except for brief periods at 0945 and 0955. At 0945 the field meter reading is perturbed for a period of roughly 4 minutes. For the remainder of the record, the nominal field-meter channel readings are both identical with those of Figure D-11, and the observations made in Section 3-e of this Appendix regarding the significance of Figure D-11 field-meter data also apply to Figure D-13.

It is interesting to examine in more detail the data outputs at the general time of payload separation. Ion-probe data from the period of payload No. 1 release are shown in Fig. D-14 together with chamber-pressure records from the ACS rockets. It is evident that each pulse of increased ion-probe current corresponds to a firing of a thruster. It is also evident that certain of the thrustors generate more of a change in ion density at a particular probe than do others. A matrix showing the degree of coupling between the various thrustors and each of the ion probes is shown in Table D-1. The locations of the various ACS motors are shown in Figure D-1. The operation of rockets No. 12 and 6 (roll CCW) produces the greatest increase in the ion density at both ion probes. (The rockets are operated in pairs.) A strong effect on ion-probe No. 1 is expected since the exhaust from engine No. 12 passes directly over ion probe No. 1 (shielded from direct impingement by the housing for ACS rockets 10 and 11). Similarly, strong coupling exists between rocket motor 6 and ion probe No. 2 because the exhaust
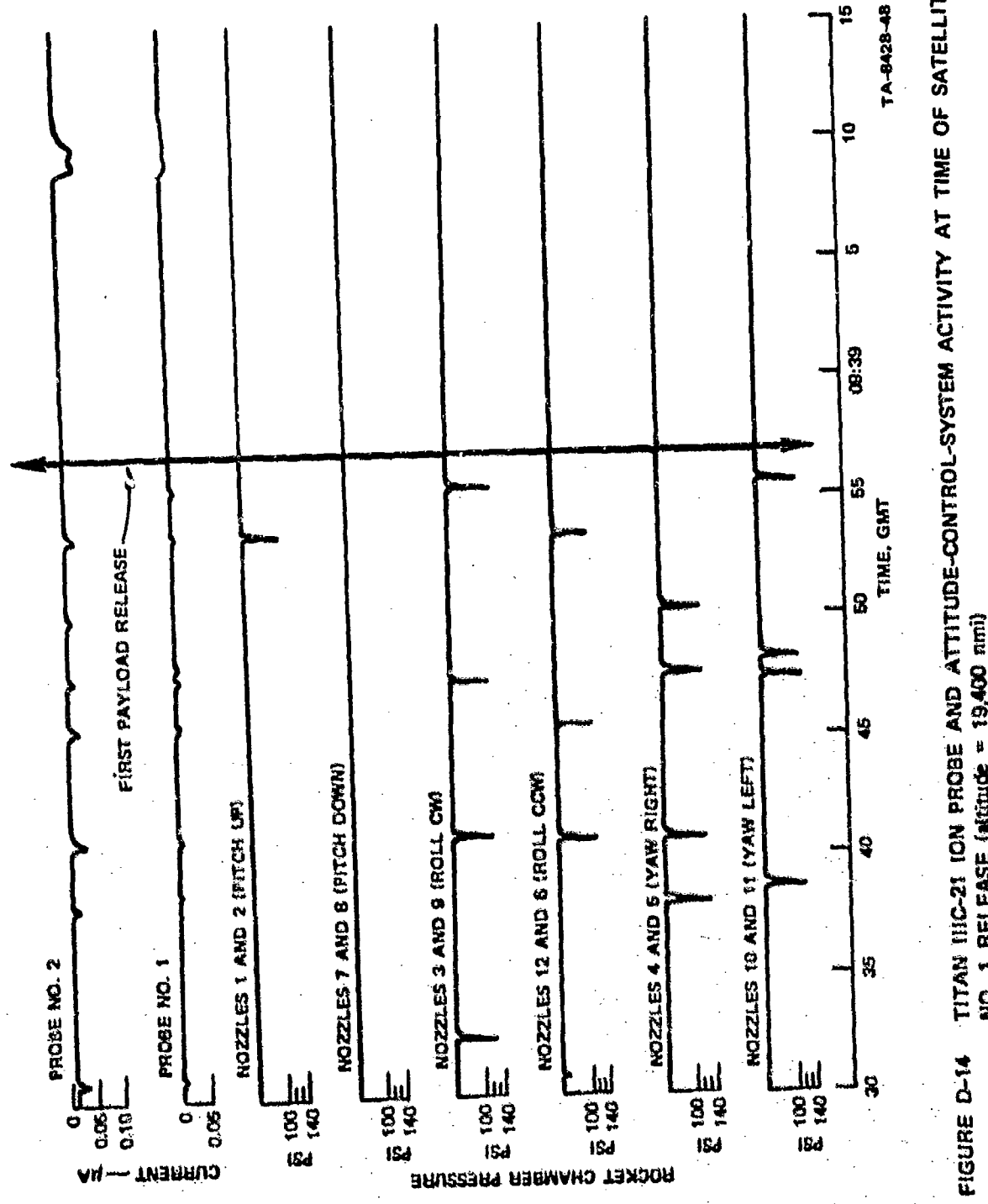
FIGURE D-14   TITAN IIIC-21 ION PROBE AND ATTITUDE-CONTROL-SYSTEM ACTIVITY AT TIME OF SATELLITE
NO. 1 RELEASE (altitude = 19,400 nmi)

142

from engine No. 6 passes directly over ion probe No. 2 (shielded from direct impingement by the housing for ACS rockets 4 and 5).

Table D-1

DEGREE OF COUPLING BETWEEN ACS ROCKET EXHAUSTS AND LANGMUIR ION PROBES

ACS Engine No.	Degree of Coupling	
	Ion Probe No. 1	Ion Probe No. 2
1,2	Weak	Weak
3,9	Weak	Weak
4,5	None	Weak
7,8	Weak	Weak
10,11	Weak	Weak
12,6	Strong	Strong

Rocket motors 3 and 9 (roll CW) are similarly located with respect to the ion probes, but their operation produces a less pronounced increase in probe current. The exhaust from motors 3 and 9 is directed away from the ion probes.

All of the pitch and yaw motors exhaust in the aft direction, and the effect of their operation on ion-probe current is less pronounced than the effect of rocket engines 12 and 6.

A very interesting and significant effect was observed following the release of the first payload at 0938:56.64. It will be noted that there was no ACS rocket activity after 0938:55.2, but there is a pulse of increased current in both ion-probe channels starting at 0939:08.8 (13.6 s after payload release) and persisting until 0939:11.5. When this unexpected current pulse was discovered by SRI personnel, speculation immediately began regarding its cause. The first possibility

143

considered was that antenna breakdown either on the transtage (considered highly unlikely) or on the payload satellite occurred at this time. A check with personnel at SAMSO/Aerospace quickly disclosed that the spinup rockets on the payload satellite were fired at this time. In fact, the time waveform of the current pulse induced in ion probe No. 2 closely duplicated the chamber-pressure variation observed during the burn of a spinup rocket. It was concluded that the ion-current pulse was undoubtedly caused by the operation of the spinup rockets on the satellite which was at this time at least 14 ft from the transtage. (At separation, the satellite moves away from the transtage with a velocity of at least 1 ft/s.) This result is significant, since it indicates that a remote measurement with a passive system such as the ion probe is able to detect rocket-motor operation on a satellite, and can provide a time history of the burn. With additional effort, it should be possible to obtain an estimate of engine thrust from ion-density change and distance from the sensor to the rocket motor.

Data from the period about the time of No. 2 payload release are shown in Figure D-15. Here there is much more ACS system activity than there was prior to the release of the No. 1 payload. Again, it is evident that both ion-probe currents are markedly affected by the operation of the No. 12 thrustor. In this record, there are several long burns of the No. 12 motor (e.g., at 0948:52.4, 0948:56.4 and 0949:01.2). Corresponding long current pulses are observed in both ion probes.

Payload No. 2 was released at 0949:18.64. Starting at 0949:29.9 (11.25 s after payload release) and persisting until 0949:33.7 a complex current pulse occurred on both ion-probe channels. When the electrostatic instrumentation data were first inspected, the ACS thrustor activity record was not available, and the informal information supplied to SRI indicated that there should be no ACS activity at the time of the observed pulse. The ion-probe data were first interpreted to mean that

144
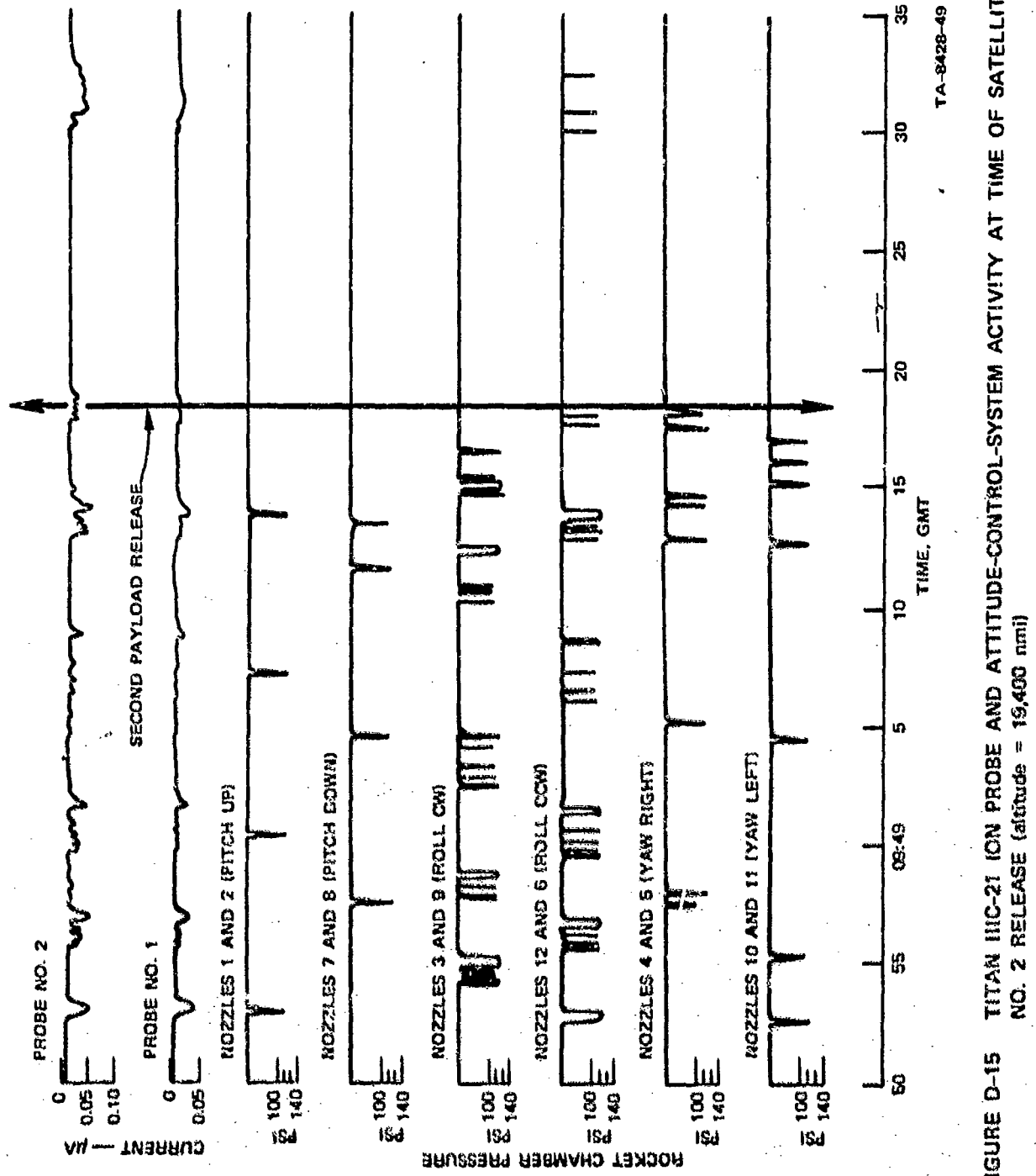
FIGURE D-15 TITAN IIIC-21 ION PROBE AND ATTITUDE-CONTROL-SYSTEM ACTIVITY AT TIME OF SATELLITE NO. 2 RELEASE (altitude = 19,400 nmi)

TA-8428-49

possibly a malfunction had occurred in the satellite spinup rocket motor, thereby generating the three additional peaks in the record (compare Figure D-14 and D-15). A second interpretation was that, on this particular flight, ACS motor activity did occur precisely during satellite spinup, thus generating the additional peaks in the No. 2 ion probe record. When the ACS motor-pressure data became available, it was immediately apparent that the complex ion-probe current record was the result of the simultaneous operation of the spinup rocket motor on the satellite and three pulses from the No. 12 motor of the transtage ACS system.

Appendix E

DESCRIPTION OF SATELLITE INSTRUMENTATION

Appendix E

DESCRIPTION OF SATELLITE INSTRUMENTATION

1. Introduction

Satellite electrification, which is known to occur under certain environmental conditions in space, is a likely cause for the unexpectedly rapid degradation of thermal-control material properties observed on previously launched synchronous-orbit satellites.

This deterioration of thermal-control properties may be caused (1) by the accelerated deposition of electrically charged or polarizable contaminants on thermal-control surfaces due to electrostatic attraction, or (2) by physical changes in thermal-control characteristics due to electrical discharges that occur between portions of satellite materials that become charged to unequal potentials. In addition, the electric fields produced by charged surfaces can interfere with the operation of field-sensitive instruments. The resulting electrical discharges may produce severe electrical noise in critical instrumentation or control circuits.

An instrumentation system for the study of satellite electrification mechanisms and charging currents has been developed by Stanford Research Institute and has been installed on a satellite that is to be launched in the near future. This instrumentation system is basically a modified and repackaged version of one that was developed by SRI and employed on the flights of Titan IIIC-20 and C-21 to study rocket electrification.

The Titan instrumentation is described in detail in Ref. 8 and again briefly in Section II of this report. The Titan instrumentation was chosen as the basis for the satellite instrumentation system, since the Titan system had already been qualified and proven in flight. Further, the time and effort required for modification and repackaging of this system for use on a satellite was minimal, thereby allowing in-orbit data regarding the electrostatic processes of interest to be obtained at the earliest possible time.

2. Satellite Instrumentation

A block diagram of the satellite instrumentation system is shown in Figure E-1, and an abbreviated description of this system is given below. A more complete description of the major components of the system is given in Ref. 8.

a. Electrostatic-Field Sensor

The electrostatic-field sensor is of the rotating-vane design. The detector head is mounted in a hole in a thermal-control panel in such a manner that the sensor vanes are exposed to the exterior of the vehicle. The depth at which the sensor is mounted has been chosen in order to maximize the sensitivity to electric fields produced by charge accumulation on the vehicle surface surrounding the sensor.

The electric-field sensor is also equipped to measure convection currents that flow to the sensor from the environment.

For the satellite system the sensitivity of the electric-field and convection-current sensors has been increased by a factor of 20 in order to allow the measurement of the magnitudes of vehicle potential and convection current that are expected during relatively quiet periods as well as during periods of increased solar activity.
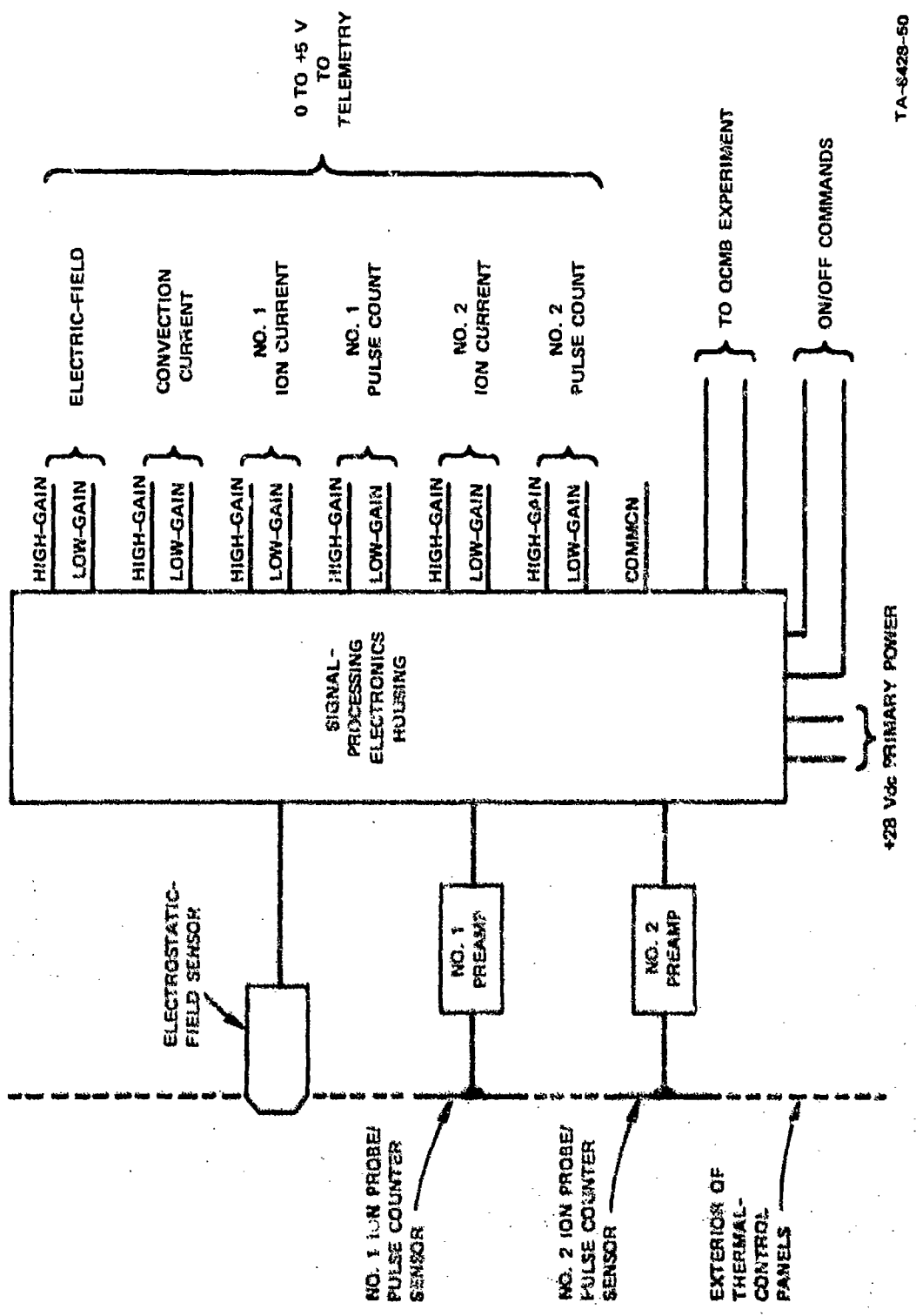
FIGURE E-1 BLOCK DIAGRAM OF SATELLITE INSTRUMENTATION SYSTEM

TA-8428-50

The location of the field-sensor on the satellite is shown in Figure E-2. Figure E-3 is a photograph of the satellite electrostatic-field sensor. It is evident from the photograph that the design of the sensor has been modified to minimize the degree to which the vanes are recessed.

b. Ion-Probe/Pulse-Counter Sensors

Two ion-probe/pulse-counter sensors are mounted on the vehicle surface as shown in Figure E-2. Each sensor consists of a stainless-steel plate with a surface area of 150 cm^2. The sensors are biased to a fixed voltage of -5.6 V with respect to the satellite frame in order to allow the collection of positive ion current.

In addition, each of the sensors is coupled to pulse-counter circuitry that allows the detection and counting of electrical pulses induced in the sensor either by electrostatic discharges that occur on thermal-control surfaces near the sensor or by charged particles, such as those that may be produced by rocket-motor operation, that strike the sensor. The amplitude and time-structure of an induced pulse determines whether or not the counter circuitry is triggered. Laboratory experiments are planned to determine the pulse-structure requirements for reliable detection, as well as the structure of pulses of the type produced by discharges on thermal-control surfaces.

Figure E-4 is a photograph of an ion-probe/pulse-counter sensor and its associated preamplifier.

c. Signal-Processing-Electronics Housing

The signal-processing-electronics housing contains the necessary on/off-command circuitry, the secondary power supply, and the major

ION PROBE/PULSE
COUNTER SENSOR
NO. 2

THERMAL-CONTROL
SURFACES

ELECTROSTATIC-
FIELD SENSOR

ION PROBE/PULSE
COUNTER SENSOR
NO. 1

-T

+T

-S NEAR SIDE
+S FAR SIDE

TA-8428-51
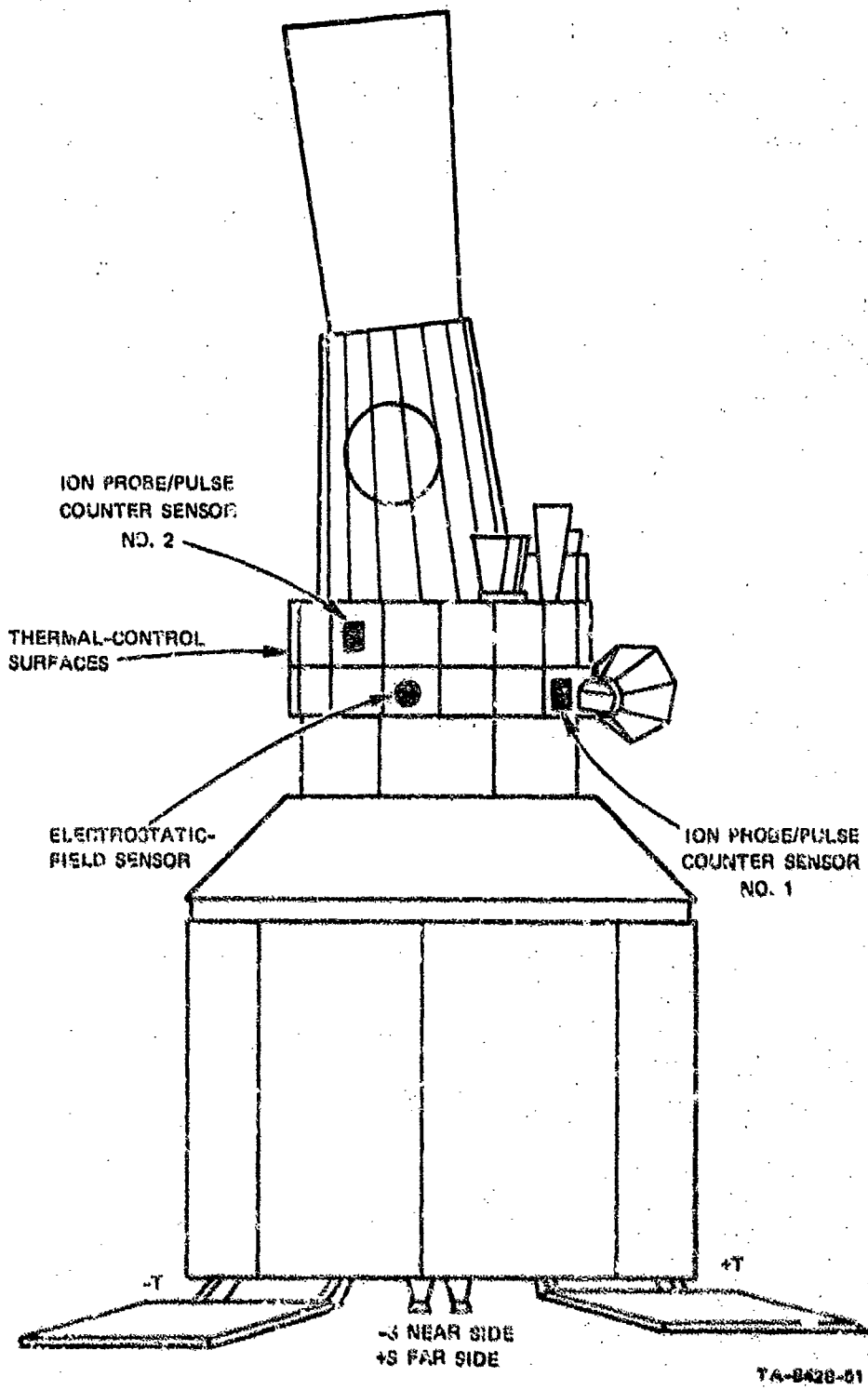
FIGURE E-2   STANFORD RESEARCH INSTITUTE SENSOR LOCATIONS

153
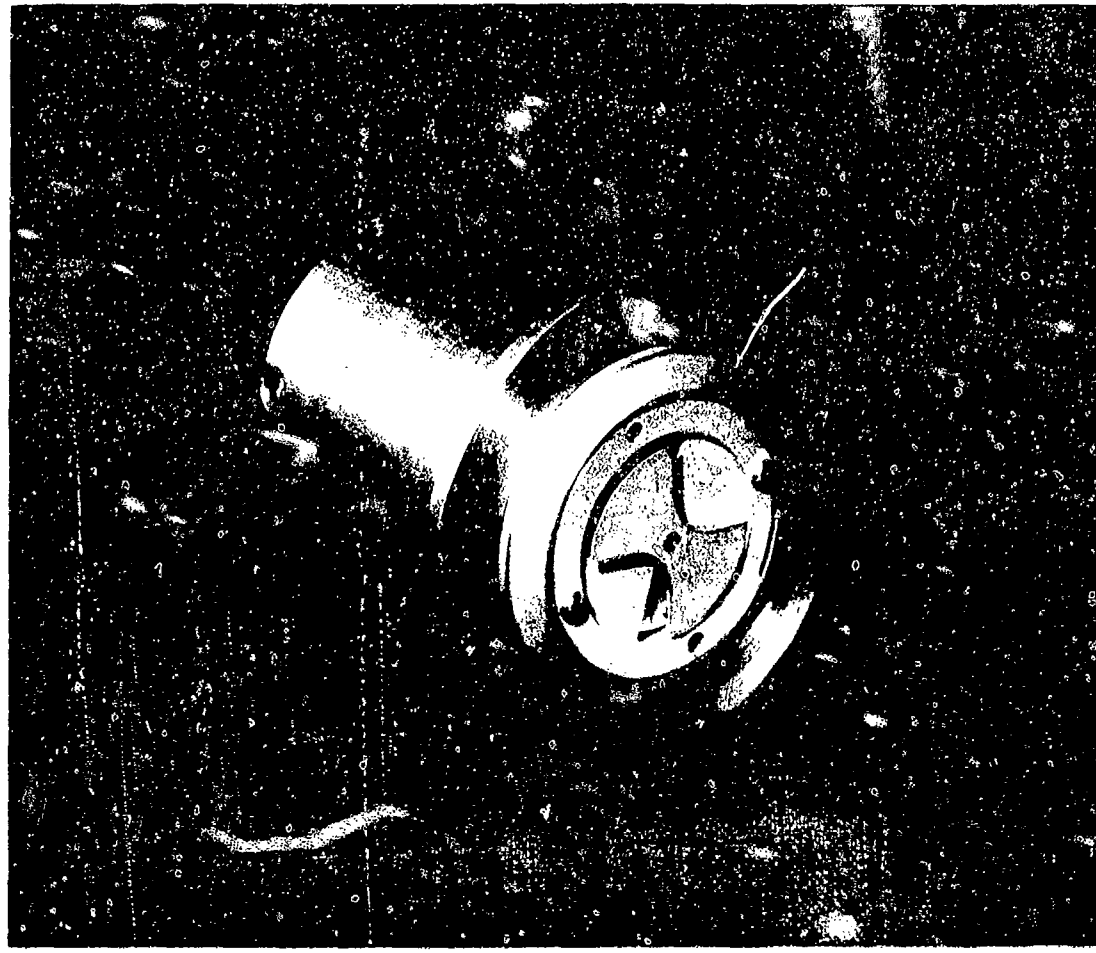
TA-8428-62

FIGURE E-3   SATELLITE FIELD-METER SENSOR

portion of the signal-processing electronics. Figure E-5 is a photo-
graph of this unit with an access cover removed,

1)   On/Off-Command Circuitry

The on/off-command circuitry is designed for fail-safe
operation, in that two separate command-signal pulses are required to
turn on the instrumentation while a single command on either line will
turn the instrumentation off. In addition, in case of single-point
command-circuit failure, the instrumentation will revert to the off
condition. A schematic diagram of one of the two identical channels
employed in the on/off-command interface circuit is shown in Figure E-6.

154
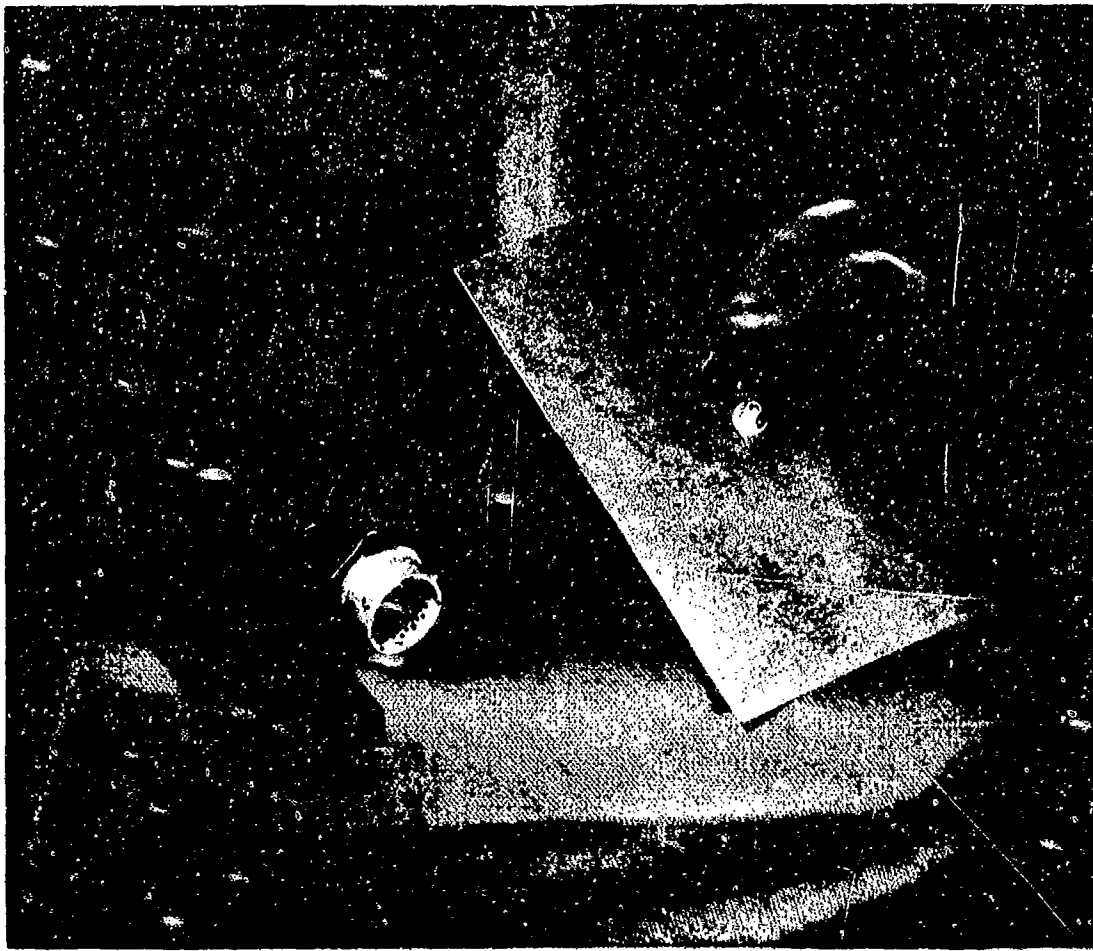
TA-8428-63

FIGURE E-4   SATELLITE PULSE PREAMPLIFIER AND LANGMUIR-ION-PROBE SENSOR

(2)   QCMB Experiment Power

The secondary power supply contained in the SRI instrumentation package is being used to supply 28-Vdc power to a quartz-crystal micro-balance system.

Power is supplied to the QCMB experiment only when the SRI instrumentation is turned on.

(3)   System Output Channels

The system output channels are shown in Figure E-1. Each channel is sampled by the telemetry system at a rate of 1 sample per second.

155
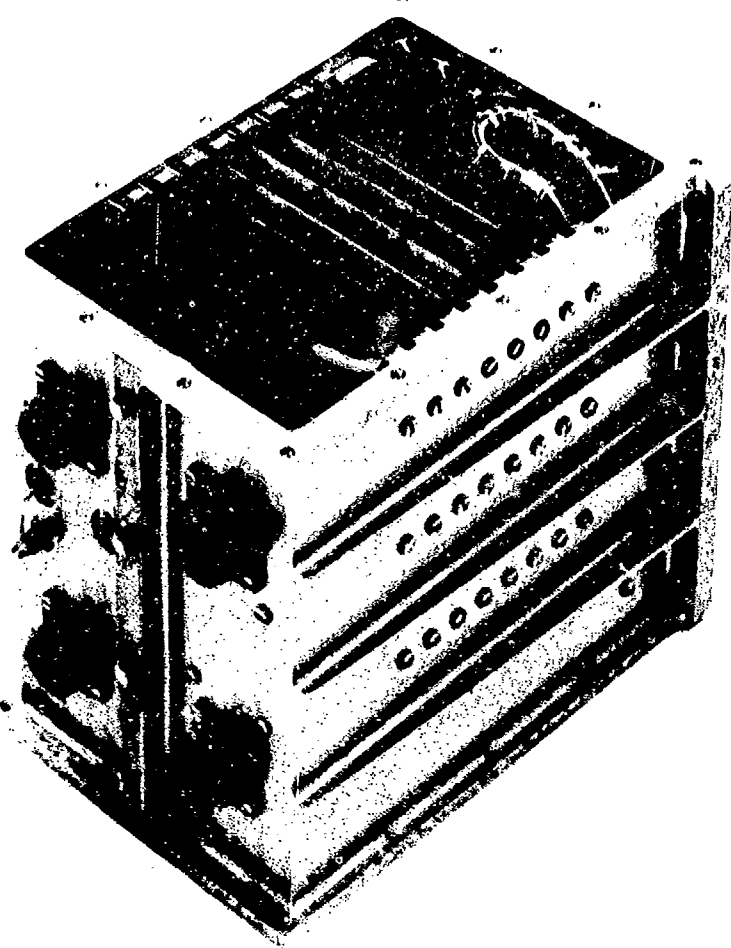
FIGURE E-5   SATELLITE ELECTRONICS PACKAGE
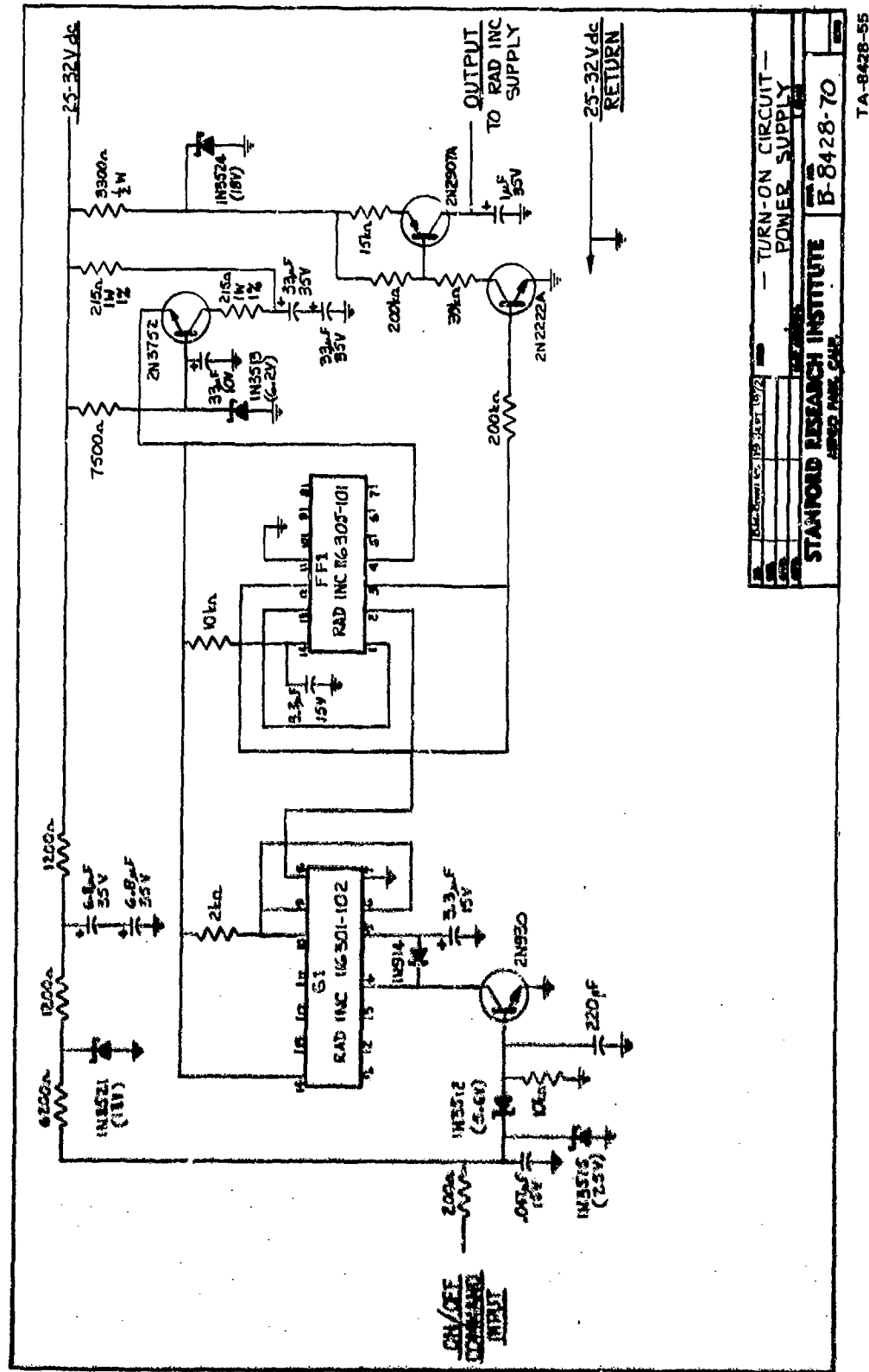
FIGURE E-6   ON-OFF COMMAND CIRCUITRY

The full-scale output range for each channel is 0 to +5 V. The output from each channel is linearly proportional to the input signal being measured. The nominal input parameter ranges for each of the channels are given in Table E-1.

Table E-1

SRI SATELLITE INSTRUMENTATION

SENSOR	PARAMETERS MEASURED	NOMINAL RANGE
Electrostatic-Field Sensor	Electric Field (high-gain)	$\pm$ 500 V/m
	Electric Field (low-gain)	$\pm$ 15 kV/m
	Convection Current (high-gain)	$\pm$ 5 $\mu A/m^2$
	Convection Current (low-gain)	$\pm$ 150 $\mu A/m^2$
Ion-probe/ Pulse counter No. 1	Ion Current (high-gain)	$0 \text{ to } +\dfrac{0.67 \text{ nA}}{cm^2}$
	Ion Current (low-gain)	$0 \text{ to } +\dfrac{20 \text{ nA}}{cm^2}$
	Pulse Count (high-gain)	0 - 50 pps
	Pulse Count (low-gain)	0 - 1000 pps
Ion-probe/ Pulse counter No. 2	Ion Current (high-gain)	$0 \text{ to } +\dfrac{0.67 \text{ nA}}{cm^2}$
	Ion Current (low-gain	$0 \text{ to } +\dfrac{20 \text{ nA}}{cm^2}$
	Pulse Count (high-gain)	0 - 50 pps
	Pulse Count (low-gain)	0 - 1000 pps

3. Progress to Date

Under the present contract, the satellite instrumentation system was constructed and installed on a satellite.

A preliminary post-installation operational and signal-injection calibration test of the satellite instrumentation system was performed. During this test the complete instrumentation system functioned as planned and the telemetry outputs were shown to be linear with respect to the system input parameters over their entire ranges.

A proposal was submitted for continued effort, including the final preflight instrument checkout and calibration, the analysis and reduction of in-orbit data, and laboratory work to support the data-analysis effort.[30] This proposal resulted in a subcontract to carry out the additional work.[31] At this writing the preflight checkout and calibration have been accomplished, and the satellite was successfully launched. Data reduction and analysis are underway.

REFERENCES

1. E. F. Vance, L. B. Seely, and J. E. Nanevicz, "Effects of Vehicle Electrification on Apollo Electro-Explosive Devices," Final Report, Contract NAS-9-3154, SRI Project 5101, Stanford Research Institute, Menlo Park, Calif. (December 1964).

2. L. Aronowitz, "Rocket-Engine-Generated Voltage as a Source of Electromagnetic Interference and Electronic Component Damage on Interplanetary Vehicles," paper presented at IEEE Space Electronics Symposium, Miami Beach, Florida, 2-4 November 1965.

3. L. Aronowitz, "Electrical Boundary Currents Generated by Plasma Flow," _Applied Physics Letters_, Vol. 6, pp. 215-216 (1965).

4. P. Molmud, "Frictional Electricity in Missile Systems," _J. Am. Roc. Soc._, pp. 73-74 (January 1959).

5. W. K. Luckow, "Spacecraft Electrostatic Phenomena," SID 64-422-1, Space and Information Systems Division, North American Aviation, Inc., Downey, Calif. (February 1964).

6. E. F. Vance and J. E. Nanevicz, "Rocket Motor Charging Experiments," Scientific Report No. 2, Contract AF 19(628)-4800, SRI Project 5359, Stanford Research Institute, Menlo Park, Calif. (December 1967).

7. J. E. Nanevicz, E. F. Vance, W. C. Wadsworth, and J. A. Martin, "Low-Altitude, Long-Range All-Weather Vehicle Interference Investigation," Tech. Report AFAL-TR-65-239, Contract AF 33(615)-1934, SRI Project 5082, Stanford Research Institute, Menlo Park, Calif. (December 1965).

8. J. E. Nanevicz, "Progress in the Study of Titan Vehicle Electrostatic Environment," Engineering Data Design Evaluation Report, Contract F33615-70-C-1406, SRI Project 8428, Stanford Research Institute, Menlo Park, Calif. (May 1971).

9. J. E. Nanevicz, E. T. Pierce, and A. L. Whitson, "Measurements in Atmospheric Electricity Designed to Improve Launch Safety During the Apollo Series," Final Report, Contract NAS9-11357, SRI Project 8940, Stanford Research Institute, Menlo Park, Calif. (June 1972).

161

10. J. E. Nanevicz, E. F. Vance, and W. C. Wadsworth, "Low-Altitude, Long-Range All-Weather Vehicle Interference Investigation: Development of Flight Test Instrumentation, Part II," Tech. Report AFAL-TR-65-239, Contract AF 33(615)-1934, SRI Project 5082, Stanford Research Institute, Menlo Park, Calif. (December 1966).

11. J. E. Nanevicz and J. B. Chown, "SRI Experiments on AFCRL Nike-Cajun Rocket AD 6.842 and on Trailblazer II," Scientific Report 8, Contract AF 19(628)-4800, SRI Project 5359, Stanford Research Institute, Menlo Park, Calif. (December 1967).

12. W. E. Scharfman and H. R. Bredfeldt, "Use of the Langmuir Probe to Determine the Electron Density and Temperature Surrounding Reentry Vehicles," Final Report, Contract NAS1-4872, SRI Project 5771, Stanford Research Institute, Menlo Park, Calif. (December 1966).

13. L. J. Paustian, Titan III-C Payload Users' Guide, Martin-Marietta Corp., Denver Division, Denver, Colorado (January 1968).

14. K. E. Bessett, "T III-C Vehicle 20 Final 3D Guidance Reference Trajectory Reissue A," MCR-70-414, Martin-Marietta Corporation, Denver, Colorado (April 1971).

15. M. A. Uman, "Electrical Breakdown in the Apollo 12/Saturn V First Stage Exhaust," Report 70-9C8-HIVOL-R1, Westinghouse Research Laboratories, Pittsburgh, PA (1970).

16. J. E. Nanevicz, E. F. Vance, R. L. Tanner, and G. R. Hilbers, "Development and Testing of Techniques for Precipitation Static Interference Reduction," Final Report, Contract AF 33(616)-6561, SRI Project 2848, Stanford Research Institute, Menlo Park, Calif. (January 1962).

17. J. C. Axtell, "Preliminary Minuteman Electrostatic Charge Studies," Model No. WS-133A, Contract AF 04(647)-580, The Boeing Company, Seattle, Washington (1963).

18. R. L. Tanner and J. E. Nanevicz, "Precipitation Charging and Corona-Generated Interference in Aircraft," AFCRL 336, Tech. Report 73, Contract AF 19(604)-3458, SRI Project 2494, Stanford Research Institute, Menlo Park, Calif. (April 1961).

19. J. E. Nanevicz, "A Study of Precipitation-Static Noise Generation in Aircraft Canopy Antennas," Tech. Report 62, SRI Project 1197, Contract AF 19(604)-1296, Stanford Research Institute, Menlo Park, Calif. (December 1957).

162

20. J. E. Nanevicz, E. F. Vance, W. C. Wadsworth, and J. A. Martin, "Low-Altitude, Long-Range All Weather Vehicle Interference Investigation," Tech. Report AFAL-TR-65-239, Contract AF(615)-1934, SRI Project 5082, Stanford Research Institute, Menlo Park, Calif. (December 1965).

21. F. S. Johnson, Satellite Environment Handbook, (Stanford University Press, Stanford, Calif., 1965).

22. B. Feuerbacher and B. Fitton, "Experimental Investigation of Photoemission from Satellite Surface Materials," J. Appl. Phys., Vol. 43, No. 4, pp. 1563-1572, (April 1972).

23. W. B. Hansen, D. D. McRibben and G. W. Sharp, "Some Ionospheric Measurements with Satellite-Borne Ion Traps," J. Geophys. Res., Vol. 69, No. 13, pp. 2747-2763 (July 1, 1964).

24. N. Matuura and T. Ondoh, "The Structure of the Topside Ionosphere Deduced from Alouette Data," Proc. IEEE, Vol. 57, No. 6, pp. 1150-1153 (June 1969).

25. E. C. Whipple, Jr., "The Equilibrium Potential of a Body in the Upper Atmosphere and in Interplanetary Space," X-615-65-296, Goddard Space Flight Center, Greenbelt, Maryland (June 1965).

26. A. P. Willmore, "Electron and Ion Temperatures in the Ionosphere," Space Science Reviews, Vol. II, No. 5, pp. 607-670 (D. Reidel Publishing Co., Dordrecht-Holland, December 1970).

27. Ju. L. Al'Pert, "On Electromagnetic Effects in the Neighbourhood of a Satellite or a Vehicle Moving in the Ionosphere or Interplanetary Space," Space Science Reviews, Vol. IV, No. 3, pp. 373-415 (D. Reidel Publishing Co., Dordrecht-Holland, May 1965).

28. E. C. Whipple, Jr., "Electrostatic Charges Acquired by Spacecraft and their Possible Effects on Instruments," AFAL-TR-72-235, Lightning and Static Electricity Conference, 12-15 December 1972, Air Force Avionics Laboratory, Wright-Patterson Air Force Base, Ohio.

29. K. P. Chopra, "Thermionic and Photoelectric Screening of Objects Moving in an Ionized Medium," Astronautica Acta, Vol. II, No. 3, pp. 157-168 (1965).

30. "Satellite Lifetime Monitoring Instrumentation (First Generation System): Orbital-Data Reduction and Laboratory Support Experiments," Proposal for Research, SRI No. ERU 72-104R, Extention to Contract F33615-70-C-1406 (26 January 1973).

31. P.O. Number 126192, Contract F04(701)-71-C-0130. From Aerojet
    Electrosystems Co., Azusa, Calif.

DISTRIBUTION LIST

Number of Copies	Addressee
15	AFAL (AAA/Capt D F Wilkerson) Wright-Patterson AFB, OH 45433
1	AFAL(TEM) Wright-Patterson AFB, OH 45433
1	AFAL(XP) Wright-Patterson AFB, OH 45433
1	AFAPL(PO) Wright-Patterson AFB, OH 45433
1	AFFDL(FGL) Wright-Patterson AFB, OH 45433
1	AFFDL(FYS) Wright-Patterson AFB, OH 45433
1	AFML(CA) Wright-Patterson AFB, OH 45433
1	AFML(LA) Wright-Patterson AFB, OH 45433
1	AFAL(TSR/Mrs Connerton) Wright-Patterson AFB, OH 45433
1	2750th ABW/SSL Wright-Patterson AFB, OH 45433
1	AFML(LC) Wright-Patterson AFB, OH 45433
2	AFML(LN/Mr H S Schwartz) Wright-Patterson AFB, OH 45433
1	AFSC(SDFC) Andrews AFB Wash DC 20332
1	AFSC(SDME) Andrews AFB Wash DC 20332

Number of Copies	Addressee
1	ASD(ENV) Wright-Patterson AFB, OH 45433
5	ASD(ENVCC/Mr C E Seth) Wright-Patterson AFB, OH 45433
1	ASD(OIP) Wright-Patterson AFB, OH 45433
1	ASD(SD4E/Mr C E Tyzzer) Wright-Patterson AFB, OH 45433
1	AUL(Air Univ Library) Maxwell AFB AL 36112
2	DDC Cameron Station Alexandria VA 22314
1	OCAMA(AFLC/MMES) Tinker AFB, OK 73145
1	OSD(DDR&E) Materials Division Office of Assistant Director (Chemical Technology) Wash DC 20301
1	HQ SAC(OAI) Offutt AFB NE 69193
1	SAMSO(SMTAE) Air Force Unit Post Office Los Angeles CA 90045
1	HQ USAF(RDPS) Wash DC 20330
1	HQ USAF(SAMID) Wash DC 20330
1	HQ USAF(SA) Wash DC 20330
1	HQ 1002 Insp Gen Gp HQ USAF Directorate of Aerospace Safety AF-IGDSFR Norton AFB CA 92409

Number of Copies	Addressee
1	HQ 3246 Test Wing TGYL/Mr R V Gressang Eglin AFB FL 32542
1	HQ 3246 Test Wing TGYL/Mr Hugh A Lindsey Eglin AFB FL 32542
1	4950/TZHM/Mr P T Marth Wright-Patterson AFB, OH 45433
1	6570th AMRL(HEF) Wright-Patterson AFB, OH 45433
1	AF Cambridge Research Labs AFCRI(CRHC/Dr D R Fitzgerald) L G Hanscom Field Bedford MA 01730
1	AF Flight Dynamics Lab (AFCR4/PTS) Mr Andre J Helten Wright-Patterson AFB, OH 45433
1	Picatinny Arsenal Plastics Technical Evaluation Ctr SMUPA-VP-3/Mr H E Pebly, Jr Dover NM 07801
1	US Army Electronics Command Attn: Dr Rudolf G Buser Ft Monmouth NJ 07703
1	US Army Electronics Command Attn: Hans E Inslerman Ft Monmouth NJ 07703
1	US Army Missile Command Redstone Scientific Information Ctr Document Section Redstone Arsenal AL 35809
2	Naval Air Systems Command AIR-53356/Mr Joseph J Fisher Wash DC 20360
1	Avco Corp Space Systems Div Attn: Mr A J Patrick Lowell Ind Park Lowell MA 01851

Number of Copies	Addressee
1	McDonnell Douglas Corp Dept 311-B33N Attn: Mr G Weinstock St Louis MO 63166
1	Martin Marietta Corp Attn: Mr Robert W Ellison P O Box 179 Denver CO 80201
2	Electromagnetic Compatibility Analysis Center, North Seven Annapolis, MD 21402 Attn: Mr W Moran/EC
20	Hdqtrs SAMSO Air Force Unit Post Office Los Angeles CA 90045 Attn: Major Wood/SCJ
1	Rand Corporation 1700 Main Street Santa Monica CA 90406 Attn: Mr A L Hiebert
2	Rome Air Development Center Griffiss AFB NY 13440 Attn: Mr Jake Scherer/RCCM
1	Werner Robins Air Material Area Robins Air Force Base, GA 31093 Attn: Mr Robinson/MMEEI
1	Sachs/Freedman Associates, Inc 7515 Annapolis Rd Hyattsville MD 20784
1	Office of Naval Research Attn: Mr James Hughes Arlington VA 22217
1	Naval Avionics Facility CODE 441 Indianapolis IN 46218

Number of Copies	Addressee
1	Naval Air Development Center STD-7-ASD/Mr Aris Pasles Warminister PA 18974
1	NASA/Lewis Research Center Attn: Mr R Lark, MS 49-1 21000 Brookpark Rd Cleveland OH 44135
1	Federal Aviation Administration Attn: Mr Robert J Auburn Wash DC 20590
1	National Bureau of Standards Div 272.70 Attn: Mr Harold E Taggart Boulder CO 80302
1	Federal Aviation Administration Office of Supersonic Transport Development SS110 (Mr E R Bartholomew) 800 Independence Ave SW Wash DC 20590
1	FAA, Eastern Region Library Federal Bldg JFK International Airport Jamaica NY 11430
1	Aerospace Corporation Attn: Mr James R Coge 2350 E El Segundo Blvd El Segundo CA 90245
1	Aerospace Corporation Attn: Dr Carl B Pearlston El Segundo Blvd, 2350 El Segundo CA 90245

DOCUMENT CONTROL DATA – R & D

(Security classification of title, body of abstract and indexing annotation must be entered when the overall report is classified)

1. ORIGINATING ACTIVITY (Corporate author)	2a. REPORT SECURITY CLASSIFICATION
Stanford Research Institute Menlo Park, Calif. 94025	Unclassified
	2b. GROUP N/A

3. REPORT TITLE

TITAN VEHICLE ELECTROSTATIC ENVIRONMENT

4. DESCRIPTIVE NOTES (Type of report and inclusive dates)

Final Report   Covering the period February 1970 through December 1972

5. AUTHOR(S) (First name, middle initial, last name)

Joseph E. Nanevicz   G. Richard Hilbers

6. REPORT DATE	7a. TOTAL NO. OF PAGES	7b. NO. OF REFS
July 1973	186	31

8a. CONTRACT OR GRANT NO.	9a. ORIGINATOR'S REPORT NUMBER(S)
Contract F33615-70-C-1406	Final Report
b. PROJECT NO. 6091	SRI Project 8428
c.	9b. OTHER REPORT NO(S) (Any other numbers that may be assigned this report)
d.	17 OCT 1973

10. DISTRIBUTION STATEMENT

Distribution limited to U.S. Government agencies only: Reason – Test and evaluation; other requests for this document must be referred to the Air Force Avionics Laboratory, AFAL/AAA, Wright-Patterson Air Force Base, Ohio 45433.

11. SUPPLEMENTARY NOTES	12. SPONSORING MILITARY ACTIVITY
	Air Force Avionics Laboratory Air Force Systems Command Systems Avionics Division Wright-Patterson AFB, Ohio 45433

13. ABSTRACT

Ground and flight instrumentation was developed and employed for the study of vehicle electrification during the launch of two Titan IIIC rockets. The flight instrumentation operated and gathered data from ignition to payload orbit injection at 19,400 nmi. The first launch occurred under clear-weather conditions and provided data on rocket-motor electrification at liftoff and in the ionosphere. On the second launch, clouds existed in the launch area so that this flight provided data on vehicle electrification during flight through precipitation.

The results of the experiment indicate that rockets become electrified by the action of the engines at liftoff, and that precipitation-particle impact also produces electrification. Streamer discharges were measured resulting from precipitation-static electrification of a dielectric surface on the front of the rocket. Results from the atmospheric portion of the flight indicate that the electrostatic behavior of a large rocket is similar to that of a jet aircraft.

In the flight through the ionosphere, it was found that operation of the main engines and altitude-control rockets produced readily detected signals in the electrostatic sensors. This indicated that rocket-exhaust constituents were being returned to the vicinity of the vehicle.

14 KEY WORDS	LINK A		LINK B		LINK C	
	ROLE	WT	ROLE	WT	ROLE	WT
Static electrification						
Rocket charging						
Rocket-motor charging						
Noise pulses						
Rocket experiments						
Ionospheric experiments						
Photoelectric currents						
Rocket-launch ground measurements						

13. ABSTRACT (Continued)

Data from the ground instrumentation indicate that the electrostatic fields in the vicinity of the pad at launch are dominated by charges on the clouds generated by the launch.

Instrumentation and the results of the tests are discussed in considerable detail. Where appropriate, results are compared to theoretical analyses or to earlier measurements on aircraft and rockets.